

Engineered ‘Nanomaterials by design’ theoretical studies experimental validations current and future prospects



S. Ahmad*

YMCA University of Science and Technology,
Faridabad, India

*) Email: drsahmad@email.com

Received 4/6/2018, Accepted 1/10/2018, Published 15/9/2019

Modulating the electron energy band structure of a nano crystalline material by varying its size, shape, and constituent species amounts to practically designing the nano size material building blocks for arriving at a known set of related physico-chemical properties in terms of the internal electronic structures for a given organization of the constituent species via covalent and non-covalent interactions operating at different length scales. In order to explore further possibilities of using synergistic combinations of nano structured materials derived from inorganic, organic and polymeric species particularly knowing through their chemical bonds involved in different forms, it is equally necessary to know about the interaction pathways among the constituent species, as mentioned above, in addition to the biomolecular species, where they form a variety of 3-d supramolecular organizations arising out of self-assembly and self-organization. After having a clear picture of these basic processes involved in the internal and external organization of the hierarchical supramolecular structures, the next step is to explore the prospects of incorporating some sort of intelligent features starting from using the biomolecular species like polypeptides, proteins and enzymes. What is emerging from the current developments taking place in the related areas can be foreseen from this review particularly viewed from material science point of view.

Keywords: Energy Band Structure; Band Structure Engineered Nanocrystals, nanostructured material species derived from inorganic, organic and biomolecular material species.

1. INTRODUCTION

The crystalline forms of the condensed state materials that have been studied in detail are represented by their characteristic energy band structures that put them into three basic categories known as metals, semiconductors and insulators (e.g. $E_G \sim 0, 1-3,$ and $>5\text{eV}$, respectively). Almost completely delocalized electron states in the metals possess very high conductivity but in the semiconductors relatively lesser number of electrons are present there possessing lower but controllable conductivities that are possible to change precisely by doping with donor/acceptor type impurities to control the concentration of majority charge carriers - electrons/holes, respectively, as well as their extrinsic conductivities that are found useful in semiconductor devices and circuits applications. The dielectrics with very high band gaps ($>5\text{eV}$) offer themselves as high quality dielectric films for separating metal, and

Exp. Theo. NANOTECHNOLOGY 3 (2019) 301-362

semiconductor layers in achieving typical interfaces required in active devices and circuits. The whole area of microelectronic device fabrication technology has practically been evolved using a number of extremely high purity, structurally almost perfect crystalline bulk as well as thin films of semiconductors, along with the thin films of metal and dielectrics combined with patterning technologies spanning over a period of about half a century in the immediate past [1,2].

Subsequently, very useful observations were made while studying the physico-chemical properties of the different families of nanoparticulate materials in the form of nanoparticles (NPs), nano crystals (NCs), quantum dots (QDs) and nano size clusters synthesized from the above-cited three basic families of materials.

In order to minimize the overlap in using different terms for nanoparticulate form of materials in different research publications coming from different fields, it is better to be familiar with the most common usages as given below.

In nanotechnology, a particle is defined as a small object that behaves as a whole unit with respect to its transport and other properties. Particles are further classified according to diameter. Nanoparticles have their sizes tentatively in the range of 1 to 100nm. On the other hand, fine aggregates of atoms or molecules containing a couple of hundred atoms are called nanoclusters. Still larger aggregates containing 1000 or more atoms are called nanoparticles (NPs). These are bound by various kinds of forces including metallic, covalent, ionic, hydrogen bonds or Van der Waal's forces. A nanocrystal is a material particle having at least one dimension smaller than 100nm comprising of atoms in either mono/poly-crystalline arrangement.

For instance, a nanoparticulate sample of metal, semiconductor or dielectric possesses additional physico-chemical properties over and above those of its parent material due to quantum confinement of the electron states in a nano size volume resulting in additional discrete allowed electron energy states superimposed upon the existing representative energy band structure of the parent material. This size/shape specific quantum confinement of the charge carriers ultimately was found responsible for their characteristic optical absorption properties, which are easy to modify for their characteristic applications in optical and optoelectronic devices [3-5].

The researchers have always been tempted to organize nanoparticulate material samples as nano size material building blocks to produce a synthetic lattice with sufficient overlap of the wave functions of the electron states from the nearest neighbors. This kind of arrangement of the nanoparticulate materials known as superlattice in 3-D is naturally expected to result into a family of high-quality nano crystalline solids that would be practically quite similar to bulk crystal in conventional form. But, controlling the inter-dot separation with the help of a large variety of molecular species known as linkers is expected to be additionally helpful in controlling the charge carrier transport, in which, it is possible to manipulate the supported excitons in terms of their dissociations into free charge carriers - electrons and holes, their separation as well as recombination, and collection by appropriately designed contact electrodes in photovoltaic devices. Phenomenon like photoluminescence (PL) and optical absorption that characterize the interaction of quantum confined charge carriers within the nano size environment inside and around them have already been studied extensively in recent past. Indeed, the overall situation regarding the energy band structure representation of a relatively smaller number of atoms and molecules in such nanoparticulate form is not that simple because of significant influence of many body effects in operation therein. In this context, continuous efforts have been made over almost hundred years in past to develop reliable theoretical models for rational designs of these material entities for exploring their numerous applications in a predictable manner. The whole exercise is ultimately aimed at finally developing 'materials by

design' approach of future material discoveries after understanding their interactions involved therein [6].

During normal preparation of these nanoparticulate material forms, most of the atoms residing on the surface that are partially bound to the atoms inside give rise to quite a few dangling orbitals per atom, which are always eager to interact among themselves in the absence of additional atoms and/or modify the band structure of the nanoparticulate form by creating extra gap states, which may act as trap centers and in case their density is sufficiently large, they may even ultimately form a band structure of their own to mix with the band structure of the core. In most of the cases already studied in recent past, the stability as well as reactivity of these nanoparticulate forms of materials has only been found dependent upon the surface conditions. Under such highly reactive conditions, it is not only advantageously possible to conjugate a large variety of hydrophobic and hydrophilic moieties for modifying their solubility in different solvents but also enable them to form conjugated supramolecular NCs with immense possibility of modifying their self-assembly and self-organizational behaviors for numerous applications involving organic-inorganic-biomolecular species in proper configurations by exploring numerous biomimetic routes.

Based on the experience of handling various kinds of nanoparticulate forms of materials starting from their design, synthesis and applications during last few decades and the success achieved in realizing numerous novel material structures, they have already been named as synthetic atoms/molecules, wherein their internal structures and optoelectronic properties are programmable over a wide range for their possible applications in synthesizing 'materials by design' in which the introduction of intelligent features have already been shown to be possible using biomolecular species in numerous compositions appropriate for chemical conjugations [7-9].

In order to assess the current status and foresee the future trend in the domain of 'materials by design' using nanoparticulate forms of materials as building blocks, an effort has been made here in this review, to briefly examine the theoretical possibilities arising due to discrete electron states in atoms, molecules and chemical compounds before proceeding towards combining them with the metal and semiconductor nano particulates along with biomolecular species by incorporating non-covalent interactions resulting into supramolecular hierarchical structures for their applications in materials development.

2. ATOMS, MOLECULES, CRYSTALS, AND NANO CRYSTALS

Applying the basic principle of quantization of energy, orbital, and angular momenta of the electrons, existing in form of negative charge cloud surrounding the positively charged nucleus, it has already been possible to estimate the discrete electron energy states characterized by a set of three quantum numbers $n, l, \text{ and } m$ along with spin quantum number s ($\pm 1/2$) for specifying the electron states adequately in an atom. Instead of an isolated individual atom, when two or more identical/different atoms approach each other in a close proximity to form a stable molecule, differing from merely an assembly of individual atoms, chemical bonds are formed as a result of overlap between the wave functions of the outermost electron states from the participating atoms as the nearest neighbors, in which, the overall energy is reduced due to stable chemical bond formation. The overlapping atomic orbitals involved in bond formation introduce delocalization of electron states as now the participating atoms jointly share the involved electron pairs. Indeed, instead of only two or few of these atoms, if fairly large number of the participating species contribute towards forming a stable crystalline lattice, a set of continuum energy bands replace the discrete energy states known as energy band structure of the periodic lattice of the crystalline materials and polymeric molecules.

Exp. Theo. NANOTECHNOLOGY 3 (2019) 301-362

In case of nano crystals (NCs) that are formed due to stable clustering of few hundreds to few thousands of atomic and molecular species under favorable conditions, the phenomenon of quantum confinement of the electrons introduces additional discrete energy states modifying the otherwise energy band gap of the core material already mentioned above.

In this process of examining the electron states belonging to different types of material species such as atoms, molecules, bulk crystalline solids, and nanometer size material species called nano crystals (NCs), unique types of structure-properties relations have been found to exist and thus have continuously been studied and updated in past with the objective of designing and preparing new materials, where their anticipated properties are known even before starting their synthesis, by using appropriate theoretical models for defining the electron states and their interactions with all kinds of external fields.

While discussing about the design of new materials using atoms, molecules, and nano crystals as building blocks, some of the characteristic features involved in the description of electron states under different circumstances are very briefly reviewed in the followings.

2.1 Electrons in Atoms and Molecules

The electronic structures of atoms and molecules are explored using the concept of quantum physics developed during the early part of the 20th Century. The spectroscopic validations carried out experimentally provided the requisite level of confidence in moving ahead with establishing the comprehensive correlations between structure and physico-chemical properties of the materials already known as briefly described in the following.

The electron states in atoms, molecules, and crystalline solids are examined using quantum mechanics for understanding the physico-chemical properties of the elements of periodic table and knowing about their precise roles in forming chemical compounds through the chemical reactions involved therein.

The Schrödinger wave equation is used to describe the interactions among the elementary particles in form of a partial differential equation expressing the time evolution of the corresponding wave function is expressed below.

$$i\hbar \frac{\partial \Psi}{\partial t} = -\frac{\hbar^2}{2m} \frac{\partial^2 \Psi}{\partial x^2} + V(x)\Psi(x, t) \equiv \tilde{H}\Psi(x, t) \quad (1)$$

Here, $\Psi(x, t)$ = time-dependent wave function, $V(x)$ = potential, and \tilde{H} = Hamiltonian operator. Separating total wave function $\Psi(x, t)$ into temporal $T(t)$ and spatial $\psi(x)$ parts using separation of variables it is expressed in the product form as given below.

$$\Psi(x, t) = \psi(x)T(t)$$

$$\frac{1}{\psi} \left[-\frac{\hbar^2}{2m} \frac{d^2 \psi}{dx^2} + V(x)\psi \right] = \frac{i\hbar}{T} \frac{dT}{dt} = E \quad (2)$$

Here, each part is set equal to a constant E with the following relationships.

$$\left[-\frac{\hbar^2}{2m} \frac{d^2}{dx^2} + V(x) \right] \psi(x) = E\psi(x), \quad (3)$$

$$T(t) = e^{-iEt/\hbar}, \text{ and} \quad (4)$$

$$\Psi(x, t) = \psi(x)e^{-\frac{iEt}{\hbar}} = \sum_n c_n \psi_n(x) \cdot e^{-iEt/\hbar} \quad (5)$$

For determining the electron states under steady state condition, time independent part of Schrödinger wave equation is solved for a known potential function to determine the allowed energy states in a given interaction.

For proceeding further to determine the allowed electron energy states in an isolated atom, the simplest case of hydrogen atom with only a pair of electron and proton is used in solving the time independent Schrödinger wave equation involving the Coulomb interactions between the two in the above atomic model where a negatively charged electron-cloud surrounds the positively charged nucleus. The earliest model of electronic structure considered only those orbitals that obeyed the principle of energy quantization using an integral quantum number n

to specify different states. This simple planetary model, although, did account for the major parts of the hydrogen spectra, the existence of fine structures, especially in presence of magnetic fields, could only be explained subsequently by solving the Schrödinger's wave equation with spherically symmetric potential function introducing additional quantum numbers l , and m corresponding to quantization of the orbital and angular momenta, respectively. Further inclusion of the Pauli's principle of electron spin introduced another set of quantum number s having two possible states ($\pm 1/2$). Thus, the electron states in a hydrogen atom are finally represented by four quantum numbers ($n, l, m, \text{ and } s$), which are sufficient to explain the hydrogen spectra observed experimentally [10,11].

The electronic structures of the atomic species beyond hydrogen in the periodic table are computed by extending the H-like solutions of the Schrödinger's wave equation with the help of 'aufbau' principle, which states that the electron orbitals are filled starting with the lowest value of the principal quantum number $n = 1$ to the subsequent higher values onward. Further, taking into account the fact that electrons among themselves repel each other in an assembly, the occupation of energetically equivalent orbitals with different orientations is preferred over their pairing according to the Hund's rule. The electronic structures of all the elements of periodic table are, thus, compiled with H-like solutions along with the help of above two basic rules, which are now available in textbooks of chemistry [10].

The atomic orbitals (AOs), determined from the H-like solution of Schrödinger's wave equation for a particular atom define the probability distributions of their locations estimated within the limit of the Heisenberg's uncertainty principle [10]. The complete one electron wave function of the H-like solution is expressed as:

$$\psi_{nlm} = \sqrt{\rho^3 (n-l-1)!/2n(n+l)!} \cdot e^{-\frac{\rho}{2}} \cdot \rho^l \cdot L_{n-l-1}^{2l+1}(\rho) \cdot Y_l^m(\vartheta, \phi); \quad (6)$$

With, $\rho = \frac{2}{na_0}$; $a_0 = \text{Bohr's radius}$; $L_{n-l-1}^{2l+1}(\rho) = \text{generalized Laguerre's polynomial of the order of } n-l-1$, and $Y_l^m(\vartheta, \phi) = \text{spherical harmonics of degree } l \text{ and order } m$. Accordingly, the energy of an electron with quantum number n , is expressed as:

$$E_n = -13.6/n^2 \quad (7)$$

It is noted from the above equation (7) that inter-level separations become smaller with the higher quantum number n before merging into continuum for very large values.

Extending the treatment of electron states represented by the H-atom like solutions of atomic orbitals (AO), it is now possible to determine the electron energy states in H₂-molecule having the overlap of the participating AOs forming molecular orbitals (MOs) that enable the electrons hold together by lowering their binding energy during bond formation [12]. In other words, the bond formations in molecules caused by inter-orbital interactions invariably lower the energy of the resulting bonding MOs leading to stability. Accordingly, the first condition for sufficient orbital overlap causing molecular bond formation is the symmetry of the orbitals such that the regions with the same sign of the wave function must overlap. Next, the energy of the AOs must be similar, as in case of different energies; the change in the energy of electrons upon formation of molecular orbitals (MOs) would be much smaller resulting in very low reduction in energy of the bound electrons for bonding. In such cases, rather, ionic bonding is proposed. Finally, the inter-atomic distance should be short enough to provide good orbital overlaps, but not so short that repulsive forces between the electrons or the nuclei start exceeding the two attractive forces. Once these essential conditions are met, the energy of the electrons in the occupied MOs is found lower than the energy of the electrons in the participating AOs. Regardless of the number of AOs involved, the number of resultant MOs is always the same as the initial number of AOs; ensuring the conservation of the total number of orbitals to hold good.

Exp. Theo. NANOTECHNOLOGY 3 (2019) 301-362

The first quantum mechanical solution of chemical bonding in H₂ molecule was, thus, attempted taking the molecular orbital as simple product of the two AOs of the hydrogen atoms A and B, as given below.

$$\psi(r_1, r_2) = \psi_{1s}(r_{1A})\psi_{1s}(r_{2B}) \quad (8)$$

Employing this kind of trial MO-function into the ‘variational integral’ formed for minimizing the binding energy gave a value energy $D_e \approx 0.25$ eV, which was indeed much smaller than the experimental value. Subsequently, several refinements were introduced based on different schemes of hybridization. For example, a symmetrized combination of two product functions, as expressed below, resulted in the next significant improvement in binding energy of $D_e \sim 3.20$ eV.

$$\psi(r_1, r_2) = \psi_{1s}(r_{1A})\psi_{1s}(r_{2B}) + \psi_{1s}(r_{1B})\psi_{1s}(r_{2A}) \quad (9)$$

In another study, replacing the exponential function of the hydrogen s-state by $e^{-\zeta r}$ improved the binding energy still further to $D_e \sim 3.782$ eV for $\zeta = 1.166$. However, in a still more recent study, a trial wave function in form of the product of exponential part with a polynomial function (comprising of 13-parameters) gave $D_e = 4.720$ eV that compared very well with the accepted value of the hydrogen binding energy 4.7467eV [13-15]. The analytical expressions used are given below.

$$\psi(r_1, r_2) = e^{-\alpha(\xi_1 + \xi_2)} \cdot \text{Polynomial}(\xi_1, \xi_2, \eta_1, \eta_2, \rho); \quad (10)$$

Where: $\xi_i = (r_{iA} + r_{iB})/R$; $\eta_i = (r_{iA} - r_{iB})/R$ and $\rho = r_{12}/R$.

The success in narrowing down the difference between the theoretical value of the binding energy and its experimentally estimated one by using complex forms of trial wave functions not only confirmed the complicated nature of hybridization involved in molecular binding but also the validity of quantum mechanical descriptions of the molecule under consideration [13,14]. The combinations of MOs resulting in the lowest energy state due to orbital overlaps have, thus, been worked out theoretically for a number of molecular compositions using quantum mechanical formulations for their further applications [16,17].

Speculating to realize an electron device involving molecular species with appropriate interactions of their MOs would ultimately offer an extraordinary type of device and circuit miniaturization well beyond the ones under development currently [18]. However, for implementing such kinds of devices in actual practice it would need appropriately right kind of device fabrication technologies for reaching to this level of miniaturization in future [18,19].

2.2 Electrons in Crystals

The most common chemical bonds that are formed due to sharing of valence electrons via interatomic interaction are called covalent, ionic, and metallic bonds, having bond energies ~ few eV. There are a number of examples to illustrate these kinds of bonds that impart characteristic properties to the resulting crystalline solids. For instance, Na atoms in sodium metal forming metallic bonds of 1.1eV/atom cohesive energy make it ductile with good electrical and thermal conductivity. In case of NaCl crystal, on the other hand, the ionic bonds with a cohesive energy of 3.28 eV/atom make it harder with very high melting point but easily dissolved in water. On the other extreme, the crystalline diamond having covalent bonds with cohesive energy of 7.4 eV/atom is the hardest natural material with high melting point of 3,800 K; but insoluble in nearly all kinds of solvents.

In addition, there are polar covalent bonds, falling between the covalent and the ionic bonds, found in most of the alloys or compounds in which different electro negativities of the participating elements decide the way sharing of the valence electrons takes place during such bond formations [20]. There is another category of non-covalent bonds, which are responsible for the behavior of biological entities due to intra and intermolecular interactions of relatively weaker nature as discussed later.

The nature of the potentials involved in these strong inter-atomic interactions during crystal formation decide the cohesive energy, the energy band structure, the dispersion relations, the allowed density of states of the valence and conduction bands, the effective masses and group velocities of the electrons in various bands. The characteristic properties of the bulk materials, such as the critical temperature for crystal structural phase transition, electronic and optical properties, hardness, elasticity, and melting point - all are closely related to the nature of the chemical bond formations. The parameters like cohesive energy and binding energy density determines the thermal stability, the elasticity, and mechanical strength, respectively [20].

The crystal structures of the condensed states are generally formed out of microscopically ordered assembly of atomic, molecular or ionic species extending in 3-D. The unit cell, the small imaginary box containing one or more constituent species in a characteristic spatial arrangement, is sufficient to describe the crystal structure, as a three-dimensional stacking of theirs forming the entire crystal. Crystalline structures are possible to realize in almost all types of materials, with all types of chemical bonds. For instance, most of the metals are commonly known to exist in polycrystalline, or amorphous states but rarely in single-crystal form produced with difficulty. Ionic crystals are generally prepared either from a molten salt or from a solution. Covalently bonded crystals include the examples of diamond, silicon, germanium, and a large variety of other semiconductors. Weak van der Waal's forces are involved in holding together the hexagonal-patterned sheets in graphite besides a whole host of biomolecular crystals.

2.3 Crystalline Lattice - Energy Band Structure

Energy band structure of a crystalline lattice represents those energy states that are allowed to exist within the lattice against the absence of those that fall in the energy band gap. Band theory of a crystalline lattice determines these allowed energy bands and the band gap by employing quantum mechanical wave functions of an electron in a large, periodic lattice of atoms or molecules using cyclic boundary conditions [2].

For exploring extended states in a periodic lattice (i.e. electron energy-band-structure), the influence of a periodic potential due to positively charged nuclei is taken into account for determining the electrical and magnetic properties of such an ensemble of quasi free electrons derived from the right kind of atomic species [2].

In order to exemplify this concept, the electron energy band structure of a simple 1-d periodic lattice is determined by solving the Schrödinger wave equation involving a periodic potential with a finite barrier height and invoking the Bloch theorem [2]. In principle, the influence of periodic potential is added to the plane wave solution in the manner defined below:

$$\psi_{\mathbf{k}}(\mathbf{r}) = \mathbf{U}_{\mathbf{k}}(\mathbf{r}) \cdot e^{i\mathbf{k} \cdot \mathbf{r}} \quad (11)$$

Here, the periodic function, defined as: $\mathbf{U}_{\mathbf{k}}(\mathbf{r} + \mathbf{T}) = \mathbf{U}_{\mathbf{k}}(\mathbf{r})$, for any lattice translation vector \mathbf{T} , contains all the details of the structural symmetry of the lattice. Using such a trial function solution and applying the required boundary conditions, a transcendental relationship was arrived at, which was further simplified by assuming δ -function potential (i.e. where $V_0 b \rightarrow$ finite value) with a period of a in the form given below.

$$\sin(Ka) \cdot (P/Ka) + \cos(Ka) = \cos(ka) \quad (12)$$

Where, the plane wave energy $E = (\hbar K)^2 / 2m$; $P = baQ^2/2$, and $\hbar K$ is the electron momentum.

It is noted from the above derivation that the effective-mass of the electron m_e , as a function of the periodic potential reflecting the capability of electron to accelerate in presence of the applied electric field, is defined as:

$$1/m_e = (1/\hbar^2) \partial^2 E / \partial k^2 = (2J/\hbar^2) \cos(ka); \text{ where,} \\ J = \pi^2 \hbar^2 / (2m_e^2 a^3 U_0); U_0 = V_0 b \quad (13)$$

Exp. Theo. NANOTECHNOLOGY 3 (2019) 301-362

The plot of the transcendental equation (12) helps in finding out the allowed energy states separated by an energy gap at the band-edge. This is known as the famous Krönig-Penny model of the electron energy bands in a 1-d periodic potential, where the complex equations are purposely simplified for qualitatively highlighting the influence of the periodic lattice [2].

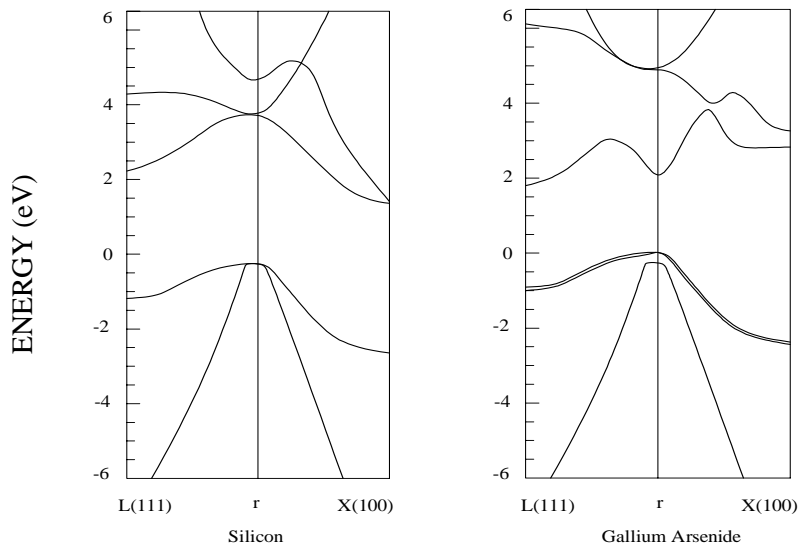


Figure 1 Theoretically calculated energy band structure of Silicon (indirect band gap) and Gallium Arsenide (direct band gap) bulk Semiconductor. The characteristic features arising out of indirect and direct band gap affect the optoelectronic properties of the materials as discussed in the text.

It is further possible to determine the electron wave functions as well as energy versus momentum variations in k -space, especially in the vicinity of the band edges, besides evaluating the effective masses from the inverse of the second derivative of energy versus k variation as expressed earlier in equation (13).

However, this discussion is concluded here, as there are more refined energy-band-structure calculations available for a number of crystalline materials, which can be used for design calculations as given in Figure. 1, for monocrystalline silicon and gallium arsenide bulk materials [2,21].

3. ELECTRONS IN NANO CRYSTALS

For determining the electron states in a NC, one has to start with the electron states corresponding to the core material involved having well defined energy band structure and then modify the wave functions by an envelope function that describes particle in a box like situation representing the phenomenon of quantum confinement [22]. Thus, the total electron wave function Ψ_{total} becomes possible to express as a product of Bloch wave function ψ_{bloch} corresponding to the crystalline structure and the envelope function ϕ_{env} as given below.

$$\Psi_{\text{total}} = \psi_{\text{bloch}} \cdot \psi_{\text{env}} \quad (14)$$

The envelope function ϕ_{env} , representing the charge carrier confinement, should in principle be the solution of the Schrödinger equation for a particle-in-a-sphere like situation where the eigen-functions are found to be the product of spherical harmonics $Y_l^m(\vartheta, \phi)$ and radial function $R(r)$ as described below.

$$\psi_{env}(\vartheta, \phi, r) = Y_l^m(\vartheta, \phi) \cdot R(r) \quad (15)$$

It is noted that the envelope function is very similar to that of an electron in a hydrogen atom except the potential function has spherical symmetry represented by $V(r) = -V_0$ for $r \leq d/2$ and $V(r) = 0$ elsewhere and the corresponding eigenvalues are given by the following relation.

$$\epsilon_{n,l}^{conf}(d) = (2\hbar^2/m_e d^2) \cdot \chi_{n,l}^2 \quad (16)$$

Here, m_e is the effective mass of electrons (or holes), and $\chi_{n,l}$ are the roots of the Bessel function depending on the principal quantum numbers n (1, 2, 3, ...) and azimuthal quantum number l (0, 1, 2, 3, ...). The lowest energy level ($n = 1$, and $l = 0$) has the symmetry of a 1s-orbital in a hydrogen atom. Because of using the spherical potential function in the nanocrystal, there is no restriction on the quantum number l with respect to quantum number n . Therefore the second energy level in a nanocrystal has quantum numbers $n = 1$ and $l = 1$ with a 1p-shaped orbital. The third level is represented by a 1d-orbital ($n = 1$, and $l = 2$), and the fourth level in a nanocrystal is a 2s level ($n = 2$, and $l = 0$). Nano crystals are very often referred to as “artificial atoms” due to the atom-like envelope wave functions of the lowest lying energy levels.

The band gap of a nanocrystal could, thus, be expressed as the sum of the fundamental band gap arising out of the bulk properties of the material used in terms of E_g^0 and the confinement energy $E_{n,l}^{conf}$ as given below.

$$E_g^{total}(d) = E_g^0 + (2\hbar^2/m_e d^2) \cdot \chi_{n,l}^2 [1/m_e + 1/m_h] \quad (17)$$

It is noted from the above simple equation (17) that the band gap of nanocrystal varies $\propto 1/d^2$ and discrete energy levels appear at the band-edges of both the conduction and valence bands as schematically depicted in Figure.2. From here it is also concluded that the optical band gap of NCs can be tuned by simply changing their morphology. There are numerous options that have been explored in this context as can be seen from the foregoing discussions.

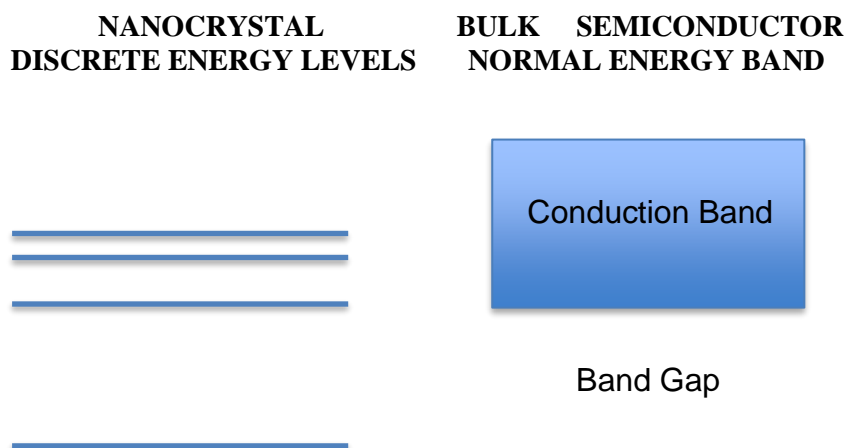




Figure 2 Schematics of the energy band structure of a quantum dot in comparison to the band structure of the bulk semiconductor used in making the quantum dot. Size dependent discrete energy levels are responsible for their characteristic physico-chemical properties.

3.1 Some Features of Nanoparticulate forms of Materials

Because of the localized discrete electron energy states present there in NCs, a detailed examination of the optical absorption spectra in colloidal form is possible using the standard methods of characterization. In one such study of optical transitions of a mono disperses quasi-spherical PbSe NCs having diameters in the range of 3.4 to 10.9 nm, however, a little more involved picture was observed [22]. For example, the plot of the lowest transition energy versus diameter of the NCs showed a relationship of the type $E \propto d^{-1.5}$ in contrast to the expected variation of $\propto d^{-2}$ as mentioned above. Indeed, the extrapolated values of this energy corresponding to infinite diameter of NCs comes to 0.3 and 1.6 eV in agreement with the band gap of bulk PbSe at the L and Σ -point in the Brillouin zone. Tight-binding calculations are found to confirm that the high-energy transitions originating from the Σ -point in the Brillouin zone [22].

Besides having the description of the ideal electronic states in a perfect NC, it is also important to know about the changes brought in by the presence of structural defects, introduced dopings, surface charges and dangling bonds, as these conditions are invariably there in any practical system comprising of NCs [23]. For instance, an incident photon in an ideal NC would excite an electron from the valence (VB) to the conduction band (CB) producing an electron-hole pair or exciton. However, in real NCs, there might be defects due to a missing or an additional atom, dopants, and/or excess charges, which would have been either introduced intentionally, as in case of Si doping, or inadvertently added by inherent surface defects such as dangling bonds, or photoionization, which would definitely complicate the excitation profiles resulting from a disruption of the normal electronic structure [24-27]. For instance, in case of a charged NC, an extra charge carrier would appear in VB or CB, leading to additional electronic transitions, whereas introduction of a hetero-valent dopant atom would create defect states near a band edge, by donating or accepting an extra electron to the CB or from the VB either from the thermal ionization of the dopant atom or confinement effects. Surface dangling bonds would, similarly, introduce discrete states into the band gap of the material [28].

In order to clarify the practical issues involved in such cases, a number of NCs comprising of PbSe, CdSe, and Si; positively and negatively charged PbSe and Si NCs besides doped PbSe and Si NCs along with dangling bonds were systematically studied theoretically as well as experimentally by measuring their optical transition spectra, from which, some interesting observations were made as summarized here [23,29]. For instance, the band structures of smaller NCs were qualitatively identical to those of much larger NCs. The small NC results showed that single excitons (SEs) are red and blue shifted for anionic and cationic NCs as compared to the neutral NCs, respectively. The multiple exciton (ME) thresholds, determined from *ab-initio* calculations with small neutral clusters agreed very well with the experimental data and more empirical calculations on the larger NCs. Dopants and dangling bonds do create defect states, irrespective of the size, and an extra electron in the CB allows new, low energy transitions, which has been observed in remote doping experiments on full-sized NCs.

In another alternate approach, the NC could also be considered like a large size molecule comprising of atomic species [30]. Under this assumption, it is, therefore, natural to start constructing the overall wave functions of the electron states in a NC using the linear combination of individual atomic orbitals. Taking the simplest case of only two atoms as an example, it is easy to see that the two atomic orbitals would combine to form a bonding and anti-bonding molecular orbitals separated by a finite energy gap as explained earlier. In case a greater number of atoms are added to this simple pair of two, there will be equally more number of energy levels and the energy spacing between the highest occupied molecular orbital (HOMO) and the lowest unoccupied molecular orbital (LUMO) would be smaller. In a NC, there are few hundred to few thousand atomic valence orbitals, forming as many molecular orbitals but still there will be discrete energy levels at the edges of the “bands” and the gap between the HOMO and LUMO levels would be subsequently smaller for larger size nano crystals. Finally, when the nanocrystal becomes even larger, the inter-level energy separation between the MO levels may be so small that the different energy levels are not distinguishable resulting in a continuous energy band structure of a bulk material and the energy spacing between the valence and conduction band is then called the fundamental band gap [30].

3.1.1 Phase Transformation in NCs

While studying the electronic properties of metallic NCs different kinds of packing behavior were observed with different core morphologies induced during synthesis. It was observed that dodecanethiol-stabilized gold NPs with similar size were found to organize into different superlattice (SL) structures depending upon the method of preparation of the nano crystals. For example, the inverse micelle technique-based NPs preferentially assembled into face centered cubic (fcc) structures with long-range translation and orientation ordering in contrast to the NPs prepared by solvated metal atom dispersion (SMAD) method organized into hexagonally close packed (hcp) nanocrystal SLs. It is significantly important to note that face centered cubic (fcc) ordering is preferred by monocrystalline NPs, while hcp is preferred in case of polycrystalline NPs [31].

Thermal treatment of Co NCs in low crystalline colloidal form is found to convert them into hcp phase without any modification in size, size distribution, and the lauric acid passivating layer. The saturation magnetization and the magnetic anisotropy of these NCs are strongly modified through annealing process. Monolayer self-assembly of the hcp cobalt NCs is also realized due to the dipolar interactions resulting in ferromagnetic behavior at room temperature [32].

Theoretical simulation of nano crystalline samples of Zr and Co undergoing plastic deformation reveals a reverse transformation from hcp to fcc structure without twinning. In Zr samples, the hcp-to-fcc transformation competes with deformation twinning [33].

Ag NCs (5nm) were noted to self-organize in colloidal crystals with various arrangements called supra-crystallinity. Phase diagrams of supra-crystals with structural transitions from fcc to hcp to bcc structures are observed depending on the chain length of the coating agent and on the solvent used to disperse the NCs before evaporation. The transition from fcc to hcp is attributed to specific stacking processes depending on evaporation kinetics, whereas the formation of bcc supra-crystals is attributed to van der Waals attractions [34].

Hexagonal close-packed Ni NPs are synthesized using reduction of nickel chloride in ethylenediamine as confirmed by XRD and selected-area electron diffraction of the as-prepared samples [35]. In another simple electrolytic deposition of Ni NCs (average diameter 9.7 ± 2.3 nm) a solution of 5.0mM $\text{NiCl}_2 \cdot 6\text{H}_2\text{O}$ is used along with 1 M NH_4Cl forming Ni NCs of almost pure hexagonal close-packed (hcp) structure, and the tuning of the final size, morphology and structural formation of these Ni NCs are possible to modify by controlling

Exp. Theo. NANOTECHNOLOGY 3 (2019) 301-362

nucleation, growth and hydrogen evolution processes in fast scan voltammetry technique used [36].

A reversible polymorphic phase transformation (i.e. from hcp to fcc) in four different nano crystalline Ti–Zr binary alloys was observed during mechanical alloying in a planetary ball mill experiment as monitored by X-ray diffraction and high-resolution transmission electron microscopy measurements [37]. For a given alloy, the lattice parameter and hence volume per atom increased with the milling time under comparable conditions. On the other hand, crystallite size, measured from X-ray peak broadening, significantly decreased with the progress of the milling process. It was suggested that structural instability due to plastic strain, increasing lattice expansion, and negative hydrostatic pressure were responsible for this hcp → fcc polymorphic transformation, which was found reversible as isothermal annealing at 1000 °C for 1h or melting the powder mass led to partial or complete transformation of the milled product from single phase fcc to hcp form [37].

Monodisperse PbS NCs of different size and shape were prepared by controlling the thermal decomposition of thioacetamide (TAA) in aqueous solution of lead acetate, with the help of cetyltrimethylammonium bromide (CTAB) surfactant and adjusting the concentration of sulfide resource in TAA, which decreased the size and changed shapes from octahedral to cubic. It was noted that the PbS NCs self-assembled into diverse superlattices, and the assembly structure strongly depending on the shape of PbS NCs [38].

While examining other materials, the bulk gold was not found in any other form like hexagonal close-packed (hcp) compared to its most stable form of fcc-structure. However, in a recent study, an *in-situ* synthesis of dispersible hcp Au square sheets on graphene oxide sheets was reported (~16 Au atomic layers thick and 200–500nm edge length). This square sheet was found to transform from hcp to fcc-structure after exposure to an electron beam during TEM analysis. In addition, with growing thickness of the square sheet (from ~ 2.4 to 6 nm), fcc-segments started appearing. This study confirmed the presence of stable pure hcp-structures in square sheets of <~ 6 nm thickness [39].

Large-area (30x40 μm^2) hcp-structured monocrystalline Au and Ag arrays appropriate for fabricating surface-enhanced Raman scattering (SERS) based biosensors, nano antennas and other plasmonic optoelectronic devices were successfully prepared on Si substrates by colloidal lithography and the surface energy driven de-wetting process [40]. Appropriate surface treatments and the metal deposition method were found out for preparing metal NC arrays with uniform size and reduced crystal size providing an inexpensive and easy route to fabricate a large-scale close-packed single crystalline metal nanocrystal arrays exhibiting excellent control for fabricating large-scale metal NC arrays with various sizes, compositions, morphologies and structures on different substrates [40].

Theoretical calculation involving genetic algorithm (molecular-dynamics) based computer simulations have revealed the presence of helical and multi walled cylindrical structures in case of thinner NWs, while bulk-like fcc-structures eventually prevailed in the thicker nanowires up to 3 nm in diameter. Though, the conductance of NWs was found increasing with wire diameter but depending on the wire structure [41]. Very thin NWs possessed molecule like behavior with DOS having many sharp and discrete peaks. In 1nm diameter NW, the discrete energy levels gradually started overlapping with each other forming continuous electronic energy bands. It was thus concluded that the bulk electronic properties were achieved in gold wire thicker than 3nm [41]

Flower-like silver nanostructures with controlled morphology and composition were prepared successfully by controlling the reaction rate by adding different amount of ammonia for determining the ratio of hcp to fcc-phases. Utilizing flower-like silver nanostructures as surface-enhanced Raman scattering (SERS) substrates, signal of Rhodamine 6G, or 4-aminothiophenol with concentration as low as 10^{-7}M could be detected [42].

3.1.2 *Electronic Properties of Metal NCs*

Having discussed the general nature of quantum confinement in a NC, it is now possible to examine the observed behaviors of the metal, the semiconductor and the insulating NCs for their possible applications in realizing intelligent materials in future.

The electrons in metals are highly delocalized due to overlap between valence and conduction bands leading to practically zero or even negative band gap in some cases exhibiting very high conductivity. Therefore, it is rather safe to assume that the metallic NCs consist of quasi-free valence electrons moving in a mean field generated out of the attractive and repulsive potentials due to the ionic cores and the rest of the electrons respectively. The confinement of such quasi-free electrons inside a finite size NCs would thus give rise to the orbitals having quantized energy levels, which are typically grouped into a number of shells. Pauli exclusion principle would allow the electrons to have a limited access to each of these shells. It is interesting to note that the metallic NCs, in principle, provided a new periodic system in contrast to the conventional atomic and nuclear periodic systems in vogue [43]. With reducing size of the NCs, more restrictions in the spatial confinements lead to enhanced separation between the valence and the conduction bands. In case, the energy gap is of the order or greater than thermal energy $k_B T$, there is a transition from metal to semiconductor. Similarly, confinement in still smaller sizes NCs may increase the energy gap such that there occurs another possible transition from semiconducting to insulating state. In the size domain, where the metal-to-insulator transition occurs, completely newer properties of NCs are indeed observed, which are not possessed either by the metal or by the molecules or atoms forming the parent metal [44]. Extraordinary features are acquired by the NCs due to quantum confinement of charge carriers and the associated boundary conditions [45]. For instance, there are situations when NCs made out of nonmagnetic materials may exhibit magnetic properties; NCs from semiconducting materials may transform into metallic ones; metal NCs may transform into semiconducting state; distinct variation in colors with size; noble material NCs may be highly reactive, and brittle NCs may be transformed into malleable state, and so on to name a few.

These features are basically manifestations of the unusual structure of the NCs and the electronic states of molecular orbitals exhibiting a finite HOMO-LUMO gap that varies with both size and composition of the NC and the way these orbitals are filled determining not only their overall stabilities but also their physical and chemical properties as well [45].

In case of examining the mass spectra of Na clusters, it has been noted that clusters comprising of 2, 8, 20, 40, . . . atoms are prominently stable. Considering Na clusters as spheres of uniform positive charges, the available valence electrons should start filling the quantized energy levels following the Pauli exclusion principle. In this process, each time, when an electronic shell is full, the corresponding cluster should exhibit pronounced stability. The confined electron energy levels in a cluster, obtained from Schrödinger wave equation solution by taking a three-dimensional square-well potential, should be represented by shell like arrangement similar to - $1s^2$, $1p^6$, $1d^{10}$, $2s^2$, $1f^{14}$, $2p^6$, and so on. Accordingly, the clusters containing 2, 8, 20, 40, electrons become very stable due to saturation [45].

In more recent investigations of Na clusters, attempts were made to locate the lowest-energy structures for all sizes up to $N = 380$, using two different forms of inter-atomic potentials, in order to identify the structures responsible for the size-dependence of the thermodynamic properties observed in various experiments [46]. Structures based on the Mackay icosahedra predominated for both the potentials, and the magic numbers showing excellent agreement with the sizes at which maxima in the latent heat and entropy change at melting were found in the experiment. In particular, the magic numbers at sizes intermediate between the complete Mackay icosahedra are due to unusual twisted icosahedral structures.

Although, initially observed similarity between magic nuclei and magic clusters appeared merely as a coincidence as the forces involved in nuclear binding are altogether different from

Exp. Theo. NANOTECHNOLOGY 3 (2019) 301-362

those that bind atoms in a NC, but the subsequent analysis of the ionization potentials, electron affinities and fragmentation energies of neutral and multiply charged NCs confirmed that these results are strikingly similar to those observed in corresponding quantities of separation energies of protons and neutrons. This similarity could, thus, further be extended, for example, in case of optical response of metal clusters *vis-a-vis* photonuclear processes. The phenomenon of photo absorption, in metal NCs, takes place via excitation of Plasmon resonance where the valence electrons move collectively against the Jellium positive background, which is quite analogous to nuclear giant dipole resonance, in which, the protons move against the neutrons. Detailed analysis of the photo absorption in alkali metal clusters predicted multi-peak profiles, which were verified experimentally but certainly differing from the simple one-peak profiles expected from the Mie theory [45].

Although the Jellium model could explain cluster stability involving nearly free electrons of metals but it did have limitations in accounting for the structural properties of clusters including geometry and atomic arrangement. For this, rigorous quantum-chemical and density-functional calculations involving electronic and nuclear degrees of freedom are necessary. For finding out the conditions when the metallic NCs would behave like metal, or when a metal cluster would mimic the structure of a bulk solid, it would necessarily involve the inclusion of the atomic and electronic structures as well as the properties and dynamics of the clusters as a function of size. Despite considerable efforts made in this area, satisfactory solutions are still not available. However, numerous studies of metal, semiconductor and insulator clusters as a function of size and morphology have provided a wealth of information that is certainly going to be very useful for further development of nano science and technology [45].

Elemental rare-gas clusters were noted to form icosahedral structures whereas covalent bonded clusters involving C and Si atoms differed from those in the bulk. For example, a 60-atom carbon cluster forms a Bucky ball structure that differs from either graphite or diamond. Ionic bonded clusters of alkali halides and metal nitrides, carbides, and oxides, retain their bulk crystalline structures. In transition metals and C clusters, the structures and stabilities have been found to depend strongly on whether the clusters were grown in a metal or carbon-rich environment. In the former case, clusters mimic the bulk carbides, whereas in the latter, they form cage-like structures.

The well-known Jellium model, explaining the metal cluster stability well, however could not account for the stability of covalently bonded transition metal magic clusters, in which, the theory of aromaticity was explored for taking care of the unusual stability of σ/π - electron systems, where electron delocalization provided extra stability. According to Hückel rule ($4n + 2$) σ/π – electrons impart extra stability in contrast to $4n$ σ/π - electrons that destabilize the system as seen in case of benzene and cyclo-butadiene. A similar rule developed for spherical systems predicted that, when the valance shells are filled by $2(N+1)^2$ electrons, there is a very stable spherical symmetry. Recently, several metallic and nonmetallic clusters obeying aromaticity rule have been predicted and experimentally verified. For example, Al_4^{2-} , having 2π – electrons, is aromatic and forms a perfect square, whereas Al_4^+ with 4π – electrons is anti-aromatic and has a rectangular shape [47]. Another example is of B_{12} clusters that are interesting from their extraordinary stability point of view having the largest HOMO-LUMO gap of 2.0 eV with a circular shape with 6π – electrons much like benzene molecules with a symmetric bond distribution [48]. Gold NCs consisting of up to 13 constituent atoms have planar arrangements according to relativistic density-functional theory whereas Au_{20} has a pyramidal structure. There were recent predictions that Au_{32} and Au_{50} would prefer hollow cage structures compared to their space-filling isomers from stability angles. Unusual stabilities of the gold cages Au_{32} and Au_{50} are attributed to spherical aromaticity following the rule of $n=3$ and 4. On the other hand, though, Au_{38} , Au_{44} , and Au_{56} are cage compounds not belonging to the magic family are less stable than the corresponding space-filling isomers.

In a recent theoretical and experimental study of a family of useful bimetallic clusters of compositions like PtZnH_5^- , PtZnH_3^- and PtZnH_4^- using negative ion photoelectron spectroscopy (PES) PtZnH_5^- was found to possess very high stability as seen in the mass spectrum, and σ -aromaticity [49].

In noble metal NCs, the decrease in sample size below the electron mean free path gives rise to intense absorption in the visible-near-UV region, and this is an outcome of coherent oscillation of the free electrons from one surface of the NC to the other and is called the surface Plasmon absorption [44]. Such absorption induces strong coupling of the NCs to the electromagnetic radiation imparting very brilliant colors to these metallic NCs in colloidal solution. It was Faraday, who recognized that such intense color was primarily due to metallic gold in colloidal form and Mie, who explained the phenomena of strong absorption by solving Maxwell's equations for explaining the absorption and scattering of electromagnetic radiation by spherical metallic particles.

In Jellium model of metal NCs, a uniformly charged background of flexible shape replaces the structural details of the ion placements present in the core. This model works very well especially for the lighter alkali metals like Na, K and Li NCs where the success has been attributed to the typical nature of the effective potential felt by the valence electrons, where inter-ionic distances are not resolved by the larger size de Broglie wavelengths associated with the valence electrons besides the thermal agitations of the core, which tend to mask their finer structural details still further [43].

3.1.3 *Electronic Properties of Semiconducting NCs*

In a semiconducting NC, also known as quantum dot (QD), each constituent atom contributes it is delocalized electrons and holes for their final distributions in the respective quantized atomic orbitals belonging to the NC in terms of S, P, D, and F orbitals correspond to the electron states respectively. This gives rise to discrete energy levels in conduction and valence bands of the semiconducting NC represented by a QW surrounded by finite barrier causing the quantum confinement of the charge carriers. The inter-level separations in the electron/hole energy states spectrum are decided by the parameters including dimension and barrier height besides the effective masses of the charge carriers that are determined from the crystalline symmetry of the parent semiconductor material. This is the kind of analogy of quasi-atom model of the semiconducting NCs that is further put to use in studying the collective electron behavior in NC-based superlattices.

For simplifying the analytical formulations of the electron states in a semiconducting NC, the geometrical shape is assumed to be of either spherical or cubic symmetry, wherein the wave function is expressed as a product of the three component wave functions, and these component wave functions are solved independently for a given potential energy function representing the background conditions. The quantized electronic states of all these valence electrons are in turn calculated by solving the corresponding Schrödinger equation in a way that is similar to that of the hydrogen atom.

Extending the simplified concept of Jellium model of NCs to determine the electronic states, it is quite natural to expect a mini band like situation especially in those cases where the NCs are situated close enough to invoke strong inter-particle interaction with the nearest neighbor. This could also be understood as electron tunneling between two NC units separated by a thin inter-particle barrier.

3.1.4 *Electrons in NC-Superlattice*

Exp. Theo. NANOTECHNOLOGY 3 (2019) 301-362

Employing the electron states in NCs, the entire problem of determining the electronic states in a NC superlattice reduces to computing the electron states responsible for miniband formation from the spillover of otherwise discrete electron energy states from each NC to its nearest neighbor. This kind of delocalization of electron states in a NC-superlattice is necessary for observing collective behavior of electrons in a superlattice where a number of useful parameters are possible to control during synthesis.

From the above description one could thus observe the followings: the signature of the quasi-free valence electrons in an individual NC is solely decided by the nature of the constituent atoms, their total number or the size of the NC and the surface passivation along with the existing functionalization meant for fixing the inter-particle separation. Considering the influence of the surface conditions is necessary because surface states may act like traps for some of the electrons from inside the NC especially where the surface to volume ratio is large and most of the constituent atoms are residing on the NC surface.

Similarly, mid band formation due to strong inter-particle interactions of the electron states is solely decided by the inter-particle separation and the symmetry of the lattice structure involved in superlattice formation. Once the signature of the valence electron from the NC is fixed the formation of electronic states in mid band becomes independent of the NCs used.

It is quite interesting to note that these conditions are exactly similar to that already observed in case of bulk crystalline solids formed using atomic building blocks but with a major difference in having immense flexibility in choosing various lattice parameters compared to condensed state lattices.

3.1.5 *Electrons in Insulating NCs*

Similar to the metallic and semiconducting NCs, described earlier, it is noted that even insulating NCs have properties to influence the electronic conduction in NC-solids. For example, an insulating NC in ground state with saturated valence and empty conduction levels behaves like an artificial atom for the purpose of adding one or more electrons, holes and excitons. For, the moment an electron is added to such a NC, it occupies the lowest energy conduction orbital that is delocalized across the nanocrystal volume having s-orbital symmetry of H-atom. Further addition of electrons continues occupying the successive higher orbitals according to Pauli Exclusion Principle. Due to quantum confinement, the inter-level separations between atom-like valence and conduction energy levels increases with reducing size and this inter-level gap could be made larger than thermal energy $k_B T$ for their uses in affecting optical transitions. Similarly, the gap between the lowest conduction and highest valence levels also increases with size reduction implying that the fundamental optical transition peak may span a broad range from near IR to near UV regions of the spectrum. The tunability of the energy levels thus makes NCs very promising building blocks for optoelectronic devices [50].

3.1.6 *Krönig-Penny Model of NC-Superlattice*

It is natural to expect realizing a periodic lattice made out of NCs in place of atomic species as discussed in case of Krönig-Penny model of crystalline solids in connection with the energy band structure. Since, basic features of NCs are possible to vary in numerous ways by controlling the size, shape and the constituent species, it is therefore anticipated to have synthetic materials out of an unprecedented number of combinations.

In case of hierarchically ordered QD/NC based SLs, there are possibilities of tuning their transport and optical properties by varying the properties of the individual constituent building blocks as well as their many-body exchange interactions [4]. Specially, the feature of long-range order achievable during synthesis in the NC SLs makes them distinctly different from

the conventional amorphous and polycrystalline solids. The existence of strong inter-particle coupling among the ordered NC assemblies causes split in the quantized discrete energy levels of the individual particles finally resulting in the formation of mini bands. Although, different types of SLs, consisting of single and multicomponent NCs building blocks, have already been self-assembled from colloidal solutions but the theoretical study of their electronic structures along with charge carrier and phonon transport still lacks details required for exploring their applications in electronic and optical devices [4]. However, the analysis of the extended states using effective mass approximation (EMA) in case of molecular beam epitaxy (MBE) grown one-dimensional QW and QD SLs has provided some insight for the collective behavior of electrons in NC based SLs as well. For simplification, simple cubic and tetragonal lattices are sufficient for solving single electron Schrödinger equation as given below [4]:

$$\left[-\frac{\hbar^2}{2} \nabla_r \frac{1}{m_e(r)} \nabla_r + V(r) \right] \varphi(r) = E\varphi(r) \quad (18)$$

The atomic structure of NCs enters the above analysis via effective mass m_e having different values in NC and barrier regions. The potential $V(r)$ represents an infinite sequence of NCs of size L_x , L_y , and L_z separated by corresponding barrier thickness H_x , H_y , and H_z . For a product form solution of $\varphi(r)$ in the above equation, $V(r)$ is expressed as a sum of three independent periodic potentials as function of coordinates x , y and z with periods of dx , dy , and dz :

$$V(r) = V_x(x) + V_y(y) + V_z(z) \quad (19)$$

Where $V_x(x) = V_y(y) = V_z(z) = 0$ in the QD region, and V_0 inside the barrier region. Applying this kind of decoupling, the total wave function is written down as follows:

$$\varphi(r) = \varphi_{n_x n_y n_z}(x, y, z) = \chi_{n_x}(x) \chi_{n_y}(y) \chi_{n_z}(z) \quad (20)$$

Corresponding quantized energy states are given as:

$$E_{n_x n_y n_z} = E_{n_x} + E_{n_y} + E_{n_z} \quad (21)$$

It is rather easy to solve these linear equations corresponding to three orientations. Such a formulation was applied to Si NCs embedded in Ge, SiO₂, Si₃N₄ and SiC matrices besides several other III-V nanocrystal superlattices. Without going into the further details that are available in the related references, it is more useful to note some general observations such as: low barrier height matrix produces higher band density and dispersions; size of NCs affects the band energy levels more than the corresponding bandwidth and mini-band energy and width are relatively independent of the electron effective mass in the dielectric barrier [4].

From the above description, it is clear that the discrete energy states are delocalized forming mini bands when the NCs are positioned very close to each other separated by a thin finite barrier. The inter-dot separation below which the sufficient overlap takes place is different for different materials like elemental and compound semiconductors. With increasing the inter-dot separation/barrier height, the wave function overlap diminishes causing the mini band to change to discrete levels. By changing the size of the NCs, inter-dot separation, barrier height and regimentation, it is easy to design the 3D mini bands in NC SLs and fine-tune electronic and optical properties of such solids to offer exciting possibilities for electronic, photovoltaic and thermoelectric devices. The schematic of mini-band formation is illustrated in Figure.3. This could possibly lead to a better route for realizing an intelligent material in future.

It is important to note that for successful realization of the extended states in mini bands it is necessary to have - perfect periodicity in the NC array, mono dispersion in NC size and shape, sufficiently small inter-dot spacing to produce strong coupling and with lower population of surface defects. Although, in actual practice, there is always some finite spread in NC size distributions and similarly unavoidable fluctuations in inter dot spacing during synthesis but, the extended states and mini band formations are still there as long as the wave function overlaps bandwidth exceeds the total broadening. Another source of disorder is caused by the fluctuations in local inter-dot coupling strengths, which is very common in colloidal solution synthesized NCs separated by disordered layers of insulating organic ligands [4].

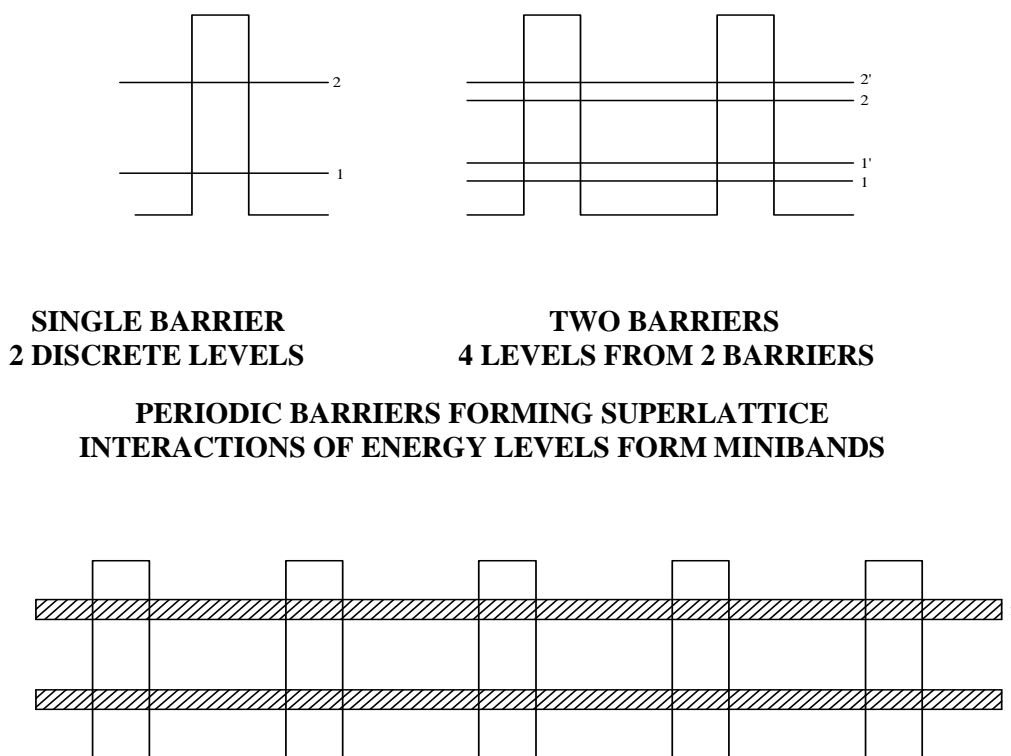


Figure 3 Schematic representation of mini-bands appearing in superlattice made out of two semiconducting materials with different band gaps. Mini-bands are formed due to interaction of the discrete energy levels participating from each unit in the superlattice similar to the broadening in a normal 3-d lattice.

Self-assembly of colloidal NCs offers very useful opportunity of designing and synthesizing novel materials possessing unique size and shape-specific physico-chemical properties different from their bulk counterparts. For example, quite similar to conventional crystals growth from constituent atoms/ions, NCs have been found to self-assemble into ordered structures known as SLs. Besides the characteristic properties of the individual NCs, these SLs possess unique set of electronic, magnetic, catalytic, and plasmonic features due to their inter-particle coupling with the neighboring NCs [4,51]. In recent past two decades, various types of NC SLs have not only been realized successfully via the controlled assembly of colloidal NPs [52-61], but also extensive computer simulation efforts were made for understanding the processes involved as well as to predict the resultant assembly patterns [62-64].

3.1.7 Properties of NC-SLs

Out of three distinct types of PbSe NC SLs namely - body-centered cubic (bcc), body-centered tetragonal (bct), and face-centered cubic (fcc) prepared, the bcc morphology was found most stable polymorph, with bct and fcc being 0.32 and 0.55 kJ/mol higher in enthalpy consistent with the decreased packing efficiency of PbSe NCs from bcc (17.2%) to bct (16.0%) and to fcc (15.2%). This study clarified several important issues related to NC SL growth from colloidal solutions [65].

Three different capping molecules like diphenylphosphine (DPP), trioctylphosphine (TOP), and oleic acid (OA), were used to control the size and shape of PbSe NCs that were prepared

involving injection of Se precursor into a hot Pb-complex solution. TEM analysis confirmed quasi-spherical morphology with an average diameter of 4.7 nm of as-prepared PbSe NCs. HRTEM images along with FFT analysis revealed the typical truncated octahedral morphology. For the assembly of PbSe NC SLs, the above-prepared PbSe NCs in either hexane or toluene were allowed to evaporate the solvent very slowly (e.g. 1.5 mL over 4 weeks). The super-crystals nucleated from hexane gave bcc SL, but those nucleated from toluene consisted of both bct and fcc SLs. The bct super-crystals were located in the corners, whereas the fcc crystals were located on the flat bottom of the vial, respectively [65].

3.2 *Closely Packed NCs Assemblies*

Distinctly discrete nature of the electron density of states in a close-packed NC solid was considered evoking considerable interests for their applications in resonant tunneling and Coulomb blockade devices [66]. Building NC arrays with well-defined conduction properties have drawn attentions while studying the carrier transport through coupled NCs and their potential applications in computational and memory devices.

Coulomb blockade-based devices have been experimentally verified at lower temperatures in 1 and 2-dimensional metal NC arrays, in which, the current threshold disappeared resulting in linear I-V characteristics at higher temperature. A portion of the I-V characteristics showing conduction gap with very small current was followed by an onset of charge carrier tunneling, and this threshold was proportional to the size of the NC array, as the applied voltage had to overcome disorder in the energy levels [67]. Subsequent attempts were also made to modify the electronic properties of metal NC arrays by manipulating the organic tunnel barrier parameters between the neighboring NCs. For instance, dodecanethiol-capped Au NCs arrays were prepared with conjugated aryl dithiol and aryl diisonitrile molecules as inter-particle covalent link to control the electronic coupling. Introducing conjugated linkers not only decreased the tunnel barrier height but also increased the inter-particle separations, from 1.3 for dodecanthiol to 1.7 nm for aryl dithiol [68].

Optically tunable properties of semiconductor NCs were explored for developing photoconductive devices [69-71] and light-emitting diodes [72-75]. Photoconductivity in semiconductors and organic solids has, since long, been used in probing carrier transport between weakly interacting molecules in otherwise insulating organic solids having large band gaps with very small population of thermally excited charge carriers under dark conditions. On the other hand, the situation in semiconductor NCs involving weak van der Waals interactions among the NCs, maintains an inter-particle separation >0.5 nm due to organic capping. Though, it is not easy to measure dark current in NC solids but a lower bound estimate of the resistivity was found close to 500 G Ohm-cm.

High-energy photons interacting with photo-conducting NCs generate electron-hole pairs that are delocalized over the entire NC volume and are subsequently dissociated by externally applied electric field producing free electrons and holes. Recombination of these electrons and holes prior to carrier separation primarily governs the efficiency of photo-carrier generation in NC solids, and charge carrier separation from the lowest excited state of the NC is another pathway besides radiative and nonradiative decay associated with the charge carrier dynamics. Externally applied bias, in such cases, helps in separating these charge carriers, but it also provides compensations for various energy needs of the system. Exciton binding energy is proportional to the inverse square of the NC diameter. Increasing the NC size not only reduces binding energy but also helps in reducing the spatial overlap of electron and hole wave functions to facilitate exciton dissociation. Further, charging energy required for two charged NCs, one with an electron and the other with a hole, from the photo excitation of a single charge neutral NC ought to be supplied by the electric field. The charging energy of the NCs is also inversely dependent on size. Finally, finite energy is required to overcome Coulomb attractions

Exp. Theo. NANOTECHNOLOGY 3 (2019) 301-362

between two neighboring, oppositely charged NCs, which is inversely proportional to the distance between charges depending on the size as it defines the electron-to-hole and site-to-site distance.

How efficiently the photo excited charges are separated also depends on the surface passivation of the NCs. Reducing the inter-particle separations by shortening the length of the alkyl chain on R_3P/R_3PO caps from octyl to butyl, increased the probability of carrier tunneling. The degree of electrostatic passivation of the NC surfaces also affected charge separations because surface traps acted as intermediate steps to facilitate charge separation and transport.

In order to explore the potential of inorganic-ligand-capped semiconductor NCs for light detection in the IR spectral region, PbS QDs were employed in a recent study for taking the advantage of its tunable band gap in the near-IR spectral region and high oxidative stability [76]. PbS NCs have been combined with $(NH_4)_3AsS_3$ (ammonium thioarsenite or ammonium sulfidoarsenite) as the inorganic capping ligand. Sulfido-arsenites have been previously identified as the chalcogenide-based ligand with the highest binding affinity to the PbS surface. Dip coating of colloidal dispersions of $(NH_4)_3AsS_3$ -capped PbS QDs produced a thin homogeneous film of electronically coupled PbS QDs in which further drying at 130 °C converted the $(NH_4)_3AsS_3$ capping ligands into a thin layer of As_2S_3 that acted as an infrared-transparent semiconducting glue. Highly photoconductive thin films of inorganic-capped PbS QDs deposited onto glass substrates showed very high values of light responsivity and detectivity of 200 A/W and 1.2×10^{13} Jones, respectively, in IR region up to 1400 nm [76].

The NC photocurrent decreases with increasing temperature. The efficiency of charge generation is inversely proportional to the radiative and nonradiative decay rates. Temperature-dependent quantum yields estimations from absorption and PL measurements of the NC solids show an exponential decrease with increasing temperature as the nonradiative rate of decay increases. The measured photocurrent increases linearly with excitation intensity. There is some commonality between the physics of charge carrier separation in close packed nano crystals solids and in NCs-doped conjugated polymers like CdS-doped poly (vinylcarbazole). Because many of the photoconductive and light-emitting devices have been prepared using close-packed nano crystals layers sandwiched between polymeric layers or as NCs-polymer composites and therefore the process of charge transport at the NCs-polymer interface is equally important.

Systematic efforts were made to understand the changes taking place in physico-chemical properties of close-packed and spatially organized QD ensembles self-organized in form of a macroscopic colloidal crystal in contrast to those of single and random NCs [52,77-79]. This kind of QD solid representing the condensed matter so realized having spatial ordering over a length scale comparable to the electron de Broglie wavelength was thus expected to possess energy bands along with the localized and delocalized electron states of an isolated QD [52]. The characteristic properties of this type of QD solid, representing a three-dimensional QD SL in real sense, were subsequently confirmed by observing a reversible modification of absorption spectrum as a function of concentration starting from a set of discrete sub-bands, characteristic feature of isolated NCs, to smoothly changing over to band-edge absorption similar to those of the bulk semiconductors [77]. This was followed by yet another study, where dense QD ensembles prepared in form of thin films comprising of small close packed CdSe NPs capped with organic group were used for studying the effect of externally applied electric field [79]. The extended states formed during the formation of QD solid were noted to be destroyed by the external electric field due to field-induced band bending known in case of planar semiconductor SLs. Consequently, above certain bias voltage, the electric field dependent band bending was found to destroy the mini-sub-band structure causing localization of electronic states. For example, in thin layers of close-packed NCs, the delocalized electron states spanning over several NCs were found to return to discrete electron states with increasing bias. Close-packed structures of NCs thus confirmed the reversible nature of positive field-

induced absorption changes, which indicated vanishing of the extended and restoration of individual confined electron states [78].

Photoluminescence (PL) and optical absorption spectroscopic measurements on NC-colloids and NC-solids comprising of TOPO and TBPO passivated CdSe QDs clarified a number of issues like inter-dot coupling, variation of band gap and binding energies with pressure, and the probability of inter-dot tunneling by changing the organic ligands or applying hydrostatic pressure [80]. The following conclusions were made on the basis of these measurements. For example, up to 60 K bar pressure there was no evidence of inter-dot coupling in both the cases. However, in each case, the overall pressure dependence could be explained by considering the cumulative influence of the pressure dependence of band gap of bulk CdSe as well as the confinement energies of electrons and holes resulting from the smaller dot dimensions. Moreover, the difference between PL energy peak and the first exciton in the absorption for NC colloids and solids increased with pressure. In contrast, a distinct difference was noted between the pressure dependence of isolated NC and NC-solid of CdSe/pyridine NCs observed in their absorption spectrum [80].

In a recent study, the optical spectra of close packed 1.6 nm CdSe NC solid with pyridine cap resembled that of the bulk CdSe but with nano crystals size reduction the electronic wave functions spilled outside the NC volume making the electronic excitations delocalized due to strong inter-particle interactions. Close-packed metal NC solids also give rise to tunable optical and electronic properties. Quite similar to that observed in the semiconductor NCs, the organic ligands attached to the metal NCs in the solids provide electronic coupling between NCs and therefore the properties of the resultant solids. For example, once the metal NCs are placed in close proximity in a solid, the surface Plasmon resonance shifts to lower energy with the increase in average dielectric constant of the surrounding medium.

In semiconductor NC solids, the inter-particle distances ≤ 0.5 nm cause strong exchange interactions as observed in pyridine-capped CdSe nano crystals. Larger size CdSe nano crystals ≥ 2.5 nm still maintain an inter-particle separation of ~ 0.7 nm and the optical absorption spectra remain unchanged. Since pyridine is a volatile solvent, applying vacuum and gently heating the NC solid removes the cap, collapsing the inter-particle separation and further heating sinters them into solid having the inter-particle separations to reduce from 0.7 to 0 nm, the optical absorption spectrum approaching that of the bulk CdSe confirming the speculations.

For inter-particle distances >0.5 nm, maintained by most organic capping groups, electronic excitations and carriers are localized in individual NCs and the solids are insulator with a Coulomb band gap. But with decreasing inter-particle separations ≤ 0.5 nm, strong exchange interactions cause significant delocalization that finally leads to insulator-metal-transition as it was experimentally verified by preparing and compressing alkanethiol-capped Ag NCs monolayers on a Langmuir trough. In this experiment, as the distance between NC centers became comparable to the NC diameter the coupling increased and the energy bands of the NC solids increased in width, decreasing the Coulomb band gap. For a ratio of inter-particle separation to diameter of ~ 1.2 , exchange interactions gave rise to the insulator-to-metal transition causing disappearance of the Coulomb band gap. The onset of electronic delocalization is observed by dramatic changes in the optical and electronic properties of the metal NCs monolayers. The phenomenon of insulator-to-metal transition was first observed in the linear and nonlinear optical absorption and reflection of these monolayers involving Ag NCs. Just before the monolayer collapsed to a bilayer structure, the distance between surfaces of NCs capped with sufficiently short chain length ligands reached ~ 0.5 nm the typical distance for the onset of exchange interactions. At these short inter-particle separations, electronic wave functions were delocalized over many nano crystals causing the monolayers to behave like a metal showing reduced reflectivity and enhanced absorption to levels characteristic of thin continuous metal films. The surface Plasmon resonance line width decreased as the delocalization of electronic wave functions enhanced the scattering length and time of

Exp. Theo. NANOTECHNOLOGY 3 (2019) 301-362

electronic carriers. The observed changes in the optical spectra from the insulator-to-metal transition were reversible. Opening the barriers used to compress the monolayer of Ag NCs increases the inter-particle separation, and the optical properties of the monolayer is again characteristic of an insulator. These changes occurring in optical properties of metal NC monolayers are consistent with more recent measurements using impedance spectroscopy and STM techniques.

In close-packed SLs, surfactant molecules covering NCs play a dominant role in overall charge carrier transport. To travel between the NCs, the charge carriers should pass through the inter-particle medium comprising of the surfactant molecules with long hydrocarbon chains behaving like tunneling barriers. In case the inter-particle coupling is weak, the electronic structure of individual metallic or semiconductor NCs can be described by discrete quantum confined wave functions localized on individual NCs. When these metallic or semiconducting NCs reside in close proximity to each other, individual wave functions start overlapping and forming “molecular orbitals” delocalized over several nano crystals or even propagating throughout the entire NC arrays.

It is known from the theoretical relation expressing the tunneling rate as a function of inter-dot spacing δ and barrier height ΔE , drops exponentially with increasing separation between the NCs. Reducing δ and ΔE by proper design of the inter-particle medium or introducing conjugated molecular linkers are generally used to enhance the inter-particle coupling strength. This kind of situation is further met during conductivity (σ) measurement of HS (CH)_{2n}SH capped Au NCs, where the conductivity varies as a function of n as $\sigma \approx \exp(-\kappa n)$, where κ is the decay constant. This observation further confirms the strong dependence of the transport properties on the inter-particle separation.

The possibility of transferring an electron from/to a NC surrounded by a dielectric medium could also be examined in terms of the charging energy of the NCs. This Coulombic charging energy E_c is the energy needed to put an additional electron on the NC because of electrostatic repulsion from already existing electrons. For individual NCs, ΔE_c can be determined by scanning tunneling spectroscopy measurements, wherefrom, it has been estimated to be $\Delta E_c \sim 0.34$ eV in case of 3nm diameter Ag nano crystals. The ΔE_c acts like a barrier against the migration of electrons from one NC to another. The actual amount of energy required to move one single electron from one isolated metal NC to another is $2\Delta E_c$ according the following process:



In an array of weakly coupled NCs and at lower bias, there is a barrier in form of charging energy $E \approx 2\Delta E_c$ that suppresses the current conduction, which is termed as Coulomb blockade. At large applied bias, the Coulomb blockade is overcome and current starts flowing through the NCs solid. The Coulomb blockade generated threshold voltage V_T depends upon the parameters including charging energy, number of NCs spanning the gap between the electrodes, operating temperature and NC packing symmetry.

It has been noted that the delocalization of electron energy states occurred only if $\beta \gg k_B T$ falling in strong coupling regime. In an array of strongly coupled metallic NCs, the discrete energy states grouped together to form a band with width proportional to the exchange coupling energy β . With the decreasing inter-particle spacing, the bandwidth is found to increase. Finally, when $\beta \ll \Delta E_c$, the Coulomb gap disappears and the carriers' move freely throughout the NC solid and this kind of sudden change in carrier conduction is termed as Mott metal-insulator transition. Above this transition point, the coherent molecular-type orbitals extend over many NCs in an analogy to ordinary crystal. The phenomenon of electronic delocalization results in sudden changes in the optical and electronic properties of the metal NC solids and this transition is verified experimentally in case of monolayers of alkylthiol-capped Ag NCs using a Langmuir trough to tune the inter-particle coupling by adjusting inter-particle separations. In a two-dimensional array of 3nm Ag NCs capped with propanethiol, the

reduction in the inter-particle spacing below $\sim 0.5\text{nm}$ produces a sharp discontinuity in the optical second-harmonic generation response, as well as the changes in the reflectance of nano crystals film, confirming the occurrence of insulator-to-metal transition. After this phase transition, the absorbance and reflectance of NC film resembled those of a thin continuous metal film supporting delocalization of carriers over many nano crystals.

3.3 *Strained Lattice NC- Solids*

The well-known lattice constant is the basic parameter besides the crystal symmetry that determines the energy band structure of a crystalline material as discussed earlier. Once the lattice parameter becomes adjustable, theoretically it offers ample opportunities to manipulate the resulting electron states. These conditions have been explored in case of bulk crystalline materials by applying pressure to affect strained lattice, where the magnitude of the change is not much. However, in case of nano size entities like NCs/QDs the volume being too small the applied stress is able to affect the lattice constants almost through and through. Unlike bulk crystalline sample there is hardly any chance to relax the strain by creating lattice defects in case of NCs/QDs. Of course, it is another problem that it may not be very convenient to apply stress as it is in case of large size bulk crystalline materials. But, via the route of heteroepitaxy, it is possible to generate strained lattice and change the related band structure of the electron states for many types of useful device applications. How are these possibilities implemented in case of NCs is briefly highlighted below to get a feel for the practically achievable conditions? Core-shell type of configuration of QDs is very appropriate structure for exploring the influence of strained lattice to tune optical and other properties associated with QD and the derived solids [81]. The basic purpose of putting a shell around the QD core is primarily needed to improve the charge carrier confinement inside the QD by choosing a shell material with larger band gap. In case, few monolayers thick shell is epitaxially grown on the QD and the core is such that it is strained easily as compared to the shell material, there is a chance that both shell as well as the core is strained simultaneously. During epitaxial growth of such a shell, the lattice constant mismatch with core material introduces strain in the growing epitaxial layers of the shell specially in case the shell thickness is not large enough to relax the strain completely. On the other side, the strain passing to the softer core can also cause radial strain quite deep inside the core. In contrast, the epitaxial growth on a solid substrate introduces strain only in the growing epitaxial layer providing only one degree of freedom to accommodate the mismatch. This “double strain” of the colloids changes the properties of both the epitaxial layer and the substrate [81]. It was subsequently demonstrated that a very high level of strain is possible to tolerate in small NCs, compared to what is achievable in bulk materials. Small NCs ($<5\text{ nm}$) have a high surface to volume ratio and highly curved surfaces, allowing the stress from a lattice-mismatched epitaxial shell to be distributed over a large fraction of the constituent atoms. In larger NCs and bulk substrates, the total number of atoms is larger and the epitaxial stress is imposed on a surface that contains a smaller fraction of the constituent atoms, favoring the formation of strain-relaxing crystalline defects rather than homogenous strain. Based on these possibilities the epitaxial growth of a compressive shell material such as ZnS, ZnSe, ZnTe, CdS, or CdSe on a small and soft nano crystalline core like CdTe was found to produce a large change in the conduction energy band of the resulting heterostructures. It was, thus, proven that lattice strain could control the locations of charge carriers, modulate the excited state lifetimes, and tune the absorption and emission spectra across a wide wavelength range [81].

It was further noted that lattice strain could also be used to induce significant band gap energy changes, when a shell material was coherently grown on a small and compressible nano crystalline core. In CdTe-ZnSe heterostructures, valence and conduction bands are aligned to localize both the electrons and holes in CdTe corresponding to type-I of SL behavior [1] in

Exp. Theo. NANOTECHNOLOGY 3 (2019) 301-362

bulk. On the nanometer scale, however, epitaxial growth of a ZnSe shell strongly compresses a CdTe nanocrystal because the lattice parameter of ZnSe (0.5668 nm) is considerably smaller than that of CdTe (0.6482 nm). For nearly all zinc blende II-VI and III-V semiconductors, the electronic energy gap increases with applied compressive force, and decreases under tensile strain, an effect that has been experimentally observed and theoretically predicted.

Applying these conditions to the epitaxial growth of ZnSe on CdTe one can estimate the changes taking place in the band structure at the interface. The compressive strain in CdTe and tensile in ZnSe increases the conduction band in CdTe and decreases in ZnSe and thus the situation corresponding to Type-I SL, as anticipated earlier, is transformed into a Type-II SL, where charge carriers are separated without any interaction [81].

With increasing epitaxial shell growth of ZnSe on CdTe, the optical absorption and fluorescence emission spectra are shifted toward longer wavelengths. In the case of (CdTe) ZnSe, however, additional shell growth continues to shift the absorption band-edge and the emission maximum, beyond the band-edge energy of bulk CdTe and ZnSe. These changes are caused by spatial separation of holes into the core and electrons into the shell, resulting in a decrease in the electron hole overlap integral. The largest spectral shifts are observed with very small cores, such as 1.8 nm CdTe, allowing tuning from the green to the near-infrared spectra. In contrast, the larger CdTe cores are not sufficiently compressed through epitaxy, and their emission spectra are not much affected by lattice strain. It is remarkable that QDs with small cores can be tuned to emit beyond the spectral ranges of larger dots, at both ends of the emission spectra. This novel phenomenon has not been observed for other types of QDs. Depending on the core size and shell thickness, these QDs can be tuned to emit between 500 nm and 1050 nm with quantum efficiency between 25-60%. The fluorescence peak width is consistently between 40 and 90 nm FWHM in the near infrared region (i.e. 700-900 nm wavelength) [81]. It is further observed that the strain-induced spectral changes are gradual and do not exhibit abrupt transformations as might be expected for a transformation from type-I to type-II. For the core sizes less than 4nm diameter, it was shown that the transition to type-II was “complete” after capping with 2–3 monolayers of shell material. Between 0 and 2–3 ML, however, the behavior of these QDs was between type-I and type-II, a regime that has been dubbed as ‘quasi-type-II’. Here, one of the charge carriers was strongly confined to one region of the NC i.e. the hole was confined to the core, whereas the electron was only weakly confined, being largely delocalized across the entire NC [81].

4. ENERGY BAND STRUCTURE OF POLYMERS

Knowing well that the AO overlaps facilitate bond formations where the electrons are confined in the bond regions and for this using the concept of hybridized AOs has been more appropriate as highlighted earlier [82] The advantage of using hybridized AOs has been illustrated in another case of C-atom possessing the electronic configuration of $1s^2 2s^2 2p^2$. According to the available electron states in the outermost shell, C- atoms should either form compounds like: CR_2 with R-C-R angle of 90° , or else $1s^2 2s^1 2p^3$ compounds (CR_4) with three p -bonds at 90° to one another and a s -bond in an unspecified direction. Since CH_4 , CCl_4 , and numerous polymeric molecules are known to have tetrahedral configuration, the simple overlap of orbitals is not able to explain the situation observed experimentally [82]. Rather, C-atoms in polymeric molecules are known to form four nearest-neighbor σ –bonds in sp^3 -hybridized form where the large electron energy band gap arising out of σ -bonded C-atoms renders them electrically insulating, and generally opaque to the visible light. For instance, in polyethylene comprising of monomeric repeat of (CH_2-CH_2) - unit, the optical band gap is on the order of 8 eV [83]. In addition, there exists a continuous chain of unsaturated C-atoms bonded in the sp^2 -hybridized form in conjugated polymers, wherein each C-atom has three σ -bonds, and one p_z -orbital forming π -overlap with the p_z -orbitals of the nearest neighbor C-atom. Such overlaps

form π -states delocalized along the polymer chain forming electronic bands with a band gap, $E_G(\pi) < E_G(\sigma)$ as confirmed by lower energy optical absorptions. Presence of these delocalized π -electrons makes these conjugated polymers different from a polymer with σ -bands in the following ways. For instance, these conjugated polymers possess a relatively smaller band gap $\sim 1.4\text{eV}$ causing low-energy excitations; get easily doped by oxidation or reduction usually through charge transfer complexes with molecular dopant species, wherein higher charge carrier mobilities give rise to higher conductivities despite the presence of charge bearing quasi particle species moving freely along un-interrupted polymer chains [83].

Although, single-electron Hückel formulation is sufficient for determining the electronic structures of conjugated polymers but it needs to include 'many-body-effect' in case of luminescence, electron-hole separation, or nonlinear optical response involving excited electronic states as well as inter-chain interactions [84]. Further, while analyzing various kinds of π -conjugated systems, the presence of electron-electron interactions as well as the profound influence of the electronic and polymer chain structures make the situations still more complex to analyze them theoretically.

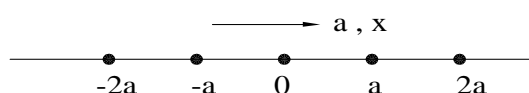
For visualizing the energy-band-structures of conjugated polymers, it is helpful to examine the simplified Hückel model of a hypothetical linear chain of one atomic orbital in each unit cell of length a , the energy is expressed as a function of wave vector k in the following form [84,85]:

$$\epsilon(k) = \alpha + 2\beta\cos(ka) \quad (23)$$

Where, α and β are the 'Coulomb' and the 'nearest neighbor resonance integrals' of the orbitals, respectively and k is the wave vector in the range of $-\frac{\pi}{a} \leq k \leq \frac{\pi}{a}$.

According to the above equation in a hydrogen chain with s -orbitals at each node, it is expected that $(0) > \epsilon(\frac{\pi}{a})$, because a positive overlap between s -orbitals results in a negative β [85].

However, the opposite holds for a linear chain of p_x -orbitals propagating along the x -axis, where a negative overlap gives positive β . Thus, the energy increases with increasing k due to interactions among the s -orbitals, while with p_x -interactions, it decreases from Γ to X in (100) direction in the Brillouin zone of reciprocal space.



MODEL POLYMER OF H-ATOMS



S-ORBITAL INTERACTION



P-ORBITAL INTERACTION

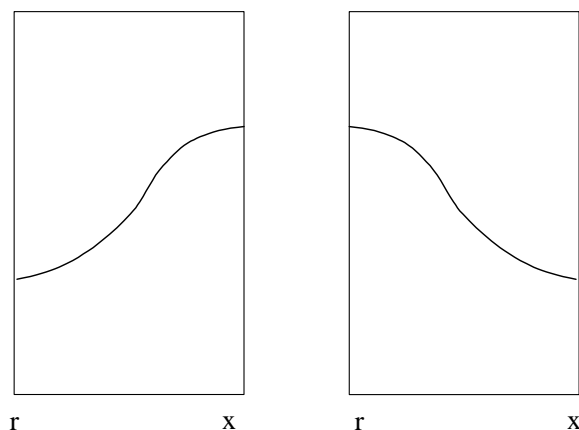


Figure. 4(a) Possible types of energy-momentum variations expected due to interactions from S and P-Orbitals (A, and B) from the nearest neighbors shown above.

This simple exercise clearly explains the energy dependence on k decided by the nature of orbital interactions involved therein as explained in Figure. 4 (a) and (b) in a schematic way using a chain of H-atoms as model [85].

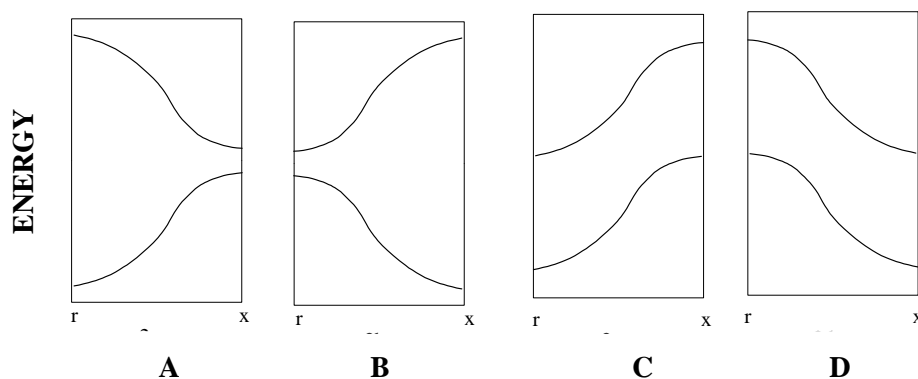


Figure. 4(b) Schematic representation of various possibilities of energy-momentum relationships under different kinds of interactions of atomic orbitals from the nearest neighbor (A, B, C, and D).

Instead of only one type of atomic orbital at each site, as mentioned above, if two different atomic orbitals are involved there on each node, it is natural to expect two non-overlapping bands to exist. For example, in case of s and p_x orbitals at each node, without any $s - p_x$ mixing, the band structure would have both the branches in two possible ways – in one case an increasing branch is situated below the decreasing one or vice versa. In case of two other possibilities, where both the bands are increasing or decreasing simultaneously, it implies that the bands originate from the orbitals having the same orbital property. This simple analysis of a hypothetical linear chain clearly shows the existence of a direct band gap where valence and conduction bands are made up of orbitals with different symmetries but in case the basis orbitals have the same topological properties, it gives rise to an indirect band gap. Applying similar consideration to one-dimensional organic semiconductors, it is possible to predict the energy band gap types for a given phase relationship of the HOMO and the LUMO of the constituent monomeric repeating units [84].

The presence of a finite energy-gap in a conjugated polymeric system is invariably due the existence of the alternate single and double bonds. Bond length variations caused by changing overlaps of the atomic orbitals involved in binding of a polymer chain determines the energy band structure and the magnitude of the energy gap. In case of long chain polymeric molecules, the translational symmetry along with cyclic boundary condition helps in arriving at an energy band structure quite similar to that of the condensed matter lattice [84].

For using conjugated polymers in realizing electron devices, it is also necessary to change the availability of charge carrier concentration by donor/acceptor impurity doping quite similar to that of the inorganic semiconductor. Since the phenomenon of doping in organic semiconductor is quite different from that in the inorganic semiconductors, it is better to examine first the response of the polymeric molecule to the addition of an electron or a hole. Because of strong coupling between an electron and the polymeric chain, it causes significant perturbation leading to formation of a mobile species that may be charged or neutral having high field mobility around $0.1 \text{ cm}^2/\text{Vs}$ [86]. In an organic molecule, in general, the strong coupling between the electronic structure, molecular geometry, and the chemical structure – all put together determine the bond formation and therefore, for including the influence of such quasi particles in the overall charge carrier transport in organic molecules, the concept of ‘polaron’ was introduced in 1980s for understanding the electronic and optical properties [87-90].

Further, it is also expected that adding an excess electron into a conjugated polymer chain would add a new band-gap state forming singly charged polaron. In polymers having non-degenerate ground states, the polarons would pair up to form spin-less, doubly charged bipolarons [83,88,89].

In a conventional semiconductor with rigid lattice, it is well-known that the transport properties of electrons and holes are governed by their interactions with lattice phonons as the major cause of momentum and energy relaxations resulting in temperature dependent mobility of the charge carriers [1,90]. However, the situations differ in case of ionic or highly polar crystalline materials like II-VI semiconductors, alkali halides, and oxides, where the charge carriers cause significant distortions in the surrounding regions due to attraction/repulsion of the surrounding ions. Representing this phonon cloud combined with electron as a source of scattering with smaller and larger displacements, charge carrier transport properties are determined accordingly [91].

5. ENGINEERED SYNTHETIC MATERIALS

One of the most significant contributions of material science development in 20th Century has been the successful growth of almost zero-defect crystal lattice in bulk and thin films by controlling the processes of nucleation and crystal growth followed by thermal treatment under different ambient conditions. Having mastered this technology on a commercial scale, numerous methods were also explored additionally to change the lattice parameters, compositions, and charge carrier confinements across band offsets to realize control on band gap of the special structures so developed. Before taking up the broader issues of band structure engineering (BSE) of NCs, it would be quite useful to have quick look into the level of success achieved in these strategies as described in the followings. The level of confidence gained in these areas has been the main drive to look for better results with the development of NCs based material syntheses.

5.1 Crystalline Inorganic Materials

Considerable efforts have been made in the recent past to develop BSE concepts of materials with special emphasis on modifying their electronic, optical, and opto-electronic properties for various applications after having access to an advanced technology of depositing single crystal

Exp. Theo. NANOTECHNOLOGY 3 (2019) 301-362

inorganic semiconducting thin films with monolayer precision during the later half of the 20th Century [1]. For implementing this strategy, several approaches have already been evolved during last several decades.

In one of the earliest approaches, alloying of the two miscible semiconducting materials having almost identical lattice constants but one with smaller band gap and the other with a larger one, exhibited a band gap between the two limits depending upon their stoichiometric ratios. This scheme of adjusting the energy band gap by alloying two miscible crystalline materials was extended further to grow ternary, and quaternary compound semiconductors for their numerous optoelectronic applications on a larger scale [92].

In another approach, the discrete energy levels, either situated below the gate oxide in a metal-oxide-semiconductor field effect transistor (MOSFET) operating under heavy inversion or present in a quantum-well formed at a hetero junction, were used to realize a two-dimensional electron gas (2DEG) channel. For instance, in MOSFETs, the electrons lying just below the gate oxide and confined to the lowest energy state, are only able to move parallel to the interface without much of scatterings. Similarly, in a hetero junction, it is equally possible to confine electrons/holes in triangular quantum wells formed due to conduction/valence band-offsets. Thus, a 2DEG/2DHG sheet, realized across hetero-interfaces, exhibited very high mobility due to almost complete absence of impurity scattering in these extremely thin layers. High electron mobility transistors (HEMTs) using such channels exhibited significant amplifications at millimeter wave frequencies required in strategic and industrial applications [93].

In another case of a double hetero structure laser (DHL), a thin layer of smaller direct band gap semiconductor sandwiched between two larger band gap layers in place of original configuration of p-i-n type of a conventional laser diode configuration, exhibited improved performance due to the presence of two heterojunctions, situated on the two sides of the active layer and acting as efficient barriers causing more efficient recombination of electrons and hole injected from the either sides. For instance, a combination of gallium arsenide (GaAs) and aluminum gallium arsenide ($\text{Al}_x\text{Ga}_{1-x}\text{As}$) with adjustable band gap by changing x was found appropriate for realizing such DH lasers performing more efficiently than the simple structure used earlier. Further reduction in the active layer thickness gave rise to discrete energy states due to quantum confinement of electrons. The modified density of states and thickness dependent inter-level separation associated with these discrete energy levels exhibited better performance for laser action. For example, only changing the active layer thickness, it could be made possible to tune the laser wavelength. Using such a simple energy-band-structured active layer offered significantly substantial improvement in the efficiency with reduced threshold current for laser action. Further improvements in the laser efficiency as well as threshold current density reduction were demonstrated by replacing the quantum well layer by quantum wires or an assembly of QDs.

The simplest hetero structure comprising of such a quantum well was prepared by depositing a thin layer of gallium arsenide (GaAs) sandwiched between two thick layers of gallium aluminum arsenide (GaAlAs) employing epitaxial deposition [94]. Instead of using inter-level transitions across these allowed discrete electron energy states, as described earlier, it is also feasible to delocalize these states by providing sufficient overlap between two nearest neighbor QWs inter-connected by a very thin barrier layer resulting in the formation of superlattice (SL) mini bands. Properties of the electrons and holes belonging to these SL-mini bands were possible to control by adjusting various parameters of the SL, so formed, involving a large number of identical QWs in a periodic structure. These kinds of superlattice structures have been prepared successfully using high precision CVD, molecular beam and atomic layer epitaxy for compound semiconductors [94].

The examples, given above, show that using high quality epitaxial growth of thin semiconducting layers it has been possible to realize confined charge carriers possessing

discrete as well as delocalized behaviors and put them to use in fabricating high performance electronic and optoelectronic devices. This could be done so because of the availability of very high precision epitaxial layer deposition technology evolved in connection with microelectronics development during last six decades.

5.2 *Conjugated Polymers*

The BSE approach developed in connection with crystalline semiconductors of inorganic origin was found equally applicable in implementing in polymeric materials having repeated units of monomers along with functional moieties and nanostructured species ensuring still more profound flexibilities and relatively simpler solution-based processing capabilities [95,96].

In the area of polymer science, the discovery of a conjugated polymer (CP) named poly (acetylene) (PA) triggered the growth of conducting polymers [97] subsequently followed by the development of poly (aniline) (PANI), poly (pyrrole) (PPy), poly (thiophene) (PTh) and more recently poly (3,4-ethylenedioxy thiophene) (PEDOT) for exploring their applications in different fields [98-103]. Originally this effort was meant for replacing copper and aluminum-based contacts and interconnects by lightweight conjugated polymers for their applications in air and space borne electronics as endorsed by the fact that heavily doped PA was more conducting than copper on conductivity per unit weight basis, but it could not be used further due to associated environmental instability. The continued search for still better alternatives led to the development of indeed newer families of polymers like PANI, PPy, PTh, and PEDOT with improved stability but, then, having much less conductivity. Thus, the failure of improving the stability along with associated higher conductivity on one hand and the successful realization of a number of promising devices including organic thin film transistors (OTFTs), flexible light emitting displays (OLEDs), chemical sensors, and nerve cell guidance channels and biological substrates, on the other hand, finally led to complete reorientation of the research and development activities from that of searching for a light-weight metal contact/interconnect replacement to more useful applications found feasible [99,101, 103-107]. The first-generation CPs including PA, PANI, PPy, and PTh were, as such, not found very useful materials for most of the industrial applications. However, PEDOT from the 2nd generation turned to be superior to PTh in terms of reduced band gap and enhanced environmental stability as a doped conductor. Having exhausted the explorations of hetero cycles for preparing 3rd generation CPs having lower band gap, aqueous compatibility, amenable to n-type doping and adequate stability, it emerged that next generation CPs would possibly come from monomers comprising of smaller functional units to incorporate electronic properties needed while maintaining polymerization as well as stability [108].

Designing materials with optimized combination of properties requires a fundamental understanding of how a particular structural modification is related to the ultimate material properties. Recent studies have clarified that most important material parameters that control the properties of CPs are the band gap and position of the edges of the conduction band and valence bands [108].

The possibility of tailoring the electronic properties of conjugated electroactive polymers (CEPs) possessing electro chemical doping/un-doping during synthesis initiated a very rapid growth in this area by modifying the characteristic properties due to changing locations of the valence and conduction bands leading to band gap modifications or modified oxidation/reduction. It was easy to verify that band gap changes were reflected in the variations of the emission wavelengths, absorptive colors in electro-chromic devices and conductivity in the neutral state. In addition, changes in the respective energy levels allowed optimization of interfacial energy level alignments between the polymer and contact electrodes in organic light emitting devices (OLEDs) [109]. Low band gap CEPs, thus, started emerging as important

Exp. Theo. NANOTECHNOLOGY 3 (2019) 301-362

materials because of their high intrinsic conductivity in the neutral state, transparency in the p-doped conducting state, and their tendency to achieve reduced band gaps through conduction band energy lowering making stable n-type doping possible [108]. There are several factors that affect the band gap in CPs as discussed in an earlier review [110], which included: reduction in bond length alternation, introducing planarity in the repeat units, inter-chain effects, resonance contributions and donor-acceptor effects [98,110-113]. Out of these several possibilities, ensuring planarity of the repeat unit was found difficult to achieve without compromising solubility [114] and inter-chain effects have sparsely been described [115,116], maximum efforts were made in enhancing the stability of the quinoid character in the neutral polymer and employing donor-acceptor effects.

In absence of any accurate design methodology to relate the structure-properties relationships for different families of materials that derive their properties from extended range inter and intra-molecular interactions; systematic studies were conducted to clarify the influence of substitutions on the band gap in a perfectly alternating donor-acceptor (D-A) copolymers [108]. In this program, poly (isothianaphene) was considered as low band gap CP having a thiophene ring fused to a benzene ring across the 3rd and 4th positions of the thiophene ring allowing the polymerization to take place through the 2nd and 5th positions of the thiophene ring, and this kind of modification enforced a competition between thiophene and benzene rings for aromaticity as it is not possible for both to be aromatic simultaneously. Detailed analysis of this process, however, revealed that benzene remained aromatic while thiophene adopted a pseudo-di-radical electronic state at the 2nd and 5th positions. Thus, during polarization, the bonds connecting the thiophenes existed in the quinoid state lowering the band gap by decreasing bond length alternation. While this was found as an effective method of lowering polymer band gap, it proved to be of only limited scope because of complex synthesis involved [108].

Later studies have confirmed that tailoring the band gap by either planarization of the repeat units by fusing hetero-cycles together, or by creating polymers with alternating donor and acceptor moieties or some combination of these two approaches was found as a better option [108]. The donor-acceptor route has, by far, been proven versatile in terms of diversity in synthesis, while avoiding solubility problems. The logic behind the donor-acceptor (D-A) route has been the possibility of achieving higher HOMO of the donor and the lower LUMO into the resulting monomer as well as polymer electronic structure [117]. In D-A approach, alternate donor and acceptor moieties result in a polymer having combined optical properties of the parent donor or acceptor monomers [108].

In another alternate approach, band gap was adjusted while synthesizing benzo [1, 2-*b*: 4, 5-*b'*] dithiophene (BDT) with different conjugated units in modifying the structure of conjugated polymers by co-polymerizing with different units [118]. The band gaps of the synthesized polymers were thus found to vary in the range of 1.0 - 2.0 eV, by effectively adjusting their HOMO and LUMO levels. It was also noted that in some cases, for example, the TPZ unit reduced the band gap by lowering the LUMO energy level and elevating the HOMO level of the polymer, but in contrast, the BT unit lowered the band gap only by depressing the LUMO level. Similarly, the influence of HOMO level on the V_{OC} in OPVSC was also examined as noted in case of a combination of BDT and TPZ being 0.5 V lower than that in case of BDT and BT. The systematic study of seven commonly used units on band gap, molecular energy level, and photovoltaic properties of the BDT based polymers gave very useful information not only for the design of the PV materials but also for the materials of various other electronic devices. In addition, the performance of PCBM and H6, based polymers exhibiting an efficiency of 1.6% indicated that BDT is a promising common unit for photovoltaic conjugated polymers [118].

A theoretical study of predicting the structure, electronic, optical and photovoltaic properties of a series of newly designed organic materials containing fluorene, thiophene, phenylene and acceptor moieties was carried out by applying density functional theory (DFT) for investigating

the photo-physical properties of alternate donor–acceptor type molecules. The insertions of fluorene, thiophene and phenylene rings-based donor units with acceptor units such as benzothiadiazol (BT), benzopyrazine (BP), pyridopyrazine (PP), benzooxadiazol (BO), thiadiazolo pyridine (TP), and oxadiazolopyridine (OP) in the co-oligomer backbone, were found to give better match to the solar spectrum resulting in more efficient light harvesting. Moreover, the acceptor linkages not only provided conjugated bridges but also reduced the steric interaction between aromatic rings and thus enhancing the effective intramolecular charge transfer between donor and acceptor parts. The low band-gap of around 1.85 eV and the calculated estimates of V_{OC} of 1.18 V were anticipated to result in efficient electron injection. The computed theoretical results suggested that both the acceptor moieties and the stable geometry contributed significantly to the electronic properties of alternating donor–acceptor conjugated co-oligomers [119].

5.3 *Nano crystalline Materials*

The conditions prevailing in nanostructured materials are more appropriate for synthesizing numerous families of future materials. For example, charge carrier confinements in a large variety of nanostructured material species as well as fullerenes, nanotubes and graphene molecules offer much wider possibilities of realizing engineered material properties as discussed in various publications [120,121]. The attempts made in this context using theoretical and experimental investigations in recent past are examined here to explore the possibility of not only using them in active devices but also in developing smart and intelligent materials for their future applications.

It is noted while determining the electronic states in various types of nanocrystalline materials, as discussed earlier, the phenomenon of quantum confinement of electrons is very much morphology dependent. Once size enters into the phenomenon of quantization, the allowed energy states and the resulting inter-level separations become morphology specific and thus opening several possibilities of controlling their electronic and optoelectronic properties by changing their sizes and shapes accordingly. But this kind of morphological sensitivity makes it practically more difficult to sort them out during their syntheses based on highly random interactions involved therein. Only possibility, which appears to help in this context, is to use some kind of self-assembly and molecular recognition based chemical conjugations for forcing these reacting species to engage, in case feasible, a precisely known morphology. Incidentally, in solution-based syntheses, it is possible to incorporate these features accordingly with advantage.

5.3.1 *Metal and Semiconductor NCs*

Detailed experimental and theoretical investigations carried out on a large number of metal/semiconductor NCs for their numerous applications primarily conceived on the basis of quantum confinement of electrons either available in delocalized states as well as the hybridization of atomic orbitals participating in chemical bond formations in NCs, which may differ considerably from the bulk. In addition, the presence of chemical moieties and functional groups on the NC surfaces are better handled experimentally in stabilizing the NCs than taking them into account properly because of complexities involved in handling many body problems. Despite problems faced in computing the energy band structure of different species of NCs with different types of surface functionalization schemes developed and used successfully, the entire areas of applications have been benefitted significantly in recent past. In future, with the

Exp. Theo. NANOTECHNOLOGY 3 (2019) 301-362

development of better theoretical models it is expected that the problems will be taken care of better.

In order, to assess the overall situation regarding the utility of their programmable features with respect to their particularly emerging applications, various developments that have taken place in connection with precise determination of microstructures, surface functionalization and stability considerations and theoretical models developed to support their observed behavior as well as predict the other unexplored features are discussed in brief in the following.

5.3.2 Metal NPs – Structures

The structural analyses of different configurations of bare/ ligand stabilized metallic NPs were carried out exhaustively using various measurement techniques like TEM, XRD, EXAFS, and Mössbauer spectroscopy to identifying the role of the core involved in further build up of the rest of the structure. For example, the analysis of stable Au₅₅ confirmed a bulk-like hexagonal close-packed (hcp) structure built around the smallest ligand-stabilized first full-shell cluster of Au₁₃ leading to further growth of the icosahedra [122-129]. Similarly, XRD analysis of Au₅₅(PPh₃)₁₂Cl₆ revealed that the final structure was arrived at after starting from a distorted hexagonal close-packed core of Au₃₉, protected by 14 PPh₃ and 6 Cl ligands. These findings were valid only for ligand-stabilized particles, which could not be extended to the bare clusters [129,130]. In another study of p-mercapto-benzoic acid (p-MBA)-protected gold NPs, comprising of 102 Au atoms and 44 p-MBAs, the starting core was a decahedron, surrounded by additional layers of Au atoms, where p-MBAs interacted not only with Au atoms but also with one another resulting a rigid surface layer having chirality, with a closing of a 58-electron shell [131]. A similar study of the internal structure of thiolate stabilized Au-NPs with the composition of [N(C₈H₁₇)₄⁺][Au₂₅(SCH₂CH₂Ph)₁₈⁻] confirmed the presence of three types of gold atoms: (i) smallest core of Au₁₃ - with one central Au atom surrounded by 12 Au atoms; (ii) 12 Au atoms forming the vertices of an icosahedron around the central atom with five bonds to Au atoms and one to a sulfur atom, and (iii) 12 Au atoms stellated on 12 of the 20 faces of the Au₁₃ icosahedron [132]. In another study, the internal structure of Au₃₈SC₂H₄Ph₂₄ NPs was found to contain a face-fused Au₂₃ bi-icosahedral core with the capping of three monomeric Au (SR)₂ staples at the waist of the Au₂₃ rod and six dimeric staples with three on the top icosahedron and other three on the bottom icosahedron. The six Au₂(SR)₃ staples were found arranged in a staggered configuration with Au₃₈S₂₄ framework having C₃ rotation axis [133].

A systematic study of very small Au NPs, carried out recently, not only confirmed that the particles < 2nm and > 2nm diameters possessed icosahedral and truncated octahedral structures, respectively, but also revealed that the lowest energy structures determined by theoretical calculations did not represent the actual condition due to significant thermodynamic effects [134].

The stability of icosahedral, decahedral and cuboctahedral NPs of other metals including Ni, Cu, Rh, Pd, Ag, Ir, Pt, and Au were theoretically explored using the local optimization of the total energy using tight-binding second moment approximation and quantum Sutton-Chen potentials. It was inferred from such a theoretical study that the icosahedral form was be most stable for Ni, and least stable for Au. The stability of Rh, and Ir NPs was found to be size and shape dependent [135].

A density functional theoretical study (DFT) of thiol, phosphine, and mixed phosphine-thiol protected Pd₁₃ and Pd₅₅ metal cores showed the feasibility of modifying their catalytic properties considerably. Due to significant interplay between the frontier orbital stabilization based on the contribution of the sulfur and the charge donation by the phosphine, the charging energy of the mixed phosphine-thiol protected cluster was found larger than that of either phosphine or thiol only systems. This study showed that it is possible to program these catalytic

NPs by varying the compositions of the protecting ligands [136]. During the study of Pd NPs, it was noted that the arrangement of Pd atoms was less ordered in thiolate-protected NPs than in amine-protected ones, in which, the S-Pd bonds in sulfide layer surrounding the NPs caused significant structural disorders [137].

The structure of thiol-protected $(\text{Au}_x\text{Ag}_{1-x})_{312\pm 55}$ clusters was studied recently as a function of composition (x) considering the structural motifs of icosahedral, fcc, and icosidodecahedral. The observed structures were found sensitive to the compositions, for example, icosahedral and fcc structures were found dominating Ag-rich and Au-rich clusters, respectively, while icosidodecahedral structures were observed only in clusters with Au content greater than 30% [138].

5.3.3 Surface Stability – Metal NPs

While the surfaces of bulk gold and 7.9, 2.9, 1.6, 1.3, and <1 nm diameter NPs were all found prone to oxidation when exposed to atomic oxygen, bare Au_{55} remained practically unaffected even during extreme oxidizing conditions [139]. This unique behavior of Au_{55} cluster was assigned to the closed-double-shell excluding any electronic contribution. Extending this argument further, it could be predicted that Au_{147} or Au_{309} cluster would also be unaffected by oxidation.

In order to study the stability of Ag NPs in detail during oxidation, surface passivated with citrate and L-glucose as well as unprotected NPs having diameters in the range of 3-5 nm and 10-12 nm were studied using UV-Vis absorption spectroscopy, SAXS, TEM, along with their electrochemical oxidations using STM, cyclic voltammetry, and XPS techniques [140]. Anodic oxidation of these Ag NPs gave Ag_2O , while only a layer of “primary” Ag (I) oxide emerged on larger uncapped nanoparticles during the potential sweep. The formation of AgO at higher potentials proceeded readily at the “primary” oxide but was retarded at the smaller NPs. Citrate and glucose-capped NPs showed substantially retarded formation of Ag_2O and AgO highlighting a non-trivial effect of particle size and transient mobilization of Ag species on the reactions of silver NPs [140].

An attempt was made to empirically correlate the influence of shape factor λ , defined as the surface area ratio between non-spherical and spherical QDs with identical volumes, along with the diameter D , in a recent publication, by taking the melting points and thermodynamic stability data of the tetrahedral, decahedral, octahedral, cuboctahedral, and icosahedral structures [141]. It was in general found that the smaller values of λ resulted in higher thermodynamic stability leading to a variation in melting point T_m as: T_m (icosahedron) $> T_m$ (cuboctahedron) $> T_m$ (octahedron) $> T_m$ (decahedron) $> T_m$ (tetrahedron). The cumulative influence of λ and D was found to enhance $T_m(D, \lambda)$ with increasing D , while decrease with λ increasing. The validity of this empirical model was confirmed by the experimental and simulation results of the size and shape-dependent thermodynamic stability in Au, Ag, Ni, Ar, Si, Pb, and in quantum dots [141].

Well-known thermodynamic instability caused by high surface energy of the bare NPs forces them in general to relax by attaching to some molecular species from the surroundings or lowering the surface energy through coagulations/agglomerations. Knowing this fact, efforts have been made for avoiding their mergers among themselves by using various types of surface stabilizations techniques based on electrostatic, steric, and electro-steric considerations [142,143].

While implementing electrostatic stabilization, it is necessary to know about the inter-particle repulsive and attractive interactions arising due to the presence of double layers formed around each NP and weak van der Waals forces operating upon these NPs, respectively [144,145]. A systematic analysis of the electrostatic interactions experienced by metallic NPs in a colloidal solution in presence of anionic and cationic species did provide an estimate of this interaction energy as a function of the number of ions around each NP, which increased with growing

Exp. Theo. NANOTECHNOLOGY 3 (2019) 301-362

number of ions and became positive for $N \geq 9$ [143]. It was further noted that this electrostatic energy could be comparable to that of the chemisorption in case of only few charged species surrounding the individual NPs. With increasing number of these surrounding charged species, the energy decreased significantly, which has particularly been found important in steric stabilization [143].

Considering the availability of sufficient cationic and anionic species in the solution it is easy to understand about the double layer formation around individual NPs. Based on electrostatics, it may be noted that the induced dipole moment in a metallic sphere is zero when two identically charged entities approach such a NP from exactly opposite directions in contrast to its enhanced values when the charges on the two species are of opposite nature. According to this law, the cationic and anionic species approaching the individual metal NPs would certainly induce many image charges - δ^+ and δ^- on the surface resulting in sufficient multi-pole moment. Further, the different chemical natures of cations and anions would result in distinctly different interactions with the metal surface forming a double layer of oppositely charged ionic species around each NP imparting repulsive inter-particle forces among them in the vicinity besides promoting the approach towards metal NPs [144]. Following this approach, it has been possible to control their agglomerations/de-agglomerations by incorporating changes in the magnitude of the dipole/multi-pole moments of the metal NPs either by increasing or decreasing the influence of polarization, respectively. This concept was applied in designing the “smart” nanomaterials [146-148]

In an alternate scheme of steric stabilization, very large size molecular or ionic species were adsorbed on the individual NPs introducing geometrical constraints around the NPs to reduce their mergers resulting in stabilization. It is worth noting in this context that an elongated or conical geometry might be advantageous in keeping the approaching NPs apart and in case the length of the stabilizer is significantly longer than the characteristic size of the NPs, spherical structures are likely to form encapsulating the NPs. Accordingly, the high molecular weight polymers have very often been found good stabilizers for NPs.

While improving adsorption properties of the stabilizing species for longer residence times by preventing their spontaneous desorption, the chelating effect has been found to increase the probability that the stabilizer remains adsorbed. Metals with more valence orbitals than valence electrons known to have an “electron deficient” surface that can very easily attach electron-donating species like divalent sulphur, trivalent phosphorus/nitrogen moieties or molecules with π -electrons. Highly charged larger size molecular species have therefore been found better for electro-steric stabilization.

According to the requirements mentioned above, the most suited stabilizers for metal NPs would, therefore, be those species that are ionic, adsorbing strongly and providing steric and electrostatic stabilization simultaneously. Ionic liquids, consisting of cations and anions, provide excess ions favoring coordination also of less strongly coordinating ions. Although, strong coordination is good for physical applications as QDs, but not suitable for applications like catalysis, where access of the substrate molecules to the metal surface is required.

In this context of NP stabilization, ionic liquids (IL's) offer particularly appropriate electrostatic features, while simultaneously it has been possible to select them in such a way that either the cations or the anions are not only strongly chemisorbed, but also have the appropriate bulky geometry providing steric hindrances. Besides, the unique combination of their physicochemical properties like negligible vapor pressure, non-flammability, high ionic conductivity, low toxicity, good solvent for organic and inorganic molecules, high thermal stability, and wide electrochemical window makes them a good choice for NP stabilization. In this context, it is useful to examine the anions/cations of tetra-octyl-ammonium bromide, out of which anions adsorb very strongly on metal surfaces, but have relatively smaller size in contrast to cations offering bulky geometry for steric repulsion. In fact, many examples of tetra-octyl-ammonium stabilized metal NPs are already reported in the literature [149]. Charged

polyelectrolytes [150] are the other well-known stabilizers of metal/metal oxide NPs and organic micelles meeting the criteria of steric as well as electrostatic stabilization together [151-158]. Metal NPs stabilized by tetra-alkyl-ammonium halides met the electrochemical as well as steric criteria, as metal surface absorbed halogen ions strongly, while the surrounding tetra-alkyl-ammonium cations restricted the close contact between the NPs [159-161]. Tetra-hexyl, tetra-butyl and tetra-octyl-ammonium bromide/chloride based molten salts were used as first ionic liquids to stabilize NPs [160,161]. Note that the use of imidazolium based ionic liquids for the stabilization of Ir NPs was reported much later in 2002 [162]. Another aspect of ionic liquids is that the thermal movement of the colloidal nanoparticles is suppressed due to the high viscosity of the surrounding medium minimizing the probability of close contacts. Imidazole IL functionalized with carboxyl and amido group has been found useful for preparing metal nano fluids (Au NFs) with improved stability as well as higher thermal conductivity [163-168].

Ionic liquid modified NPs form a system with many degrees of freedom and particularly because of sufficient tunability of their physical properties like viscosity, conductivity, and melting point by changing the structure of cation and anion, besides their solubility, dispersion, and accessibility which are possible to tailor for specific applications. Functional groups are possible to introduce into the cation or anion for improving stability of the NPs as well as modify their catalytic properties. A mixture of two/more ionic liquids with one/two types of NPs offers an altogether new combination of physicochemical properties, which are different from those of the single components.

Anion in ionic liquids (IL's) are found to play a comparatively more significant role than cation in stabilizing metal NPs due to its stronger interaction with metal surfaces, which may be used for modifying the stability accordingly. Although, non-functionalized IL's interacting very weakly with metal surfaces are good for improved catalytic activity, but offer poor stability/recyclability of the NPs. Using hydroxyl group functionalized ILs has been found effective in taking care of this problem of NP stabilization by interacting with halide anion as seen in case of stabilized Pd species using this route. Functionalized IL's are found very effective when used in conjunction with polymers and ligands exploring strategies involving electrostatic, steric and coordination along with electron donating ligands as discussed earlier. Various aspects of applying IL's in metal NP stabilization have been reviewed in detail elsewhere providing more information [143, 169,170].

5.3.4 *Semiconductor NCs*

A quantum dot (QD) is a semiconductor nanocrystalline material supporting bound electron-hole pairs called excitons due to quantum confinement in a small volume created by high-energy photons discovered in early 1980's. QDs possess their electronic properties somewhere between those of bulk semiconductors and of discrete molecules.

Size-specific optical, electronic, and optoelectronic properties of the nanosize QDs exhibiting discrete electronic transitions, as well as possessing useful properties of crystalline materials have been observed due to interaction of the quantum confined excitons with electric, magnetic, and the electromagnetic fields. High-energy photons (i.e. energies $> E_G$) irradiating these QDs excite electrons from the valence to the conduction band leaving holes in the valence band producing excitons, out of which, the relaxing excited electrons returning to the valence band and annihilating the parent excitons emit photons in form of radiative recombination.

These excitons, extending over a length scale of 1-100 nm according to the material used, when confined in a volume with dimension smaller than the exciton extension enable the QDs to exhibit size-specific absorption and fluorescence spectra with discrete electronic transitions including size-specific energy band gap. Thus, due to strong quantum confinement of excitons in QDs, it has been possible to tune the band gap as a function of the dimensionality and degree

Exp. Theo. NANOTECHNOLOGY 3 (2019) 301-362

of confinement as verified in case of CdSe QDs, quantum wires/rods, and quantum well/disc [171].

Because of their tunability over a wide range QDs have been considered particularly useful in bio labeling, whereas elongated nanostructures have been found emitting linearly polarized light with a wide energy separation between the absorption and emission maxima, which can reduce light reabsorption for light emission applications [172]. Similarly, very familiar quantum wells used in optoelectronic devices, and their colloidal disc analogues have recently been found possessing novel piezoelectric properties once confined in a polar lattice [173]. Most of the atoms in smaller size QDs residing onto the surface with partial bindings with the atoms inside the core, possess one/two dangling orbitals directed towards outside the facet involved. These atoms that are residing on each facet may form a periodic array of unpassivated orbitals with two-dimensional translational symmetry, which may give rise to energy band structure similar to that of the three-dimensional crystal [174,175]. Since these surface energy states generally fall within the semiconductor band gap, they act as charge carrier traps at the surface, and thereby reduce the overlap between the electron and hole, increasing the probability of nonradiative decay events. However, these QDs are either embedded in a solid matrix or suspended in a colloidal solution coated with some surface passivating organic ligands. Under these circumstances, bonds with atoms/molecules present in the immediate neighborhood minimize the intra-band gap surface states and reduce the surface reconstruction during dangling bond passivation. For example, in colloidal suspensions, molecules like TOPO and HDA adsorb onto the QD surface by forming ligand-metal bonds, which make them soluble in nonpolar solvents. Similarly, polar end groups and hydrophilic polymers could also be conjugated to the QDs for solubilizing them in polar solvents [176].

Because of the strong influence of the prevailing conditions on the nanocrystal facets, the phenomenon of fluorescence has been found sensitive to the nature of the structural defects present there at the facet. For example, very small colloidal CdSe QDs often show two distinctly different fluorescence emission bands, one corresponding to the band edge and the other resulting from recombination at intra-band gap defect sites on the surface [175]. Indeed, nano crystals with surfaces terminated by anions typically have very little or no fluorescence emission due to the overwhelming number of surface trap states leading to nonradiative recombination [81].

Spherical QDs having the smallest number of surface atoms are not only the most stable structures, but are also very useful for those applications, where fluorescence modulation from external stimuli is required to be minimum. On the other hand, elongated structures like nano rods and nano wires, with a large fraction of their constituent atoms on their surfaces, are useful for those applications where the charge carriers interact with the surrounding environment, such as for redox chemistry, energy transfer, photo-catalysis, and sensing applications [81].

QDs have been found generating polarization-entangled photons efficiently involving bi-exciton-exciton cascaded emissions. Employing an electric field has been found useful facilitating the integration of these QDs into optoelectronic devices. In this context, generation of polarization-entangled photons from a single biased QD was demonstrated confirming the concept involved [177]. In this context, the exciton binding energy in an asymmetrical cylindrical QD was studied as a function of electric field using EMA and a variational calculation procedure, in which, it was concluded that in absence of the electric field the binding energy was a decreasing function of the QD radius and height and for a fixed geometry, it became a decreasing function of the electric field strength [178].

The melting point of the nano crystals has been found decreasing with size reduction, as a larger fraction of atoms resides onto disordered, and partly passivated surfaces [179]. The surface energy differences between different crystal phases have also been used to explain

pressure-induced phase transitions in high surface-area semiconductor QDs relative to their bulk counterparts [180].

QD surface passivation using an insulating inorganic shell has been found to stabilize as well as maximize the fluorescence efficiency by minimizing the influence of surface defect states and trap sites besides another environmental parameter [73,181, 182].

The energy band gaps of QDs have been modified by changing their sizes, shapes, and compositions, in which, the quantum confinement could easily change the associated band gap by over 1 eV, giving an enormous range of continuous tunability. Besides, independent tuning of band gap has also been realized well by using alloyed materials such as $\text{CdSe}_y\text{Te}_{1-y}$ and $\text{Cd}_x\text{Zn}_{1-x}\text{S}$ [183,184]. More recently, the manipulation of nanocrystal hetero-structures has also been employed enabling flexible control over charge carrier wave functions resulting in newer types of optical properties. For example, using the concept of band offsets in different types of core-shell QDs, it has been possible to segregate the electrons and the holes in the core and shell regions [185]. In a specific case of core-shell QDs of CdTe-CdSe, the conduction band minimum has been found in the CdSe shell, whereas the valence band maximum lying in the CdTe core could help in segregating the electrons to the shell and the holes to the core, and carrier recombination could occur across the interface at a lower energy than the band gaps of either of the constituent semiconductor materials. This type band alignment known as type-II has been found useful in photovoltaic devices [186]. These type-II nano crystals have been found useful in independently controlling charge carriers that are accessible to the surface for charge transfer applications.

A. Silicon NCs

The discovery of photoluminescence in porous silicon as well as in silicon clusters triggered interest in exploring further by looking into the possibilities of size specific band gaps responsible for the inter-band transition-based luminescence in the visible range, and the observed high transition probability [187-195]. A number of methods to prepare Si clusters have subsequently been evolved using techniques like liquid-solution-phase growth, silane slow combustion, microwave plasma discharge, chemical vapor deposition, gas evaporation, sputtering or ablation, ultrasonication of porous silicon and various other techniques [196-204]. It was, however, noted that photo luminescent Si clusters were invariably surface passivated, whereas non-passivated clusters did not emit any light after UV excitation. This led the researchers to particularly investigate hydrogen passivated and oxidized Si clusters in more detail [205-217]. Size-specific energy gaps of Si cluster have been examined in more detail due to particular observations made in porous and nanocrystalline silicon samples [187,188,208,209, 218,219]. For example, the associated energy gaps were found increasing significantly with reducing diameters as observed in case of 1-5 nm diameter clusters between 1.3 and 2.5 eV [217].

The energy band gaps of QDs have been estimated under effective mass approximation (EMA) using the variational calculation of the Schrodinger wave equation of electron and hole in an exciton having Coulomb interactions in terms of the band gap of the core material E_{Bulk} , Planck's constant \hbar , quantum dot diameter d , as well as the effective mass of the excited electron and hole as m_e and m_h [220,221]. The simplified form of equation based on asymptotic variations is expressed as given below.

$$E_{QD} = E_{\text{Bulk}} + (2\hbar^2/\mu d^2) - 3.572(e^2/\epsilon d) - 0.248E_{RYD},$$

where, $1/\mu = (1/m_e + 1/m_h)$; d = diameter; e = electron charge; ϵ = dielectric constant; E_{RYD} = Rydberg energy.

The third term in the above equation represents the columbic interaction of exciton having d^{-1} dependence; often neglected due to high dielectric constant of the material. The multiplying

Exp. Theo. NANOTECHNOLOGY 3 (2019) 301-362

factor of 3.572 has come from the above-referred variational solution of the Coulomb interactions involving only the nearest neighbors [221].

Although, EMA based predictions described above, could be used for Si clusters, but its applicability has been questioned particularly due to not considering the influence of atomic structure, unsaturated surface dangling orbitals, and the significant changes in MO-hybridization occurring during size reductions [222].

Theoretically, smaller Si clusters with $N < 10$ have been found possessing compact cubooctahedral or icosahedral structures with average coordination number above 4 of the bulk Si in clusters with $N = 12-24$ as confirmed by Raman and anion photoelectron spectroscopic measurements [223-232]. Observed changes in electronic properties of Si clusters from crystalline semiconducting to closed packed metallic entities must arise from some sudden transformation. Because of numerous factors influencing the structure as well as physico-chemical properties of these smaller clusters, HOMO-LUMO gaps of these particularly non-passivated ones have not yet been properly understood well despite having good experience in handling electronic structure and band gap of porous silicon and large passivated Si nano crystals [209, 213, 233-237]. Band gaps ranging between zero and several electron volts have been predicted for small un-passivated silicon clusters as estimated in several cases such as: near zero gap for Si_{28} to Si_{45} ; 1.2 for Si_{20} and Si_{46} ; and 0.3–3 eV for Si_3 - Si_{11} [223,230, 238-240].

The proposed prolate shapes of the clusters with $N \sim 27$ could be one of the reasons for observing this difference as compared to more spherical larger clusters [241]. Abrupt changes in the properties of medium-sized Si clusters have already been clearly reflected in photoionization measurements on clusters with $N = 20-30$ indicating about the sudden change in the electric polarizability of the clusters due to the associated structural changes at $N > 20$ [242,243]. Disordered Si clusters have also been, in general, formed during fast cooling of Si molecular beam or vapor, where the participating atoms do not find time to adjust to the low-energy positions and thus result into significantly different structures from both the bulk and the nanocrystal structures [244,245].

Scanning tunneling spectroscopic (STS) measurement has been found useful for determining the band gaps of Si clusters by identifying the zero tunnel current regions situated symmetrically around zero bias. In case, no states are there inside the band gap of the cluster, the tunneling electrons would pass through the cluster without interaction making the substrate visible in the STM image. At relatively higher bias voltages of either polarity, electrons tunnel from the tip to the sample and vice versa resulting in relatively larger current in the positive bias ranges than those in the negative bias regions, showing that the cluster has a higher state density at the conduction band edge compared to the valence band edge. In one of the measurements, carried out on clusters ranging between 1.5 and 4.0 nm, zero gaps were observed. For smaller clusters, non-zero gaps became more predominant along with zero gaps. Below 1.5 nm, the band gaps started showing an increase with decreasing cluster size with the largest gap of 450 meV, for clusters with 0.5 and 0.85 nm with not only a large scatter in data but also showing different band gaps for clusters of similar size [246].

Considering the bulk Si with a band gap of 1.1 eV, the expected increase in case of smaller size NPs due to the quantum-size effect could increase the band gaps up to 4eV, as confirmed by experiments and theory in surface passivated Si clusters [190,193,194, 205-209, 211-215, 217,219, 222, 247- 250]. Theoretically calculated HOMO-LUMO gaps of Si_2 to Si_{61} clusters showed large variations subject to the calculation methods, assumptions, and types of approaches used including DFT, tight-binding, and self-consistent-field algorithms. These clusters were found to possess zero as well as non-zero band gaps extending up to 3.5 eV [223, 230,231, 251-253]. In a more recent study, a general method of reconstructing the electronic band structure of Si NCs from ordinary real-space electronic structure was also introduced, which could include full geometric and electronic relaxations with different types of non-

polarizing and polarizing surface passivating groups [254]. By combining with large-scale DFT calculations, it became possible to have insight into the luminescence properties of silicon nano crystals of up to 3 nm in size depending on the surface passivation and geometric distortion. It was further proved that the band structure concept was still applicable to Si NCs with diameter > 2 nm with certain limitations [254].

The presence of high-density dangling bonds creating partially filled surface states in the energy band gap around the Fermi level due to directional properties of the sp^3 -hybrids and the missing neighbors at the extended surface of bulk Si, as demonstrated by tunneling spectroscopy as well, have been expected to give rise to similar conditions in un-passivated Si clusters surfaces [246]. For example, theoretical calculations of Si_{29} , Si_{87} , and Si_{357} cluster showed zero HOMO-LUMO gaps, while the passivated clusters like $Si_{29}H_{36}$, $Si_{87}H_{76}$, and $Si_{357}H_{204}$, showed the band gaps of the order of 3.44, 2.77, and 1.99 eV, respectively, just as expected for the particles in this size range [246]. These observations clearly showed that the zero band gaps of the pristine clusters indeed originated from the surface states due to excessive dangling bonds.

The role of surface reconstruction in reducing the density of dangling bonds was estimated in earlier studies but was found inadequate in removing the band gap states, as confirmed by tunneling spectroscopy measurements at very low bias confirming the presence of a high density of states near Fermi level [255,256]. However, in subsequent investigations of photoelectron spectroscopy for electronic structures and band gaps of Si_3 - Si_{45} clusters it has been observed that almost all clusters possessed either zero or a band gaps that were much smaller than that of bulk Si, which was attributed to covalent bond formation and surface reconstructions on single-crystal surfaces [257]. Besides, band gaps of 0.6 and 0.4 eV observed in case of Si_{30} and Si_{33} were supported by spherically stable structures. Out of these, only two clusters, S_7 and Si_{10} , had a band gap larger than that of bulk Si, in contrast to quantum confinement considerations. The phenomenon like surface reconstruction and covalent bond formation reducing the number of dangling bonds were found to dominate and most of the medium-size clusters ($N = 20 - 45$) were found to be like open-shell metallic clusters, which could be possible due to reconstruction of Si (111) surface. The clusters including Si_{11} , Si_{14} , Si_{17} , Si_{18} , Si_{30} , and Si_{33} , only a few had closed-shell electronic configurations in the neutral state with a band gap of 0.4-0.6 eV [257].

Zero band gaps arising due to the metallic surface state density, observed in combined photoemission and inverse photoemission studies could be explained by either of the two transport mechanisms involving either high density surface states overlaps forming a conduction band or lower surface states density resulting in thermally activated hopping between the localized surface states. In case of ~ 1.5 nm diameter cluster with $N \sim 90$, a major change in the cluster properties occurred in form of a sudden opening up of the band gap which went wider for still smaller clusters [246].

This kind of change over from zero to non-zero band gap indicated a substantial change in the electronic structure of the clusters, as mentioned earlier, which was explained in case of large silicon clusters using sp^3 -hybridized strong covalent bonds and rigid bond angles resulting in high surface state density. Around a critical size of N^* , the sp^3 -nature of the bonds gradually changed to some other form of MO-hybridization as highlighted in *ab-initio* calculations that sp^3 was not the favored hybridization for small silicon clusters. The change of the electronic structure around N^* also amounted to a definite change in the atomic structure of the clusters, and below this critical size, the clusters could no more be treated as fragments of the bulk crystal but rather had their own cluster-specific close packed structures similar to those of metal clusters confirming a covalent to metallic transitions. It has also been noted that some of the Si clusters examined showed zero band gaps even below N^* because of having surface states similar to those above N^* . It also showed that the transition around $N^* = 90$ did not occur for

Exp. Theo. NANOTECHNOLOGY 3 (2019) 301-362

all Si clusters as some clusters did have sp^3 -coordinated bonds even at very small size coexisting with the compact clusters as structural isomers [246].

Single photon vacuum ultraviolet photoionization conducted on small Si_1 - Si_7 clusters using laser ablation of Si helped in resolving various conflicting experimental observations [258]. The adiabatic ionization energies (AIE) estimated in eV from such a set of experiments gave the following values as: Si_1 (8.13), Si_2 (7.92), Si_3 (8.12), Si_4 (8.2), Si_5 (7.96), Si_6 (7.8), and Si_7 (7.8) for different clusters. Most of the experimental AIE values were in agreement with density functional electronic structure calculations. In order to explain the observed difference between the experimental and theoretical AIEs for Si_4 and Si_6 , a theoretical search of other possible isomers was also performed [258].

There were further indications of such transitions as observed in chemical reactions showing significant changes in the chemisorption probabilities at $N = 29-36$ and dissociation energy of ionized Si cluster started deviating from the smooth size behavior below about $N=40$ and photoionization threshold suddenly dropping at $N \sim 20-30$ [246].

Using tight binding approximation and DFT combined, the HOMO-LUMO gaps of hydrogen-terminated silicon NPs has been studied as function of shape and size. It has been shown that optical properties of these NPs were strongly dependent upon nanoparticle shape, and in particular that octahedral NPs had band gap in excess of up to 0.2 eV than cubic or pseudo-spherical NPs of equal volume. In this study, it was found feasible to have silicon NPs with emission wavelengths covering the full visible range [259].

5.3.5 Engineered Materials – Some Results

After studying the electronic states in metallic and semiconducting NCs, using quantum mechanical formulations, attempts were made in parallel to explore their band-structure-engineering aspects for their uses in numerous applications. Some of the theoretical and experimental results reported in published literature are included in the followings to highlight the degree of success achieved while trying to explore future applications.

For instance, the energy band structure adjustment of a NC is not only tunable by adjusting the morphology that changes the confinement of the electrons and holes causing shifts in the range of ~ 1 eV but also by adjusting the energy band gap of the parent material employing alloy compositions with more flexibilities such as $CdSe_yTe_{1-y}$, and $Cd_xZn_{1-x}S$ [183,184]. In addition, employing a core-shell type of configuration of NCs provides added flexibility; where extensive control over electron and hole wave functions exhibits newer optical properties. These core-shell type NCs, in general, involve a hetero structure with staggered conduction and valence band edges in the core and shell regions accordingly [185]. For example, the CdTe core with CdSe shell has a lower conduction band edge in the CdSe shell, and a higher valence band edge in the CdTe core, due to which electrons and holes are segregated in the shell and the core regions, respectively, forcing the charge carrier recombination to occur primarily across the interface. The reduced spatial overlap between the electron and hole wave functions also results in reduction in band edge oscillator strength causing significant increase in excited state lifetimes. This kind of band alignment is, thus, found useful in photovoltaic devices by radially enhancing the directional charge transport [186]. These NCs also enable independent control of the charge carrier accessible to the surface for charge transfer applications.

Besides, in colloidal (CdSe)ZnS NCs, it is also possible to support significant strain due to large difference in their lattice constants (e.g. $\sim 12\%$) in the core and shell materials without causing any structural disruptions. It is important to note that during the overgrowth of a shell layer in an isolated NC, it is possible to adjust relatively larger magnitude of such a strain during the overgrowth by forcing the material to adopt to an unnatural lattice constant, which ultimately alters the electronic band gap substantially without causing strain induced lattice

defects. In a recent study, however, the influence of the core lattice in causing strain generation in the shell layer was reduced to zero by choosing the core diameter less than a certain critical value in a colloidal heterostructures [260]. For example, even with a 11.4 % difference in the lattice constants of CdTe and CdS, CdTe cores; it was practically seen that < 4 nm diameter cores were over-coated with almost any thickness of CdS shell through coherent growth. Knowing that the compressive strain shifts both the conduction and valence bands to higher energies, and tensile strain shifts the bands to lower energy; the coherent growth of compressive shells like ZnSe or CdS on CdTe core is expected to cause significant changes in the relative energy bands with widely tunable band gaps. For this type of band-gap-engineering, CdTe NCs being much softer compared CdSe, ZnS and CdS; are very useful for this purpose. Furthermore, the strain produced during formation of (core) shell NCs has also been employed in realizing different fluorescence behaviors of (CdSe) CdTe and (CdSe) ZnTe NCs, where CdTe shell exhibits quantum yields of 20-40% compared to <1% in ZnTe shells. In an alternate scheme of controlling the band gap of CdTe NCs, alkanethiol capping was employed as reported recently, where, precursor concentration and reaction time adjustments during capping were found to influence the size and hence energy band gap due to the formation of CdTe_{1-x}(SC₁₀)_x shell [261].

It has been possible to fabricate nanowires, nanocables, and coaxial shells structures employing directed assembly of NCs as discussed earlier. Since, it involves NCs in various arrangements, it becomes easy to vary the electronic structure by varying the parameters involved there. Some of the attempts made in this context are summarized below.

For instance, attempts were made to explore better light harvesting, improved charge carrier separation and faster charge carrier transport properties of the core/shell type nano cables, in which the staggered type heterojunctions present there could extend their absorption bands extensively [262]. These nano cables not only offered larger interfaces, better charge separation, improved collection efficiency, straight 1-d path for efficient collection of photo generated carriers, but also provided effective passivation reducing nonradiative recombination of percolated electrons in 1-d oxide with electrolyte and corrosion protection to the oxide cores. Arrays of type-II ZnO/Zn_xCd_{1-x}Se core/shell nano cables with tunable shell composition (0 < x < 1) and band gaps from 1.62 to 2.33 eV were prepared, which gave PCE of 4.74% in PVSC devices [262].

The possibility of varying composition and structure along and across a NW and coaxial shell opens up numerous possibilities of employing band-structure-engineering in realizing novel device structures. Introducing variations in composition and structure to change its energy band structure is possible to confine carriers within the nanowire resulting in the formation of local 2, 1 and 0-dimensional structures within the NW. Various aspects of this development were reviewed in detail in a recent paper [263].

A number of Zn_xCd_{1-x}Se nano-multipods were synthesized by changing the ratio of Zn/(Zn+Cd) from 0.08 to 0.86 by varying the ratio of precursors, which resulted in band gap energy varying linearly from 1.88 to 2.48 eV [264]. The presence of oleylamine resulted in the predominant formation of nano-multipods. Theoretical calculations indicated that dissimilarities of electronic band structures and orbitals determined the tunable band gap of the as-synthesized nano-multipods.

Three-dimensional hierarchical NW-networks possessing longer optical path for efficient light absorption, high-quality one-dimensional conducting channels for rapid electron-hole separation and charge carrier transport, and high surface areas for fast interfacial charge transfer and electrochemical reactions, have been considered for preparing high quality electrodes in PVSCs. By growing TiO₂-NRs onto dense Si-NWs array backbones, it was successfully shown that 3-d architecture of 20 μm long wet-etched Si-NWs and dense TiO₂-NRs exhibited a photo-electrochemical efficiency of 2.1%, which was almost three times that of TiO₂ film-Si-NWs having a core-shell structure [265]. The efficiency, however, could

Exp. Theo. NANOTECHNOLOGY 3 (2019) 301-362

further be improved by optimizing the number of over-coating cycles and the length/density of NW backbones.

With special reference to explore band-structure-engineering in a number of new nano crystalline materials with a diverse range of chemical, elastic, and optical properties, ZnO is an excellent shell material for NC capping due to its wide band gap and resistance to oxidative degradation. Additionally, it is also possible to tune the energy band gaps of IV-VI and II-VI semiconductors by exploring their positive deformation potentials and spontaneous cation exchange reactions, respectively. It is further anticipated to engineer NCs for multi-exciton generation and efficient charge carrier separation in PV applications of future generations. It is possible to minimize the overall size of bio-conjugated NCs for reducing the steric hindrance and nonspecific protein adsorption, while developing NCs for multicolor super-resolution optical microscopy, and to understand the potential toxic effects of semiconductor materials [266].

In one of the novel studies, it was reported how to divide a semiconducting nanotube into multiple quantum dots with lengths of about 10 nm by inserting Gd@C₈₂ endohedral fullerenes [267]. The spatial modulation of the nanotube electronic band gap resulting from such a modification was measured with a low-temperature STM, where it was found reducing from ~0.5 eV to ~0.1 eV at the locations of endohedral metallo-fullerenes. This kind of energy band gap modification was ascribed to the local elastic strain and charge transfer at metallo-fullerene sites.

The influence of water on the electronic properties of fullerenes was also studied using Monte Carlo and DFT, in which, a red shift of 0.8 eV was observed in the energy band gap of hydrated system [268].

In another case, the energy band gap of photo luminescent nano-peapods was examined over a wide range of diameters from 1.25 to 1.55 nm, and the observed behavior was possible to explain by the strain-induced band gap shifts due to the C₆₀ insertion and the hybridization between the electronic states of SWCNTs and C₆₀ [269]. These results provide significant insights into band gap engineering of SWCNTs in future nano devices.

A number of donor-acceptor copolymers were synthesized possessing low and high-energy optical transitions by changing one atom strategically situated in benzochalcogenodiazole from S to Se to Te [270]. It was noted that heavy atom substitution resulted in low energy transitions band gaps of 1.59, 1.46, and 1.06 eV for sulfur, selenium and tellurium containing polymers, respectively. This kind of study established that in D-A type copolymers, it is possible to adjust the energy band gap by changing the heavy atom.

To clarify the conceptual issues related to the energy band gap tuning in low band gap copolymers, efforts were made to find out the minimum requirements for accurate prediction of polymer band gaps from those of finite length oligomers [271]. Comparison with experimental results helped in identifying the suitability of the functionals available for this purpose.

Semiconducting polymers having energy band gaps higher than 2 eV are able to harvest about 30% of the solar photons. In this attempt of better harvesting of the solar spectrum, conjugated polyaromatic polymers with thiophene moieties were developed with tunable band gaps, from 1.0 to 2.0 eV [272]. For adjusting solubility and energy levels, a variety of radicals were attached to the polymer backbones so that morphology and performance of the electro active layer were optimized.

The electronic structure of CdTe nanotube-fullerene nanocomposite was studied using the self-consistent-charge density-functional tight-binding (SCC-DFTB) method [273], in which the modifications occurred into the NT band gap by introducing the molecular states of fullerene into the band gap region. The effect of the band alignment modulation through the wall thickness of the CdTe NTs on the electron injection rate from the NT to C₆₀ in hybrid systems was explored [273]. Increasing the concentration of the C₆₀-thiol moieties, it was possible to

maximize the light harvesting efficiency of these nano hybrids by changing the composition of the CdTe–fullerene hybrid nano composite.

The study of post deposition thermal annealing in a particular solvent was carried out on low band gap polymer (LBG): fullerene mixtures that are found useful in OPVSCs [274]. While examining the morphological evolution of PCPDTBT: PCBM mixtures in terms of the final device performance, it was noted that the solvent vapor not only controlled the ordering of PCPDTBT and PCBM phase separation but also inverted the morphology - from a polymer aggregate dispersed in a polymer: fullerene matrix to fullerene aggregates dispersed in a polymer: fullerene matrix [274].

5.3.6 Graphene

Out of several types of configurations of nanostructured species, already mentioned earlier, the case of graphene is unique, as it possesses altogether different type of electronic band structure and charge carrier properties. For instance, graphene, although found promising for replacing silicon in coming generations of electronics and optoelectronics, but, due to its zero-energy band gap and massless Dirac fermions, it has not yet been possible to harness their superior features in device fabrications. Numerous attempts, made in recent past to create semiconducting graphene by resorting to periodic patterning; passivation, doping, and nanoscale perforations, although, appear promising but it still needs more development before it is put to use. For instance, despite extensive theoretical studies made so far, the role of periodic modulations on electronic structures of graphene is still not a reality. Employing tight binding and first-principles based electronic structure calculations, it was concluded recently that the band gap in a patterned graphene has an origin in its geometric symmetry [275].

Referring to the schematics of energy band diagrams of single/double layer graphene compared to that of graphite as shown in Figure. 5, using graphene material in semiconductor device applications, a 'wide energy gap' of at least 0.5 eV must be opened without the introduction of associated atomic defects. However, such a wide energy gap has not been realized in graphene, except in the cases of narrow, chemically terminated graphene nanostructures with inevitable edge defects. Despite having massless charge carrier based ballistic transport in graphene, it is not possible to control its conductivity electronically as it lacks a band gap around the Fermi level. Though, periodic modulation of graphene lattice was predicted to result in a tunable band gap but still it is not a reality. In a recent study, patterned absorption of hydrogen demonstrated the existence of a band gap opening in graphene grown on Ir substrate [276].

In some experiments, conducted sometime back, the lateral charge carrier confinement in a patterned graphene ribbon was found exhibiting an energy gap near the charge neutrality point as confirmed during a measurement carried out on ribbons of varying widths and different crystallographic orientations [277]. The temperature dependent conductance measurements carried out at low temperature showed that the energy gap varied inversely with the ribbon width [277].

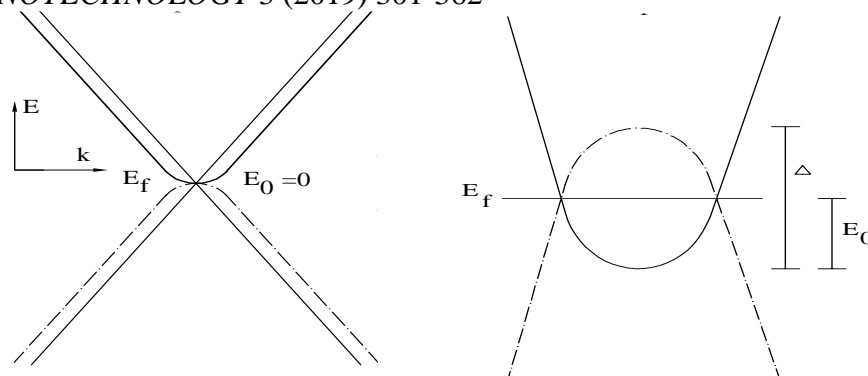


Figure 5 The schematic energy band structure of mono and bilayer of graphene lattice (A) as compared to the band structure of bulk graphite (semi metal) (B) shown having overlapping valence and conduction bands with respect to the position of Fermi level (E_f).

In another alternate experiment, a wide energy gap of 0.74 eV was created reversibly in a graphene monolayer without introducing atomic defects through the alternate adsorption of self-assembled twisted sodium nano strips and oxygen [278]. The success of experimentally observing this kind of behavior is expected to improve the utility of graphene in semiconductor devices resulting in a major advancement in graphene technology.

For using graphene in device applications, besides proper band gap, it also needs a suitable substrate material. In this context, graphene on hexagonal boron nitride (hBN) substrate appears a reasonable choice. In order to resolve the conflict between theory and experiment, density functional and many-body perturbation theories were employed in finding out the electronic states in graphene on hBN substrate, in which it was observed that stacked graphene on hBN did possess a band gap of about 0.1 eV, which disappeared with misalignment [279]. In contrast, the hydrogenated graphene supported on hBN (graphone) exhibited > 2.5 eV band gap, which was reduced by ~ 1 eV when supported on hBN due to the polarization effects at the graphone/hBN interface. The realized band offsets at the interface indicated that hBN couldn't be used as a substrate alone but also as a dielectric for FET devices with graphone channel [279].

With better understanding of the band-structure of graphenes, a number of extraordinary improvements are expected in their product features affecting their market values and field applications. For example, in medicine, their applications in realizing biosensors, bio-imaging devices, drug and gene deliveries, disinfectants, and DNA sequencing, are some of the representative areas that are getting benefitted significantly [280-284]. The possibility of having direct access to the neural systems using highly conducting graphene are currently being explored for diagnostic purposes besides their use in surgery related to spinal injuries [285,286].

Use of graphene in fabricating computer chips has shown considerable promise in improving their processing speeds resulting in CPUs having several orders of magnitude better performance than those of the existing ones of today [287]. Researchers have also been toying with the idea of replacing silicon with graphene for not only to remove the restriction arising due to the finite band gap of silicon but also to avail the additional advantages associated with its transparency and flexibility. In addition, novel applications in diverse fields including fast charging batteries, quality headphones, flexible electronics, photo-sensors, and unbreakable touch screens, are also emerging fast in this context [288-292]. The integration of graphene and optoelectronic devices is expected to make the development of e-papers a reality in near future [293].

Though, graphene water filters developed by Lockheed Martin claimed to reduce the costs of desalination plants by 99% but it is yet to come in the market due to non-availability of a large-scale production of graphene as yet [294].

Graphene applied to other materials may render them either superabsorbent or super-repellent with vast commercial potentials when used as waterproofing materials in electronics, and building construction [295]. Graphene is explored for its use in photovoltaic applications in form of wearable solar cells, which are very useful in field applications to power military equipment [296]. Graphene is used as an additive in a number of material preparations including paints, plastics, and polymers with added advantages due to their superior mechanical strength and very light weight [297].

6. NON-COVALENT INTERACTIONS

The biological macromolecules, in general, contain linear polymers having repeating subunits covalently bonded with bond energies in the range of $100 - 150k_B T$, which are not at all disrupted by any thermal fluctuations. Besides, there are in addition a number of other weaker and non-covalent types of interactions such as electrostatic attractions; hydrogen, and halogen bonding; π -orbital couplings; van der Waals interactions; and hydrophobic effects with bond energies in the range of 1-5 kcal/mol, in contrast to electrons sharing involved in common covalent bonding [298]. Non covalent bonds, although being relatively weaker in strength, ultimately decide the overall morphology of the macromolecules like proteins and nucleic acids. Such intermolecular interactions are responsible for many biological processes, in which, large molecules get attached/detached specifically but dynamically to one another. The nature of water molecules and protein folding are the typical examples to illustrate the relevance of these inter and intra-molecular interactions [298].

Although, electrostatic attractions between oppositely charged ions or ionized molecules are sturdier than covalent bonds, but they are otherwise vulnerable to break after adding water or any other highly polar solvents.

Hydrogen and halogen bonds involving interactions between a partially positive hydrogen/halogen atom and a highly electronegative and partially negative oxygen, nitrogen, sulfur, or fluorine atom, represent a strong dipole-dipole type of interaction compared to a covalent bond. The presence of hydrogen bonds in water, for instance, enables water to exist in form of liquid even with its lower molecular weight. The energy involved in hydrogen bonds is in the range of 0 - 4 kcal/mol, but sometimes it could be an order of magnitude higher even.

The van der Waal bonds form a part of electrostatic interactions involving permanent/induced dipoles/multi-poles causing various types of permanent dipole-dipole, dipole-induced dipole, and induced dipole-induced dipole interactions also named as 'Keesom', 'Debye', and 'London' dispersion forces, respectively. Although, hydrogen/halogen bonds are also of the dipole-dipole interaction type, but are not included in van der Waals interactions [298]. For example, in dipole-dipole interaction, it is the electrostatic attraction between the dipoles of the two molecules, which try to align to reduce the potential energy in three different modes. Dipoles are generally but not limited to electronegative species like oxygen, nitrogen, sulfur, and fluorine. In case of acetone, for instance, it has a net dipole due to more electronegative oxygen than the carbon atom that is covalently bonded to it, and the electrons associated with this bond are closer to the oxygen than the carbon, creating a partial negative charge (δ^-) on the oxygen, and a partial positive charge (δ^+) on the carbon. They are not full charges because the electrons are still shared through a covalent bond between the oxygen and carbon atoms. The bond energies of C-O, C-C, C-H, C=C, and C=O are 340, 360, 430, 600, and 690 kJ/mol, respectively.

Exp. Theo. NANOTECHNOLOGY 3 (2019) 301-362

In a dipole-induced dipole type of interaction of Debye force, it is interaction between molecules approaching to nonpolar molecules with permanent dipoles. In such cases, the electrons of the nonpolar molecules are polarized either toward or away from the dipoles of the approaching molecule causing an attraction or a repulsion of the electrons from the nonpolar molecules, depending on the charge of the incoming dipole. Considering a dipole with a full or partial positive or negative charge approaching a nonpolar molecule, it will induce an attracting dipole with the correspondingly organized induced dipole. Atoms with larger atomic radii are considered more "polarizable" and therefore experience greater attraction.

London dispersion forces arise due to induced dipole-induced dipole interactions involving molecules that inherently do not possess permanent dipoles. They are the results of temporary repulsion of electrons away from the electrons of a neighboring molecule, leading to a partially positive dipole on one molecule and a partially negative dipole on another molecule. In this context, it has been noted in hexane, with no polarity or high electronegativity, is yet a liquid at room temperature because of London forces. Even though, these interactions are very weak and short-lived but are otherwise responsible for some nonpolar molecules to be liquid at room temperature.

6.1 Electrostatic Attraction and Repulsions

Considering the presence of the most common form of Coulomb force of attraction/repulsion between two charges q_1 , and q_2 separated by a distance r , where both are residing either on free ions or biomolecular subunits in a solution, the potential energy U is found to vary as $\propto q_1q_2/r$, which is a long-range interaction. The typical U values, in vacuum, are around $\sim 30 k_B T$ in case of two electrons separated by 2 nm distance, which reduces to $0.4 k_B T$ in an aqueous medium. In addition, the presence of mobile ions in a solution causes screening of the charge surfaces mainly because of clustering of the free ions, also known as counter-ions, where the strength and range of the Coulomb interactions is further reduced. These counter-ions are in close proximity with the charged objects with energies in excess of $\sim 5 k_B T$ and are not easily disrupted by thermal energy.

6.2 Dipolar Interactions

A number of molecules possess permanent dipoles because of their asymmetric distributions of the electron cloud around the positively charged nuclei while maintaining overall charge neutrality individually. For example, water molecule has a permanent dipole because the electron density is greater near the more electronegative O atom.

It is possible to estimate the potential energy of a dipole \vec{p} interacting with an electric field, free charges, permanent, and induced dipoles in the environment for assessing the relative importance of various noncovalent interactions.

For example, the potential energy of a dipole in presence of an electric field \vec{E} is $-pE \cdot \cos\theta$, where, θ is the angle between the vectors \vec{p} and \vec{E} .

Similarly, in case of interaction between a charge and a dipole, it is necessary to replace the electric field \vec{E} in earlier case of dipole-field interaction by the field produced by the point charge at a distance r from the charge i.e. $E = kq/r^2$. In this way, the potential energy of a charge-dipole system is $U = -k|q|\cos\theta/r^2$ falling off as $1/r^2$, more rapidly than the charge-charge system. For taking care of the angular dependence of the potential energy on θ it is necessary to apply averaging due to Brownian motion by taking into account the Boltzmann probability that the dipole makes an angle θ with the \vec{E} field as $\propto \exp(-U/k_B T)$; the average value of the potential energy is given below:

$$\langle U \rangle = -pE [\coth\{pE/k_B T\} - k_B T/pE] \quad (24)$$

Which, in the limiting case of $pU \ll k_B T$, simplifies to the following:

$$\langle U \rangle = -(kqp)^2 / 3k_B T r^4 \quad (25)$$

This clearly shows that the charge-dipole types of interaction fall off as $\propto 1/r^4$.

Following a similar approach for describing the interaction between two dipoles \vec{p}_1 and \vec{p}_2 ; the expression for potential energy reduces to the following form.

$$U = k \cdot (p_1 \cdot p_2 / r^3) \cdot F(\theta_1, \phi_1, \theta_2, \phi_2) \quad (26)$$

Where, $F(\theta_1, \phi_1, \theta_2, \phi_2)$ is an angular function dependent upon the positions of \vec{p}_1 and \vec{p}_2 . Carrying out the thermal averaging, as mentioned earlier and applying the condition of $U \ll k_B T$, it reduces to the following form:

$$\langle U \rangle = -2 [k^2 \cdot p_1^2 \cdot p_2^2] / 3k_B T r^6; \quad (27)$$

In this case, the potential energy between two dipoles falls off as $\propto 1/r^6$ power.

In case of a permanent dipole interacting with an induced dipole in another polarizable molecule involved in interaction, it is necessary to consider the potential energy involved in interaction of \vec{p}_1 with \vec{p}_2^* ; where \vec{p}_2^* is the induced dipole directed along the electric field \vec{E}_1 and the associated potential energy of interaction takes the form as:

$$U = -kp_1 p_2^* f(\theta) / r^3; \quad (28)$$

where, θ defines the angular position of \vec{p}_2^* relative to \vec{p}_1 . The magnitude of \vec{p}_2^* depends upon the strength of the electric field at position (r, θ) , so that $p_2^* = \epsilon_0 \alpha_2 \cdot E_1(r, \theta)$, and $\alpha_2 =$ polarizability of the second molecule. The following relation gives the interaction potential:

$$U = -\alpha_2 \cdot \epsilon_0 \cdot (kp_1)^2 f^2(\theta) / r^6, \quad (29)$$

where, it shows a $1/r^6$ type dependence on distance in absence of thermal averaging. Since \vec{p}_2^* always follows the instantaneous direction of the electric field \vec{E}_1 , the process of thermal averaging adds a constant factor giving $\langle U \rangle \sim 1/r^6$ as in case of dipole-dipole interactions.

In presence of a fluctuating electric field around each atom, a fluctuating dipole moment is natural to induce proportional to the polarizability of the atom. These instantaneously induced dipoles would result into an attractive potential having $\sim 1/r^6$ dependence.

In case, the atoms get too close, at some point there is a strong repulsion arising due to overlapping electron clouds and Pauli's exclusion principle, whereby filled electron shells of an atom cannot accommodate any more electrons. A general analytical form that lumps together all dipole-dipole interactions and includes both the attractive and the repulsive terms is described as the Lennard-Jones potential, where the repulsive term is approximated as having a $1/r^{12}$ dependence:

$$U(r) = U_0 \{r_0/r\}^{12} - 2U_0 \{r_0/r\}^6 \quad (30)$$

This form of the potential energy function has a minimum at $r = r_0$ with $U(r_0) = -U_0$.

Treating atoms as spheres, the van der Waals radius is a measure of how close another atoms can come before a strong, very short range, repulsive force sets in. Some typical values of r_0 in case of different types of atoms are as $\sim 0.12, 0.14, 0.16,$ and 0.2 nm, for hydrogen, oxygen, nitrogen, and carbon, respectively.

The most important interaction responsible for the structure and properties of water, as well as the biomolecules, is the hydrogen bond representing an interaction between a proton donor group D-H and a proton acceptor atom A. A *D-H-type bond* is strongly polar in which the electron density is primarily around the electronegative atom and the acceptor atom A is strongly electronegative.

In a hydrogen bond type of interaction, the distance between H and A is less than the sum of their respective van der Waals radii. The hydrogen bond is strongest in case of the three atoms D, H, and A have a collinear geometry. The hydrogen bond-strength in biological macromolecules lies in the range of $2 - 5k_B T$.

6.3 Hydrophobic Interactions

Exp. Theo. NANOTECHNOLOGY 3 (2019) 301-362

Hydrophobic interactions deciding the reorientations of water molecules in presence of natural clustering of hydrophobic species are necessary to understand about the changes taking place in enthalpy and entropy at molecular levels (Note-5). Hydrophobes, being nonpolar molecules with long chain of carbon atoms, do not interact with water molecules as seen in case of mixing of fat molecules in water. This phenomenon was discovered while examining the natural clumping up of the fat molecules in a water medium causing minimal contacts with water molecules.

Adding a hydrophobe in an aqueous medium breaks some hydrogen bonds between water molecules to accommodate the hydrophobe leading to an endothermic reaction, because bonds breaking generate heat. Water molecules that are distorted by the presence of the hydrophobe attempt form new hydrogen bonds resulting in a cage like structure called *clathrate* cage around the hydrophobe. This orientation makes the system (hydrophobe) more structured with decrease of the total entropy of the system; therefore ΔS is negative.

Depending upon the disruption of hydrogen bonds by the entry of the hydrophobes, the ΔH of the system can be negative, zero, or positive according to the make up for the partial, complete, or over compensations. The change in enthalpy, however, is insignificant in determining the spontaneity of the reaction (mixing of hydrophobic molecules and water) because the change in entropy ΔS is large. Thus according to Gibb's free energy formula: $\Delta G = \Delta H - T \cdot \Delta S$, with smaller unknown values of ΔH and large negative values of ΔS , the value of ΔG is positive. Consequently, the mixing of hydrophobes with water is nonspontaneous. During inter-hydrophobe interactions, the change in total free energy ΔG is negative as the changes in enthalpy and entropy are positive and negative, respectively, due to breakage of the clathrate cage hydrogen bonds. This confirms that inter-hydrophobe interactions are instantaneous in nature. Hydrophobic interactions are relatively stronger than other intermolecular forces like van der Waals interactions or hydrogen bonds.

6.4 The Phenomenon of Screening

The interaction of mobile ions with charged surfaces immersed in an aqueous solution is possible to analyze in form of a many-body-problem outlined here in brief using Poisson-Boltzmann (PB) equation [299]. While examining the interactions of the mobile ions present there in the solution, it is necessary to take into account the screening of the charged surfaces by the mobile ions present in the vicinity along with the local electric field produced by the charged surface expressed as:

$$E(x) = -\nabla \varphi(x).$$

The flow of drift and diffusion currents caused due to movement of the i -th species of the mobile ions with $Z_i e$ charge on each, is given as:

$$J_{drift}^i = -\mu Z_i e c_i \nabla \varphi; J_{diff}^i = -D \nabla c_i \quad (31)$$

In which, the mobile-ion density, mobility and diffusion coefficient are represented by c_i , μ , and D , respectively, beside connecting mobility and diffusion coefficient by Einstein's relationship given as $D = k_B T / \mu$. The total current due to the movement of mobile ion species is expressed as:

$$J_{Tot}^i = -c_i \mu \nabla [k_B T \ln(c_i / c_{i0}) + Z_i e \varphi] \quad (32)$$

By applying the boundary condition of the total current to be zero at thermal equilibrium, the value of c_i found to vary with distance as:

$$c_i(x) = c_{i0} \cdot \exp \left[-\frac{Z_i e \varphi(x)}{k_B T} \right], c_{i0} = c_i (@\varphi(x) = 0). \quad (33)$$

For finding out the potential energy in terms of the existing charge distribution, it is necessary to use the well-known Poisson's equation relating the potential $\varphi(x)$ to the total charge density $\rho(x)$ as given below:

$$\nabla^2 \varphi(x) = -[1/4\pi\epsilon] \rho(x) \quad (34)$$

Here, the total charge density is expressed as a sum of all mobile ions species and external fixed charges immersed in the solution described as:

$$\rho(x) = \sum_i Z_i e c_i(x) + \rho_{ext}(x). \quad (35)$$

Combining these charge distributions, the final equation reduces to the form as:

$$\nabla^2 \varphi(x) = - \sum_i (e/4\pi\epsilon) Z_i c_{i0} \exp\{-Z_i e c_i(x)/k_B T\} - (1/4\pi\epsilon) \rho_{ext}(x). \quad (36)$$

This kind of the Poisson-Boltzmann's equation describes the electrostatic potential variation in terms of mobile counterion density in space, subjected to the boundary conditions determined by the external charges and the overall charge neutrality condition, i.e. $-\int d^3x. \rho(x) = 0$. The general nature of the above-described equation is highly nonlinear, and the exact solutions are only sought in special cases, e.g. with planar and cylindrical symmetries. Before attempting to solve the above equation for specific geometries, it is convenient to convert the whole equation into a dimensionless form as given below. Multiplying by $e/k_B T$ and rescaling the potential $\varphi \rightarrow e\varphi/k_B T$, one can rewrite the above as:

$$\nabla^2 \varphi(x) + l_B \left[\sum_i Z_i c_{i0} \exp\{-Z_i \varphi(x)\} + \rho_{ext}(x)/e \right] = 0, \text{ and}$$

$$l_B = e^2/4\pi\epsilon k_B T \quad (37)$$

Where, $l_B =$ Bjerrum's length, at which, the electrostatic potential energy of a pair of charges equals their thermal energies. This is also described by two oppositely charged particles with magnitude e and separated by a distance r : they are "bound" if $r < l_B$, and ionized if $r > l_B$ (by thermal fluctuations). In an aqueous solution of dielectric constant $\epsilon = 80$ (H_2O) at room temperature, $l_B \approx 0.7nm$ giving some idea of the distances involved.

In an electrolyte medium, where, an equal number of positively and negatively charged particles of valence Z are there without any external fixed charges, the PB-equation reduces to:

$$-\nabla^2 \varphi(x) + 8\pi l_B Z c_B \sinh Z \varphi(x) = 0, \quad (38)$$

Where, c_B is the bulk ion density. The solution of this equation is trivial: i.e. $\varphi(x) = 0$, since the mean electric field vanishes in an overall neutral system of two uniform and independent charge distributions of opposite signs.

In order to understand correlations, it is helpful to single out a positive charged particle fixed at x' and consider the electrostatic potential at x by linearizing the above equation.

$$[-\nabla_x^2 + \kappa_s^2] G(x, x') = 4\pi Z^2 l_B \delta(x - x') \quad (39)$$

Where, $\kappa_s^2 = 8\pi l_B Z^2 c_B$. This is the *Debye-Hückel* (DH) equation, in which, the response function $G(x, x')$ should be regarded as a fluctuating potential at point x generated by the test charge in the presence of fluctuating charges around it and this is also called the Green's function, containing information about the correlations of the system. It can also be interpreted as the electrostatic interaction between two Ze test charges located at x and x' in the presence of the fluctuating ions in the bulk. It is noted that in the limit $c_B \rightarrow 0$, $G(x, x')$ reduces to the usual Coulomb's interaction. The Yukawa potential, as defined below, gives the solution to the above equation.

$$G(x, x') = [4\pi l_B Z^2 / |x - x'|] \exp\{-\kappa_s |x - x'|\} \quad (40)$$

Here, $1/\kappa_s$ defines the decay or screening length as the test charge is screened by the induced charges, which surround it. The screening length $1/\kappa_s$ associated is given as:

$$\kappa_s = \sqrt{4\pi l_B \sum_i Z_i c_{bi}}, \quad (41)$$

This classical parameter plays an important role in DH theory of electrolytes. Physically, due to accumulation of oppositely charged ion cloud near the test charge, the magnitude of its charge is screened and the potential decays exponentially with distance. For 1 mM of monovalent salt concentration, this screening length is ~ 10 nm.

It will be helpful to have some idea about the values of several parameters encountered during discussions. For example, the distance between two electrons, having Coulomb interaction energy of $k_B T$, is estimated from the relation: $r = k e^2 / (\epsilon k_B T)$ by substituting values of $k = 9 \times 10^9 N \cdot m^2 / C^2$, $\epsilon_0 = 1.6 \times 10^{-19} C$, $\epsilon = 80$, and $k_B T = 4 \times 10^{-21} J$, and this comes to 0.7 nm. This distance is often called the Bjerrum's length as defined earlier.

Exp. Theo. NANOTECHNOLOGY 3 (2019) 301-362

For appreciating the role of screening in studying the interaction of charged particle with the charged surfaces immersed in an electrolyte, it is necessary to define the volume considered. For example, in case of short-range interactions, where there is no other ion present in the vicinity, the Coulomb force is defined as: $kq_1q_2/\epsilon r$, which modifies to: $(q_1q_2/4\pi\epsilon r)$. $\text{Exp}(-\kappa_s r)$ in presence of screening provided by the mobile ions in the immediate vicinity of the charged surface. These two forces are correspondingly defined as short- and long-range forces and it is implicit that while considering short range interactions, the volume considered is such that there is no other charged ion present in the vicinity, but, in case of long-range interactions, there are sufficiently large number of mobile ions to screen the fixed surface charges immersed in the electrolyte. This Debye screening length is defined as: $1/l_D = \kappa_s = [4\pi l_B \sum Z_i c_{bi}]^{1/2}$. For a monovalent electrolyte like NaCl, this screening length is 0.3 nm for 1M solutions. The values of Debye's screening length are 0.3, 0.18 and 0.15 nm for 1:1, 2:1 and 2:2 electrolytes of Na^+ : Cl^- , Mg^{2+} : 2Cl^- and Mg^{2+} : SO_4^{2-} , respectively.

The surfaces of large proteins, nucleic acids, cell membranes, and many other surfaces relevant to biology, are often *charged*. The charged surfaces of these macromolecules, when immersed in solution where ions are present, will attract a thin 'atmosphere' of opposite-charge counter ions [299].

7. FORESEEABLE PATHWAYS OF NANOMATERIALS DEVELOPMENT IN FUTURE

Having studied the basic concepts of nano science in detail including the proof of concept the process of translating them into something practical has to go through two distinctly different stages of development termed as 'nano bulk' and 'nano world' according to the recommendations of the European Project of 'GENNESYS' (Grand European Initiative on Nano science and Nanotechnology using Neutron and Synchrotron Radiation Sources) after examining the Nanotechnology and the Future of Advanced Materials in detail [300].

In the 'nano bulk' category of nanomaterials development that has already started and is expected to continue for two decades, the nanomaterials would be prepared for their macro scale applications in which the macro scale objects are targeted instead of realizing nanoparticles, nanowires, DNA strand, or like that. For fabricating such components and devices the sizeable quantity of nanomaterials (solid, liquid or gas phase) is to be produced with their unique properties determined by their nanoscopic internal constituent structures. Some of the examples that highlight this stage of development include nano cosmetics, nano suspensions, nano emulsions, nano gels for drug and gene delivery applications besides nano composites (extraordinary mechanical properties) of automotive and infrastructure sectors to name only a few besides many more.

In order to meet the basic requirement of nano bulk development the major task ahead is to reduce the overall costs by using more cost effective and green synthesis of large quantity of nanoparticulate materials besides taking care of their storage and handling without contamination, degradation and agglomeration. In this context, a great support is anticipated from microbial route of nanoparticulate synthesis in some specific areas of applications.

While implementing the nano bulk stage of development, the most important parameter to consider is the process yield during cost effective mass scale production processes besides controlling uniformity, purity, toxicology, and stability. The current examples of semiconductor nano crystals production using solution-based processes, and vapor-phase bulk production of carbon nanotubes via arc-discharge or CVD highlight the scale-up potential of both liquid-phase and vapor-phase techniques for mass-scale nanomaterial synthesis.

A number of recommendations made in this useful project include the development of micro fluidics based continuous synthesis of nanomaterials in solution, cost effective bulk

nanomaterial production in vapor phase, and biochemical reaction based green synthesis of nanomaterials in bulk quantity in some specific areas [300].

In this context, it is necessary to develop the characterization strategies that are especially based on in-situ, real-time techniques dealing with non-destructive, high-resolution means of characterization while following the evolution of the synthesis process. The techniques that are useable include Raman, optical absorption and fluorescence, x-ray diffraction, transmission electron microscopy besides neutron scattering, high-resolution and high-sensitivity EXAFS or XPS based on synchrotron radiation.

Modeling and simulation tools for nanomaterials growths that are currently available include classical to density functional theory and molecular dynamics covering a large temporal and special scales necessary for describing the growth process.

The nano world stage of nanomaterials development anticipated in 15 – 40 years from now in the future would be a long-term vision aiming to take advantage of integrating the natural or induced diversity among nano blocks instead of nano components. In this context, the proposed synthesis strategy should have a very precise and independent degree of control over the structure of every single nano-object and/or the location where to assemble or grow it. The randomness of nano bulks must be replaced with a deterministic control at the nanoscale. The anticipated applications of the nano world approach would be to produce small objects, taking the advantageous features of in terms of high-integration, low power consumption, and non-invasive monitoring involving novel computing resources, with complex nano machines possessing a sort of embedded intelligence. Applications span from neural computing, sensing and ambient intelligence to nano machines for self-surgery and intelligent drug delivery [300]. Having reached to this level of development the emphasis will shift from preparing cost effective bulk quantities of nanomaterials towards fabricating an "intelligent" nano system with targeted functionalities by involving high precision synthesis and characterization technologies where the fundamental understanding of the process becomes priority instead of relying on empirical methods.

Consequent upon the basic requirement of nano world level of developments in terms of their highly deterministic precisions, the top-down approach would be combined with bottom-up strategies leading to "Hybrid Fabrication Methods" will be essential. The simplest example that can be cited here is to conceive about a combined method of depositing patterned catalysts on a substrate using top-down approach along with the deposition of nano wires and nano tubes using CVD method of bottom-up approach in the same run with controlled features producing active components grown from point to point in an intelligent fashion [300].

8. DISCUSSIONS

The current status of nano material syntheses based on the systematic development of the associated technologies along with the fundamental understanding of the related processes facilitated by numerous theoretical simulation techniques has reached to a stage where the basic requirements of nano bulk and nano world stages are getting clarified for ensuring the progress of the further developments. Now the question is to have a technology to produce a nano element with precise specifications by combining right kind of mixes of top-down and bottom-up approaches of nanoscience and technology already established. Now the stage has reached where deterministically precise controls of nano features are becoming necessary for the successful development of nano world based small system in the near future. This deterministic precision replacing random growth of features would certainly put a commensurate pressure on developing fundamental concepts accordingly. In other words, picking individual atomic and molecular species and placing them at the right locations with the help of molecular recognition based self-assembly would be almost essential for arriving at the desired precision as mentioned. This also necessitates using some form of biomimetic processes already

Exp. Theo. NANOTECHNOLOGY 3 (2019) 301-362

observed in nature to help in arriving at the goals in reasonable time frame. For the success of such a deterministic precision in-situ characterization techniques would be an essential component with the precision of handling atomic and molecular species during process growth as mentioned.

9. CONCLUSIONS

Realizing a large variety of the nanostructured entities to explore their additional features in terms of their characteristic properties arising out of the quantum confinements of electrons has been established during the last few years as can be seen from the brief descriptions included in this review. There are adequate proof of concept studies already reported to clarify the processes involved at atomic and molecular levels as highlighted in the discussions included here. The roles of engineered inorganic, organic and biomolecular materials have been highlighted with the help of experimental results corroborating the theoretical understanding of the processes involved. From these discussions it is amply clear that introduction of smart and intelligent features required for the development of the products for the nano world domain would be foreseeable to achieve in the anticipated form in near future. Learning from the study of biomimetic processes taking place in natural form would provide additional support in accelerating the progress in this direction.

ACKNOWLEDGEMENTS

The stay of the author at Hamdard University, New Delhi, India, and interactions with the learned faculty there triggered the interest of examining the biological processes on the basis of engineered nanomaterials particularly derived from phytochemical origin. While pursuing this approach the essential touch of technological considerations has always been there in the background as can be seen from the inclusion of these aspects discussed in the main text. Particularly, the author's involvement in the industrial applications of engineered nanomaterials while working with Center of Excellence in Nanotechnology provided the required impetus to examine these aspects of nanomaterials in detail. These studies undertaken during last 10 years have resulted into a number of publications and the current one is one of those as mentioned. The author acknowledges the encouragement and support extended by the scientists and academics wholeheartedly. The excellent academic environment provided by Hamdard University, New Delhi, and CII Center of Excellence in Nanotechnology, Ahmedabad, has been extremely useful in pursuing a rather involved area of nano science and technology.

References

- [1] S. Ahmad, *Microwave and Millimeter wave semiconductor materials technology*, Tata-McGrawHill, N. Delhi, (1998)
- [2] C. Kittel, *Introduction to Solid State Physics*, 8th Edition, John Wiley & Sons, Inc., (2004)
- [3] Y. Yin, A. P. Alivisatos, *Nature* 437 (2005) 664
- [4] D. V. Talapin, J.-S. Lee, M. V. Kovalenko, E. V. Shevchenko, *Chem. Rev.* 110(1) (2010) 389
- [5] B. Diaconescu, L. A. Padilha, P. Nagpal, B. S. Swartzentruber, V. I. Klimov, *Phys. Rev. Lett.* 110 (2013) 127406
- [6] S. Ahmad, *Ind. J. Engineering and Material Science* 12 (2005) 299
- [7] S. Ahmad, *Int. J. Nanoelectronics and Materials* 8 (2015) 129
- [8] S. Ahmad, *Int. J. Material Science* 6(1) (2016)
- [9] S. Ahmad, *J. Nano pharmaceuticals and Drug Delivery* 3(1) (2016) 1

- [10] T. Jevremovic, *Nuclear Principles in Engineering*, Chapter 2, Atomic Structure, Springer US; Springer Science+Business Media, LLC (2009).
- [11] Chemistry LibreTexts, *The Atomic Spectrum of Hydrogen*; Text available @ https://chem.libretexts.org/LibreTexts/Solano_Community_College/Chem_160/Chapter_07%3A_Atomic_Structure_and_Periodicity/7.03_The_Atomic_Spectrum_of_Hydrogen
- [12] H. B. Gray, *Electrons and Chemical Bonding*, W. A. Benjamin, Inc. New York. (1965); <http://resolver.caltech.edu/CaltechBOOK:1965.003>
- [13] *MO-Theory*, R. S. Mulliken Lecture, December 12, (1966). Text @ www.nobelprize.org/nobel_prizes/chemistry/laureates/1966/mulliken-lecture.pdf
- [14] M. O. Scully, R. E. Allen, Y. Dou, K. T. Kapale, M. Kim, G. Chen A. Svidzinsky. *Chemical Physics Letters* 389 (2004) 385
- [15] D. Sprecher, C. Jungen, W. Ubachs, F. Merkt, *Faraday Discussions* 150 (2011) 51.
- [16] P. Atkins, R. Friedman, *Molecular Quantum Mechanics*, Fourth Edition; Oxford University Press, Great Clarendon Street, Oxford AC OX2 6DP
- [17] M. Orchin, R. S. Macomber, A. R. Pinhas, R. M. Wilson, *The Vocabulary and Concepts of Organic Chemistry, 2nd ed.*; Wiley-Interscience: Hoboken, NJ, (2005)
- [18] M. Ratner, *Nature Nanotechnology* 8(6) (2013) 378
- [19] Y. Chen¹, G.-Y. Jung, D. A. A. Ohlberg, X. Li, D. R. Stewart, J. O Jeppesen, K. A. Nielsen, J. F. Stoddart, R. S. Williams, *Nanotechnology* 14 (2003) 462
- [20] Polar Covalent Bonds: Electronegativity, *Lecture Notes* available @ www.csus.edu/indiv/s/spencej/chem%2031%20summer%2014%20web/day%202%20lecture.pdf
- [21] S. Richard, F. Aniel, G. Fishman, *Phys. Rev. B* 70 (2005) 235204; Erratum *Phys. Rev. B* 71 (2005) 169901
- [22] R. Koole, G. Allan, C. Delerue, Andries Meijerink, D. I. Vanmaekelbergh, A. J. Houtepen, *small* 4(1) (2008) 127
- [23] T. C. Fischer, D. M. Crenshaw, S. B. Kraemer, H. R. Schmitt, R. F. Mushotsky, J. P. Dunn, *Astrophys. J.* 727(71) (2011)
- [24] X. D. Pi, R. W. Liptak, J. D. Nowak, N. P. Wells, C. B. Carter, S. A. Campbell, U. Kortshage, *Nanotechnology* 19 (24) (2008) 245603
- [25] O. V. Prezhdo, *Acc. Chem. Res.*, 42 (2009) 2005
- [26] C. M. Isborn, O. V. Prezhdo, *J. Phys. Chem. C*, 113 (2009) 12617
- [27] T. C. Fischer, D. M. Crenshaw, S. B. Kraemer, H. R. Schmitt, M. L. Trippe, *Astron. J.* 140(2) (2010)
- [28] D. J. Norris, A. L. Efros, S. C. Erwin, *Science* 319(5871) (2008) 1776
- [29] B. G. Lee, J. W. Luo, N. R. Neale, M. C. Beard, D. Hiller, M. Zacharias, P. Stradins, A. Zunger, Quasi-Direct Optical Transitions in Silicon Nanocrystals with Intensity Exceeding the Bulk, *Nano Lett.* 16(3) (2016) 1583
- [30] M. G. Bawendi, M. L. Steigerwald, L. E. Brus, *Annu. Rev. Phys. Chem.* 41 (1990) 477
- [31] S. I. Stoeva, B. L. V. Prasad, S. Uma, P. K. Stoimenov, V. Zaikovski, C. M. Sorensen, K. J. Klabunde, *J. Phys. Chem. B* 107 (30) (2003): 7441
- [32] C. Petit, Z. L. Wang, and M. P. Pileni, *J. Phys. Chem. B* 109 (2005) 15309
- [33] G. Zheng, MRS Spring Meeting, *MRS Proc.* 924 (2006)
- [34] M. P. Pileni, *J. Phys.: Condens. Matter* 23 (2011) 503102
- [35] Y. Mi, D. Yuan, Y. Liu, J. Zhang, Y. Xiao, *Mater. Chem. and Phys.* 89(2–3) (2005) 359
- [36] R. M. A. Tehrani, S. A. Ghani, *J. Colloid and Inter. Sci.* 339(1) (2009) 125
- [37] S. Bera, I. Manna. *J. Alloys & Compounds*, 417(1–2) (2006) 104
- [38] Z. Zhao, K. Zhang, J. Zhang, K. Yang, C. He, F. Dong, B. Yang, *Colloids and Surfaces A: Physicochem. Eng. Aspects* 355 (2010) 114

Exp. Theo. NANOTECHNOLOGY 3 (2019) 301-362

- [39] X. Huang, S. Li, Y. Huang, S. Wu, X. Zhou, S. Li, C. L. Gan, F. Boey, C. A. Mirkin, H. Zhang, *Nature Communications* 2, Article number: 292 (2011)
- [40] H.-W. Ting, Y.-K. Lin, Y.-J. Wu, L.-J. Chou, C.-J. Tsai, L.-J. Chen. *J. Mater. Chem. C* 1 (2013) 3593
- [41] B. Wang, S. Yin, G. Wang, A. Buldum, J. Zhao, *Phys Rev. Lett.* 86(10) (2001) 2046
- [42] N. Zhou, D. Li, D. Yang, *Nanoscale Research Letters* 9 (2014) 302
- [43] M. Brack, *Rev. Mod. Phys.* 65 (1993) 677
- [44] M. A. El-Syed, *Acc. Chem. Research* 34(4) (2001) 257
- [45] P. Jena, A. W. Castleman Jr., *PNAS* 103(28) (2006) 10560
- [46] E. G. Noya, J. P. K. Doye, D. J. Wales, and A. Aguado, *Eur. Phys. J. D* 43 (2007) 57
- [47] X. Li, A. E. Kuznetsov, H.-F. Zhang, A. I. Boldyrev, L.-S. Wang, *Science* 291 (2001) 859
- [48] H. Bai, H. J. Zhai, S. D. Li, L. S. Wang, *PhysChemChemPhys.* 15(24) (2013) 9646
- [49] X. Zhang, G. Liu, G. Ganteför, K. H. Bowen, A. N. Alexandrova, *J. Phys. Chem. Lett.* 5 (2014) 1596
- [50] A. L. Roest, A. J. Houtepen, J. J. Kelly, D. Vanmaekelbergh, *Faraday Discuss.* 125 (2004) 55
- [51] T. Wang, J. Zhuang, J. Lynch, O. Chen, Z. Wang, X. Wang, D. LaMontagne, H. Wu, Z. Wang, Y. C. Cao, *Science* 338(6105) (2012) 358
- [52] C. B. Murray, C. R. Kagan, M. G. Bawendi, *Science* 270(5240) (1995) 1335
- [53] C. T. Black, C. B. Murray, R. L. Sandstrom, S. Sun, *Science* 290(5494) (2000) 1131
- [54] S. Sun, C. B. Murray, D. Weller, L. Folks, A. Moser, *Science* 287(5460) (2000) 1989
- [55] Y. Yin, Y. Xia, *J. Am. Chem. Soc.* 125(8) (2003) 2048
- [56] Z. Tang, Z. Zhang, Y. Wang, S. C. Glotzer, N. A. Kotov, *Science* 314(5797) (2006) 274
- [57] A. Tao, P. Sinsersuksakul, P. Yang, *Nat. Nanotechnol* 2(7) (2007) 435
- [58] M. Rycenga, J. M. McLellan, Y. Xia, *Adv. Mater.* 20(12) (2008) 2416
- [59] Z. Quan, J. Fang, *Nano Today* 5(5) (2010) 390
- [60] Y. Xia, T. D. Nguyen, M. Yang, B. Lee, A. Santos, P. Podsiadlo, Z. Tang, S. C. Glotzer, N. A. Kotov, *Nat. Nanotechnol.* 6(9) (2011) 580
- [61] R. J. Macfarlane, M. R. Jones, B. Lee, E. Auyeung, C. A. Mirkin, *Science* 341(6151) (2013) 1222
- [62] C. Knorowski, S. Burleigh, A. Travasset, *Phys. Rev. Lett.* 106(21) (2011) 21550
- [63] P. F. Damasceno, M. Engel, S. C. Glotzer, *Science* 337(6093) (2012) 453
- [64] A. P. Kaushik, P. Clancy, *J. Comput. Chem.* 34(7) (2013) 5232
- [65] Z. Quan, D. Wu, J. Zhu, W. H. Evers, J. M. Boncella, L. D. A. Siebbeles, Z. A. Navrotsky, H. Xu, *PNAS* 111(25) (2014) 9054
- [66] B. Wang, S. Yin, G. Wang, A. Buldum, J. Zhao, *Phys Rev. Lett.* 86(10) (2001) 2046
- [67] A. A. Middleton, N. S. Wingreen. *Phys. Rev. Lett.* 71 (1993), 3198
- [68] R. P. Andres, T. Bein, M. Dorogi, S. Feng, J. I. Henderson, C. P. Kubiak, W. Mahoney, R. G. Osifchin, R. Reifenberger, *Science* 272 (1996) 1323
- [69] H. Bach, N. Neuroth (*Editors*), *The Properties of Optical Glass*. Schott Series on Glass and Glass Ceramics, Springer-Verlag Berlin Heidelberg, Springer-Verlag Berlin Heidelberg (1998)
- [70] B. O'Regan, M. Graetzel, *Nature* 353 (1991) 737
- [71] L. Cao, H. Chen, M. Wang, J. Sun, X. Zhang, F. Kong, *J. Phys. Chem. B* 106 (35) (2002) 8971
- [72] V. L. Colvin, M. C. Schlamp, A. P. Alivisatos, *Nature* 370 (1994) 354
- [73] B. O. Dabbousi, J. Rodriguez-Viejo, F. V. Mikulec, J. R. Heine, H. Mattoussi, R. Ober, K. F. Jensen, M. G. Bawendi, *J. Phys. Chem. B* 101 (1997) 9463.
- [74] M. V. Artemyev, V. Sperling, U. Woggon, *J. Appl. Phys.* 81 (1997) 6975

- [75] M. C. Schlamp, X. Peng, A. P. Alivisatos, *J. Appl. Phys.* 82 (1997) 5837
- [76] S. Yakunin, D. N. Dirin, L. Protesescu, M. Sytnyk, S. Tollabimazraehno, M. Humer, F. Hackl, T. Fromherz, M. I. Bodnarchuk, M. V. Kovalenko, W. Heiss, *ACS Nano.* 8(12) (2014) 12883
- [77] M. V. Artemyev, A. I. Bibik, L. I. Gurinovich, S. V. Gaponenko, H. Jaschinski, U. Woggon, *Phys. Stat. Sol. (b)* 224(2) (2001) 393
- [78] M. V. Artemyev, U. Woggon, H. Jaschinski, L. I. Gurinovich, S. V. Gaponenko, *J. Phys. Chem. B* 104 (2000) 11617
- [79] M. V. Artemyev, A. I. Bibik, L. I. Gurinovich, S. V. Gaponenko, U. Woggon, *Phys. Rev. B* 60 (1999) 1504
- [80] B. S. Kim, M. A. Islam, L. E. Brus, I. P. Hermana, *J. App. Phys.* 89(12) (2001) 812
- [81] A. M. Smith, S. Nie, *Acc. Chem. Res.* 43(2) (2010) 190
- [82] F. Rioux, A Molecular Orbital Approach to Bonding in Methane; Text available @ www.users.csbsju.edu/~frioux/h2bond/MethaneMOBonding.pdf
- [83] W.R. Salaneck, R. H. Friend, J. L. Breddas, *Physics Reports* 319 (1999) 231
- [84] D. K. Seo, R. Hoffmann, *J. Solid State Chem.* 147(1)(1999) 26
- [85] R. Hoffmann, C. Janiak, C. Kollmar, *Macromolecules* 24(13) (1991) 3725
- [86] N Tessler, S. C. Graham, R. H. Friend, *Phys. Rev. B* 57 (20) (1998) 12951
- [87] M. P. Samanta, W. Tian, S. Datta, J. I. Henderson, C. P. Kubiak, *Phys Rev B Condens Matter* 53(12) (1996) R7626
- [88] J. L. Brédas, J. P. Calbert, D. A. da Silva Filho, J. Cornil, *PNAS* 99(9) (2002) 5804
- [89] A. J. Heeger, S. Kivelson, J. R. Schrieffer, W. P. Su. *Rev. Mod. Phys.* 60 (1988) 781,
- [90] S. Ahmad, O. P. Daga, W. S. Khokle, *Phys. Stat. Solidi. B* 40(2) (1970) 631
- [91] S. J. F. Byrnes, (2008); Text available @ www.scribd.com/document/47249066/Basic-theory-and-phenomenology-of-polarons-2008
- [92] M. A. Littlejohn, J. R. Hauser, T. H. Glisson, *Solid-State Electronics* 21(1) (1978) 107
- [93] S. Hoshi, M. Itoh, T. Marui, H. Okita, Y. Morino, I. Tamai, F. Toda, S. Seki, T. Egawa, *The Japan Society of Applied Physics, Appl. Phys. Express* 2(6)(2009)
- [94] Chapter 9, *Two Dimensional Electron Gas, Quantum Wells & Semiconductor Superlattices*; Text available @ http://web.mit.edu/6.732/www/new_part1b.pdf
- [95] J. Roncali, Molecular Engineering of the Band Gap of π -Conjugated Systems: Facing Technological Applications, *Macromol. Rapid Commun.* 28(2007) 1761
- [96] R. Gutzler, *Phys. Chem. Chem. Phys.* 18 (2016) 29092
- [97] C. K. Chiang, C. R. Fincher, Jr., Y. W. Park, A. J. Heeger, H. Shirakawa, E. J. Louis, S. C. Gau, Alan G. MacDiarmid, *Phys. Rev. Lett.* 39 (1977) 1098
- [98] J. Roncali, *Chem. Rev.* 92 (1992) 711e738
- [99] J. J. M. Halls, C. A. Walsh, N. C. Greenham, E. A. Marseglla, R. H. Friend, S. C. Moratti, A. B. Holmes, *Nature* 3776 (1995) 498
- [100] H. S. O. Chan, S. C. Ng, *Prog. Polym. Sci.* 23 (1998) 1167
- [101] A. Kraft, A. C. Grimsdale, A. B. Holmes, *Angew. Chemie. Int. Edition* 37(4) (1998) 402
- [102] J. Roncali, *J. Mater. Chem.* 9 (1999) 1875
- [103] R. H. Friend, R. W. Gymer, A. B. Holmes, J. H. Burroughes, R. N. Marks, C. Taliani, D. D. C. Bradley, D. A. Dos Santos, J. L. Brédas, M. Lögdlund, W. R. Salaneck, *Nature* 397 (1999) 121
- [104] D. L. Ellis, M. R. Zakin, L. W. Bernstein, M. F. Rubner, *Anal. Chem.* 68(5) (1996) 816
- [105] C. E. Schmidt, V. R. Shastri, J. P. Vacanti, R. Langer, *Proc. Natl. Acad. Sci. USA* 94 (1997) 8948
- [106] K. J. Albert, N. S. Lewis, C. L. Schauer, G. A. Sotzing, S. E. Stitzel, T. P. Vaid, D. R. Walt, *Chem. Rev.* 100(7) (2000) 2595
- [107] D. T. McQuade, A. E. Pullen, T. M. Swager, *Chem. Rev.* 100(7)(2000) 2537

Exp. Theo. NANOTECHNOLOGY 3 (2019) 301-362

- [108] C. A. Thomas, Dissertation presented to Graduate School of University of Florida for PhD degree, 2002.
- [109] H. Ishii, K. Sugiyama, E. Ito, K. Seki, *Adv. Mater.* 11(8) (1999) 605
- [110] J. Roncali, *Chem. Rev.* 97 (1997) 173
- [111] F. Wudl, M. Kobayashi, A. J. Heeger, *J. Org. Chem.* 49 (1984) 3382
- [112] M. Kobayashi, N. Colaneri, M. Boysel, F. Wudl, A. J. Heeger, *J. Chem. Phys.* 82 (1985) 5717
- [113] Q. T. Zhang, J. M. Tour, *J. Am. Chem. Soc.* 120(22) (1998) 5355
- [114] Y. Yao, Q. T. Zhang, J. M. Tour. *Macromolecules* 24 (1998) 8600
- [115] D. Hu, J. Yu, K. Wong, B. Bagchi, P. J. Rossky, P. F. Barbara, *Nature* 405 (2000) 1030.
- [116] R. C. Smith, H. Deng, W. M. Fischer, D. L. Gin, *Mater. Res. Soc. Symp. Proc.* 488 (1998) 419
- [117] E. W. Havinga, E. E. ten Hoeve, H. Wynberg, *Synt. Metals* 55(1) (1993) 299
- [118] J. Hou, M.-H. Park, S. Zhang, Y. Yao, L.-M. Chen, J.-H. Li, Y. Yang, *Macromolecules* 41 (2008) 6012
- [119] H. Zgou, S. Boussaidi, A. Zahlou, M. Bouachrine, M. Hamidi, *Int. J. Adv. Res. in Comp. Sci. and Software Engg.* 4(5) (2014) 10
- [120] O. A. Shenderova, V. V. Zhirnov, and D. W. Brenner, *Crit. Rev. Solid State Mater. Sci.* 27 (2002) 227
- [121] F. Schwierz, *Nature Nanotechnology* 5 (2010) 487
- [122] J. W. A. van der Velden, F. A. Vollenbroek, J. J. Bour, P. I. Beurskens, J. M. M. Smits, W. P. Bosman, J. R. Neth, *Chem. Soc.* 100 (1981) 148
- [123] C. E. Briant, B. R. C. Theobald, J. W. White, C. K. Bell, D. M. P. Mingos, *J. Chem. Soc., Chem. Comm.* (1981) 201
- [124] G. Schmid, R. Boese, R. Pfeil, F. Bandermann, S. Meyer, G. H. M. Calis, J. W. A. van der Velden, *Chem. Ber.* 114 (1981) 3634
- [125] H. H. A. Smit, R. C. Thiel, L. J. de Jongh, *Z. Phys. D* 12 (1989) 193
- [126] M. C. Fairbanks, R. E. Benfield, R. J. Newport, G. Schmid, *Solid State Comm.* 73 (1990) 431
- [127] P. D. Cluskey, R. J. Newport, R. E. Benfield, S. J. Gurmman, G. Schmid, *Z. Phys. D* 26 (1993) 8
- [128] G. Schmid, R. Pugin, Th. Sawitowski, U. Simon, B. Marler, *Chem. Commun.* (1999) 1303
- [129] G. Schmid, B. Corain, *Eur. J. Inorg. Chem.* (2003) 3081
- [130] B. K. Teo, X. Shi, H. Zhang, *J. Am. Chem. Soc.* 114 (1992) 2743
- [131] P. D. Jadzinsky, G. Calero, C. J. Ackerson, D. A. Bushnell, R. D. Kornberg, *Science* 318(5849) (2007) 430
- [132] M. W. Heaven, A. Dass, P. S. White, K. M. Holt, R. W. Murray, *J. Am. Chem. Soc.* 130(12) (2008) 3754
- [133] H. Qian, W. T. Eckenhoff, Y. Zhu, T. Pintauer, R. Jin, *J. Am. Chem. Soc.* 132(24) (2010) 8280
- [134] B. G. Wang, X. B. Wang, W. J. Lou, J. C. Hao, *J. Colloid Interface Sci.* 362 (2011) 5
- [135] V. Myshlyavtsev, P. V. Stishenko, *Adsorption* 19(2-4) (2013) 795
- [136] B. Fresch, F. Remacle, *J. Phys. Chem. C* 118 (18) (2014) 9790
- [137] G. Corthey, J. A. Olmos-Asar, G. Casillas, M. M. Mariscal, S. Mejía-Rosales, J. C. Azcárate, E. Larios, M. José-Yacamán, R. C. Salvarezza, M. H. Fonticelli, *J. Phys. Chem. C*, 2014, 118 (42) (2014) 24641
- [138] N. Jian, R. E. Palmer, *J. Phys. Chem. C* 119 (20) (2015) 11114
- [139] H.-G. Boyen, G. Kästle, F. Weigl, B. Koslowski, C. Dietrich, P. Ziemann, J. P. Spatz, S. Riethmüller, C. Hartmann, M. Möller, G. Schmid, M. G. Garnier, P. Oelhafen, *Science* 297 (2002) 1533

- [140] Y. L. Mikhlina, E. A. Vishnyakova, A. S. Romanchenkoa, S. V. Saikova, M. N. Likhatski, Y. V. Larichevc, F. V. Tuzikov, V. I. Zaikovskii, S. M. Zharkov, *Appl. Surf. Sci.* 297 (2014) 75
- [141] H. Li, H.-J. Xiao, T.-S. Zhu, H.-C. Xuan, M. Li, *J. Phys. Chem. C* 119 (21) (2015) 12002
- [142] J. D. Aiken III, R. G. Finke, *J. Mole. Catalysis A - Chemical* 145(1-2) (1999) 1
- [143] A. Kraynov, T. E. Müller (2011). *Concepts for the Stabilization of Metal Nanoparticles in Ionic Liquids, Applications of Ionic Liquids in Science and Technology*, S. Handy (Editor), ISBN: 978-953-307- 605-8.
- [144] E. J. Verwey, J. T. G. Overbeek, *Theory of the stability of lyophobic colloids*, Elsevier, Amsterdam, (1948).
- [145] J. Lekner, *Proc. R. Soc. A* 468 (2012) 2829
- [146] A. M. Kalsin, M. Fialkowski, M. Paszewski, S. K. Smoukov, K. J. M. Bishop, B. A. Grzybowski, *Science* 312 (2006) 420
- [147] R. Klajn, K. J. M. Bishop, M. Fialkowski, M. Paszewski, C. J. Campbell, T. P. Gray, B. A. Grzybowski, *Science* 316 (2007) 261
- [148] R. Klajn, P. J. Wesson, K. J. M. Bishop, B. A. Grzybowski, *Ange. Chem. Int. Edition* 48 (38) (2009) 7035
- [149] H. Bönemann, W. Brijoux. (1996). Chapter 9. *Catalytically Active Metal Powders and Colloids*. In: *Active Metals: Preparation Characterization Applications* (Editor: A. Fürstner), Wiley-VCH, Weinheim.
- [150] J. Ruhe, M. Ballauff, M. Biesalski, P. Dziezok, F. Grohn, D. Johannsmann, N. Houbenov, N. Hugenberg, R. Konradi, S. Minko, M. Motornov, R. R. Netz, M. Schmidt, C. Seidel, M. Stamm, T. Stephan, D. Usov, H. N. Zhang, *Polyelectrolyte Brushes*. In: *Polyelectrolytes with Defined Molecular Architecture I*. M. Schmidt, (Ed.), *Advances in Polymer Science* 165 (2004) 79.
- [151] S. Creutz, R. Jerome, *Langmuir* 15 (1999) 7145
- [152] H. Mori, A. H. E. Muller, J. E. Klee, *J. Amer. Chem. Soc.* 125 (2003) 3712
- [153] H. Mori, M. G. Lanzendorfer, A. H. E. Muller, J. E. Klee, *Langmuir* 20 (2004) 1934
- [154] S. Forster, V. Abetz, A. H. E. Muller (2004). *Polyelectrolyte Block Copolymer Micelles*. In: *Polyelectrolytes with Defined Molecular Architecture II*, M. Schmidt, (Ed.), *Advances in Polymer Science* 166, 173
- [155] G. Sharma, M. Ballauff, *Macromolecular Rapid Comm.* 25 (2004) 547
- [156] Y. Mei, G. Sharma, Y. Lu, M. Ballauff, M. Drechsler, T. Irrgang, R. Kempe, *Langmuir* 21 (2005) 12229
- [157] Y. Mei, Y. Lu, F. Polzer, M. Ballauff, M. Drechsler, *Chem. Mater.* 19 (2007) 1062
- [158] S. Proch, Y. Mei, J. M. R. Villanueva, Y. Lu, A. Karpov, M. Ballauff, R. Kempe, *Adv. Synthesis & Catalysis* 350 (2008) 493
- [159] J. Kiwi, M. Grätzel, *J. Amer. Chem. Soc.* 101 (1997) 7214
- [160] H. Bönemann, W. Brijoux, *Euro. J. Inorg. Chem.* 10 (2001) 2455
- [161] M. T. Reetz, W. Helbig, S. A. Quaiser, Chapter 7, *Electrochemical Methods in the Synthesis of Nanostructured Transition Metal Clusters*. In: *Active Metals: Preparation Characterization Applications* (Editor: A. Fürstner), VCH, Weinheim, (1996)
- [162] J. Dupont, G. S. Fonseca, A. P. Umpierre, P. F. Fichtner, S. R. Teixeira, *J. Am. Chem. Soc.* 124(16) (2002) 4228
- [163] K. S. Kim, D. Demberelnyamba, H. Lee, *Langmuir* 20 (2004) 556
- [164] S. Gao, H. Zhang, X. Wang, W. Mai, C. Peng, L. Ge, *Nanotechnology* 16 (2005) 1234
- [165] R. Marcilla, D. Mecerreyes, I. Odriozola, J. A. Pomposo, J. Rodriguez, I. Zalakain, I. Mondragon, *Nano.* 2 (2007) 169
- [166] N. Shalkevich, W. Escher, T. Burgi T, B. Michel, L. Si-Ahmed, D. Poulidakos, *Langmuir* 26 (2009) 663

Exp. Theo. NANOTECHNOLOGY 3 (2019) 301-362

- [167] Y. P. Zheng, J. X. Zhang, L. Lan, P. Y. Yu, R. Rodriguez, R. Herrera, D. Y. Wang, E. P. Giannelis, *ChemPhysChem*. 11 (2010) 61
- [168] B. Wang, M. Liu, Y. Wang, X. Chen, *J. Phys. Chem. C* 115 (23) (2011) 11374
- [169] H. Zhang, C. Hua, S. Yao, K. Zhang, H. Tao, H. Meng, *Nanoscale Res. Lett.* 7(1) (2012) 583
- [170] B. Zhang, N. Yan, *Catalysts* 3 (2013) 543
- [171] J. W. Sun, L. W. Wang, W. E. Buhro, *J. Am. Chem. Soc.* 130 (2008) 7997
- [172] E. C. Scher, L. Manna, A. P. Alivisatos, *Philos. Trans. R. Soc. London, Ser. A* 361 (2003) 241
- [173] S. Ithurria, B. Dubertret, *J. Am. Chem. Soc.* 130 (2008) 16504
- [174] S. Pokrant, K. B. Whaley, *Eur. Phys. J. D* 6 (1999) 255
- [175] D. F. Underwood, T. Kippeny, S. J. Rosenthal, *J. Phys. Chem. B* 105 (2001) 436
- [176] C. B. Murray, D. J. Norris, M. G. Bawendi, *J. Am. Chem. Soc.* 115 (1993) 8706
- [177] M. Ghali, K. Ohtani, Y. Ohno, H. Ohno, *Nature Comm.* 3, Article number: 661 (2012)
- [178] R. E. Acosta, A. Zapata, C.A. Duque, M. E. Mora-Ramos, *Physica E: Low-dimensional Systems and Nanostructures.* 44(9) (2012) 1936
- [179] A. P. Alivisatos, *J. Phys. Chem.* 100 (2996) 13226.
- [180] S. H. Tolbert, A. P. Alivisatos, *Ann. Rev. Phys. Chem.* 46 (1995) 595
- [181] M. A. Hines, P. Guyot-Sionnest, *J. Phys. Chem* 100 (1996) 468
- [182] J. McBride, J. Treadway, L. C. Feldman, S. J. Pennycook, S. J. Rosenthal, *Nano Lett.* 6 (2006) 1496
- [183] R. E. Bailey, S. M. Nie, *J. Am. Chem. Soc.* 125 (2003) 7100
- [184] X. H. Zhong, Y. Y. Feng, W. Knoll, M. Y. Han, *J. Am. Chem. Soc.* 125 (2003) 13559
- [185] S. Kim, B. Fisher, H. J. Eisler, M. Bawendi, *J. Am. Chem. Soc.* 125 (2003) 11466
- [186] S. Kumar, M. Jones, S. S. Lo, G. D. Scholes, *small* 3 (2007) 1633
- [187] L. T. Canham, *Appl. Phys. Lett.* 57 (1990) 1046
- [188] H. Takagi, H. Ogawa, Y. Yamazaki, A. Ishizaki, T. Nakagiri, *Appl. Phys. Lett.* 56 (1990) 2379
- [189] H. Morizaki, F. W. Ping, H. Ono, K. Yazawa, *J. Appl. Phys.* 70 (1991) 1869
- [190] K. A. Littau, P. J. Szajowski, A. J. Muller, A. R. Kortan, L. E. Brus, *J. Phys. Chem.* 97 (1993) 1224
- [191] X.-N. Liu, X.-W. Wu, X.-M. Bao, Y.-L. He, *Appl. Phys. Lett.* 64 (1994) 220
- [192] P. D. Milewski, D. J. Lichtenwalner, P. Mehta, A. I. Kingon, D. Zhang, R. M. Kolbas, *J. Electron Mater.* 23 (1994) 57
- [193] S. Nozaki, S. Sato, H. Ono, H. Morisaki, *Mater. Res. Soc. Symp. Proc.* 351 (1994) 399
- [194] A. A. Seraphin, S.-T. Ngiam, K. D. Kolenbrander, *J. Appl. Phys.* 80 (1996) 6429
- [195] V. G. Baru, S. Bayliss, L. Zaharov, *Yu. Microelectron, Eng.* 36 (1997) 111
- [196] A. Frojtik, H. Weller, S. Fiechter, A. Henglein, *Chem. Phys. Lett.* 134 (1987) 477
- [197] S. Iijima, *Jpn. J. Appl. Phys.* 26 (1987) 357
- [198] S. Iijima, *Jpn. J. Appl. Phys.* 26 (1987) 365
- [199] M. F. Jarrold, *Science* 252 (1991) 1085
- [200] J. R. Heath, *Science* 258 (1992) 1131
- [201] J. L. Heinrich, C. L. Curtis, G. M. Credo, K. L. Kavamagh, M. J. Sailor, *Science* 255 (1992) 66
- [202] J. M. Hunter, J. L. Fye, M. F. Jarrold, J. E. Bower, *Phys. Rev. Lett.* 73 (1994) 2063
- [203] R. A. Bley, S. M. Kauzlarich, *J. Am. Chem. Soc.* 118 (1996) 12461
- [204] R. A. Bley, S. M. Kauzlarich, H. W. H. Lee, *Chem. Mater.* 8 (1996) 1881
- [205] W. L. Wilson, P. F. Szajowski, L. E. Brus, *Science* 262 (1993) 1242
- [206] D. Zhang, R. M. Kolbas, J. M. Zavada, *Appl. Phys. Lett.* 65 (1994) 2684
- [207] L.-W. Wang, A. Zunger, *J. Chem. Phys.* 100 (1994) 2394
- [208] L.-W. Wang, A. Zunger, *J. Phys. Chem.* 98 (1994) 2158

- [209] M. Hirao, T. Uda, Surf. Sci. 306 (1994) 87
- [210] G. Onida, W. Andreoni, Chem. Phys. Lett. 243 (1995) 183
- [211] B. Delley, E. F. Steigmeier, Appl. Phys. Lett. 67 (1995) 2370
- [212] Y. Kanemitsu, S. Okamoto, M. Otobe, S. Oda, Phys. Rev. B 55 (1997) R7375
- [213] S. Oeguet, J. R. Chelikowsky, S. G. Louie, Phys. Rev. Lett. 79 (1997) 1770
- [214] G. Allan, C. Delerue, M. Lannoo, Phys. Rev. Lett. 78 (1997) 3161
- [215] A. B. Filonov, A. N. Kholod, F. d'Avitaya, X. Arnaud, Phys. Rev. B 57 (1998) 1394
- [216] M. O. Watanabe, T. Miyazaki, T. Kanayama, Phys. Rev. Lett. 81 (1998) 5362
- [217] T. van Buuren, L. N. Dinh, L. L. Chase, W. J. Siekhaus, L. J. Terminello, Phys. Rev. Lett. 80 (1998) 3803
- [218] A. Kux, M. B. Chorin, Phys. Rev. B 51 (1995) 17535
- [219] H. Yorikawa, H. Uchida, S. Muramatsu, J. Appl. Phys. 79 (1996) 3619
- [220] L. Brus, J. Phys. Chem. 90 (12) (1986) 2555
- [221] Y. Kayanuma, Solid State Comm. 59(6) (1986) 405
- [222] B. Delley, E. F. Steigmeier, Phys. Rev. B 47 (1993) 1397
- [223] D. Tomanek, M. A. Schlüter, Phys. Rev. B 36 (1987) 1208
- [224] J. R. Chelikowsky, Phys. Rev. Lett. 60 (1988) 2669
- [225] C. M. Rohlifing, K. Raghavachari, Chem. Phys. Lett. 167 (1990) 559
- [226] N. Binggeli, J. L. Martins, J. R. Chelikowsky, Phys. Rev. Lett. 68 (1992) 2956
- [227] M. Menon, K. R. Subbaswamy, Phys. Rev. B 47 (1993) 12754
- [228] E. C. Honea, A. Ogura, C. A. Murray, K. Raghavachari, W. O. Sprenger, M. F. Jarrold, W. L. Brown, Nature 366 (1993) 42
- [229] X. Jing, N. Troullier, Y. Saad, Phys. Rev. B 50 (1994) 12234
- [230] X. G. Gong, Phys. Rev. B 52 (1995) 14677
- [231] X. G. Gong, Q. Q. Zheng, Y.-Z. He, J. Phys. Condens. Matter 7 (1995) 577
- [232] C. Xu, T. R. Taylor, D. M. Neumark, J. Chem. Phys. 108 (1998) 1395
- [233] H. Kimura, S. Imanaga, Y. Hayafuji, H. Adachi, J. Phys. Soc. Jpn. 62 (1993) 2663
- [234] B.-L. Gu, Z.-Q. Li, J.-L. Zhu, J. Phys.: Condens. Matter 5 (1993) 5255
- [235] T. van Buuren, T. Tiedje, J. R. Dahn, B. M. Way, Appl. Phys. Lett. 63 (1993) 2911
- [236] D. J. Wales, Phys. Rev. A 49 (1994) 2195
- [237] S. Fouad, Naseer Sabri, P. Poopalan, Z.A.Z. Jamal, Exp. Theo. NANOTECHNOLOGY 2 (2018) 115
- [238] S. Saito, Phys. Rev. B 51 (1995) 2628(R)
- [239] E. Kaxiras, In "Cluster Assembled Materials" (K. Sattler, Ed.), 232: 67. Trans. Tech. Publications, Zurich (1996)
- [240] S. Saito. In "Cluster Assembled Materials" (K. Sattler, Ed.), 232: 233. Trans. Tech. Publications, Zurich, (1996)
- [241] M. F. Jarrold, V. A. Constant, Phys. Rev. Lett. 67 (1991) 2994
- [242] K. Fuke, K. Tsukamoto, F. Misaizu, J. Chem. Phys. 99 (1993) 7807
- [243] P. Jackson, K.J. Fisher, G.E. Gadd, I. G. Dance, D. R. Smith, G. D. Willett, Int. J. Mass. Spectrom. Ion. Process. 164 (1997) 45
- [244] S. Hayashi, H. Abe, Jpn. J. Appl. Phys. 23 (1984) L824
- [245] J. A. Cogordan, L. E. Sansores, A. A. Valladares, J. Non-Cryst. Solids 181 (1995) 135
- [246] B. Marsen, M. Lonfat, P. Scheier, K. Sattler, J. Electron Spectroscopy and Related Phenomena 109 (2000) 157
- [247] J. P. Proot, C. Delerue, G. Allan, Appl. Phys. Lett. 61 (1992) 1948
- [248] P. E. Batson, J. R. Heath, Phys. Rev. Lett. 71 (1993) 911
- [249] Y. Kanemitsu, H. Uto, Y. Masumoto, T. Matsumoto, T. Futagi, H. Mimura, Phys. Rev. B 48 (1993) 2827
- [250] C. Delerue, E. Martin, J.-F. Lampin, G. Allan, M. Lannoo, Le Journal de Physique IV(3) (1993) C5 -359

Exp. Theo. NANOTECHNOLOGY 3 (2019) 301-362

- [251] J. L. Gavartin, C. C. Matthai, *Mater. Sci. Eng. B* 35 (1995) 459
- [252] A. Sieck, D. Porezag, T. Frauenheim, M. R. Pederson, K. Jackson, *Phys. Rev. A* 56 (1997) 4890
- [253] E. Kaxiras, *Phys. Rev. B* 56 (1997) 13455
- [254] P. Hapala, K. K^ousov[´]a, I. Pelant, P. Jel[´]inek, *Phys. Rev. B* 87 (2013) 195420
- [255] R. S. Becker, J. A. Golovchenko, D. R. Hamann, B. S. Swartzentruber, *Phys. Rev. Lett.* 55 (1985) 2032
- [256] R. J. Hamers, P. Avouris, F. Bozso, *Phys. Rev. Lett.* 59 (1987) 2071
- [257] M. Maus, G. Ganteför, W. Eberhardt, *App. Phys. A* 70 (5)(2000) 535
- [258] O. Kostko, S. R. Leone, M. A. Duncan, M. Ahmed, *J. Phys. Chem. A.* 114(9) (2010) 3176
- [259] H. F. Wilson, L. McKenzie-Sell, A. S. Barnard, *J. Mater. Chem. C* 2 (2014) 9451
- [260] A. M. Smith, A. M. Mohs, S. Nie, *Nature Nanotech.* 4 (2009) 56
- [261] K. Akamatsu, S. Takei, M. Mizuhata, A. Kajinami, S. Deki, S. Takeoka, M. Fujii, S. Hayashi, K. Yamamoto, *Thin Film Solids* 359 (2000) 55
- [262] J. Xu, X. Yang, Q.-D. Yang, T.-L. Wong, S.-T. Lee, W.-J. Zhang, C.-S. Lee, *J. Mater. Chem.* 22 (2012) 13374
- [263] J. Arbiol, M. de la Mata, M. Eickhoff, A. Fontcuberta i Morral, *Materials today* 16(6) (2013) 213
- [264] H. Wei, Y. Su, Z. Han, T. Li, X. Ren, Z. Yang, L. Wei, F. Cong Y. Zhang, *Nanotechnology* 24(23)(2013)
- [265] J. Shi, Y. Hara, C. L. Sun, M. A. Anderson, X. D. Wang, *Nano Lett.* 11 (2011) 3413
- [266] A. M. Smith, A. M. Mohs, and S. Nie, *Nat Nanotechnol.* 4(1) (2009) 56
- [267] J. Lee, H. Kim, S.-J. Kahng, G. Kim, Y.-W. Son, J. Ihm, H. Kato, Z. W. Wang, T. Okazaki, H. Shinohara, Y. Kuk, *Nature (London)* 415 (2002) 1005
- [268] R. Rivelino, F. de Brito Mota, *Nano letters* 7 (6) (2007) 1526
- [269] S. Okubo, T. Okazaki, N. Kishi, S.-K. Joung, T. Nakanishi, S. Okada, S. Iijima, *J. Phys. Chem. C* 113 (2009) 571
- [270] G. L. Gibson, T. M. McCormick, D. S. Seferos, *J. Amer. Chem. Soc.* 134(1) (2011) 539
- [271] M. Wykes, B. Milián-Medina, J. Gierschner, *Front Chem.* 1 (2013) 35
- [272] T. Xu, L. Yu, *Materials today* 17(1) (2014) 11
- [273] S. Sarkar, S. Saha, S. Pal and P. Sarkar, *RSC Adv.* 4 (2014) 14673
- [274] H. Chen, J. Peet, S. Hu, J. Azoulay, G. Bazan, M. Dadmun, *Adv. Funct. Mater.* 24 (214) 140
- [275] M. Dvorak, W. Oswald, Z. Wu, *Scientific Reports* 3, Art. No. 2289 (2013)
- [276] R. Balog, B. Jørgensen, L. Nilsson, M. Andersen, E. Rienks, M. Bianchi, M. Fanetti, E. Lægsgaard, A. Baraldi, S. Lizzit, Z. Sljivancanin, F. Besenbacher, B. Hammer, T. G. Pedersen, P. Hofmann, L. Hornekær, *Nature Materials* 9 (2010) 315
- [277] M. Y. Han, B. Oezylmaz, Y. Zhang, P. Kim, *Phys. Rev. Lett.* 98(20) (2007)
- [278] C. Jeon, H.-C. Shin, I. Song, M. Kim, J.-H. Park, J. Nam, D.-H. Oh, S. Woo, C.-C. Hwang, C.-Y. Park, J. R. Ahn, *Scientific Reports* 3, Article number: 2725 (2013)
- [279] N. Kharche, S. K. Nayak, *Nano Lett.* 11 (12) (2011) 5274
- [280] W. Yang, K. R. Ratinac, S. P. Ringer, P. Thordarson, J. J. Gooding, F. Braet, *Ang. Chemie. Int. Edition* 49(12) (2010) 2114
- [281] H. W. Ch. Postma, *Nano Lett.*, 10 (2) (2010) 420
- [282] F. Mena, *J. Mol. Imaging Dynam* 3:e103(2013)
- [283] M. Yang, X. Zhang, *Environ. Sci. Technol.* 48 (20) (2014) 11846
- [284] S. Upadhyay, U. J. Phukan, S. Mishra, R. K. Shukla, *BMC Genomics* 15 (2014) 746
- [285] Y.-Q. Li, M.-F. Zhang, H.-Y. Wen, C.-L. Hu, R. Liu, H.-Y. Wei, C.-M. Ai, G. Wang, X.-X. Liao, X. Li, *Clinics (Sao Paulo)*. 68(1) (2013) 75

- [286] T. A. Mattei, A. A. Rehman, *Neurosurgery* 74 (5) (2014) 499
- [287] S. Ulstrup, J. C. Johannsen, F. Cilento, J. A. Miwa, A. Crepaldi, M. Zacchigna, C. Cacho, R. Chapman, E. Springate, S. Mammadov, F. Fromm, C. Raidel, T. Seyller, F. Parmigiani, M. Grioni, P. D. C. King, P. Hofmann, *Phys. Rev. Lett.* 112 (2014) 257401
- [288] S. Kannappan, K. Kaliyappan, R. K. Manian, A. S. Pandian, H. Yang, Y. S. Lee, J.-H. Jang, W. Lu, eprint arXiv:1311.1548 (2013).
- [289] H. Tian, Y. Shu, Y.-L. Cui, W.-T. Mi, Y. Yang, D. Xie, T.-L. Ren, *Nanoscale*, 6 (2014) 699
- [290] G. Eda, G. Fanchini, M. Chhowalla, *Nature Nanotechnology* 3(2008) 270
- [291] Y.-P. Hsieh, M. Hofmann, J. Kong, *J. Carbon* 67 (2013) 417
- [292] H. Brody, *Nature* 483 (2012) S29
- [293] Y. Zhang, T. Liu, B. Meng, X. Li, G. Liang, X. Hu, Q. J. Wang, *Nature Communications* 4, Article number: 1811 (2013)
- [294] Lockheed Martin (2013), Text available @ www.businessinsider.in/Lockheed-Martin-Says-This-Desalination-Technology-Is-An-Industry-Game-Changer/articleshow/21232574.cms
- [295] R. Sanna, E. Fortunati, V. Alzari, D. Nuvoli, A. Terenzi, M. F. Casula, J. M. Kenny, A. Mariani, *Cellulose* 20 (2013) 2393
- [296] S. Pan, Z. Yang, P. Chen, J. Deng, H. Li, H. Peng, *Angew. Chem. Int. Ed. Engl.* 53 (24) (2014) 6110
- [297] N. Nuraje, S. I. Khan, H. Misak, R. Asmatulu. *ISRN Polymer Science* (2013), Article ID 514617.
- [298] E. Anslyn (2004), *Modern Physical Organic Chemistry*, Sausalito, CA: University Science. ISBN 978-1-891389-31-3.
- [299] A. W.-C. Lau (2000), Fluctuation and Correlation Effects in Electrostatics of Highly Charged Surfaces. PhD thesis submitted to ^[1]Physics Department, University of California, Santa Barbara
- [300] Nanowerk, 2010; text available @ <http://www.nanowerk.com/spotlight/spotid=16047.php>

© 2019 The Authors. Published by IFIA (<https://etn.iraqi-forum2014.com/>). This article is an open access article distributed under the terms and conditions of the Creative Commons Attribution license (<http://creativecommons.org/licenses/by/4.0/>).